

**OPTICAL MODULATION OF FLUOROPHORES BASED ON DARK STATE
PHOTOPHYSICS**

A Dissertation
Presented to
The Academic Faculty

By

Daniel P. Mahoney

In Partial Fulfillment
Of the Requirements for the Degree
Of Doctor of Philosophy in the
School of Chemistry & Biochemistry

Georgia Institute of Technology
August 2017

Copyright © Daniel P. Mahoney 2017

OPTICAL MODULATION OF FLUOROPHORES BASED ON DARK STATE PHOTOPHYSICS

Approved by:

Dr. Robert M. Dickson, Advisor
School of Chemistry and Biochemistry
Georgia Institute of Technology

Dr. Jennifer E. Curtis
School of Physics
Georgia Institute of Technology

Dr. Kenneth R. Brown
School of Chemistry and Biochemistry
Georgia Institute of Technology

Dr. Jeffrey T. Petty
Department of Chemistry
Furman University

Dr. Christoph J. Fahrni
School of Chemistry and Biochemistry
Georgia Institute of Technology

Date Approved: June 7, 2017

ACKNOWLEDGEMENTS

I would like to thank all of the people who helped me through my PhD. My advisor Prof. Robert Dickson has guided me through, requiring me to take ownership and initiative in my projects, but always being available for feedback and consultation on all things research related: equipment and experimental setup, data analysis, theoretical insight, and manuscript publication. Thank you for helping me develop from an undisciplined undergraduate to a PhD graduate ready to begin an industry position. Thank you to my thesis committee: Profs. Ken Brown, Christoph Fahrni, Jennifer Curtis, and Jeff Petty. Your insights and feedback in discussions and presentations helped me improve and think about my projects in new ways. Thank you also to all of my group members, past and present. Drs. Chaoyang Fan, Saugata Sarkar, and Jagnyaseni Tripathy helped me get my start in lab and showed me how to conduct research. Jung-Cheng Hsiang was extraordinarily helpful with expertise in all things experimental and theoretical, as well as developing very useful computer programs for data acquisition and analysis. Thank you also to Amy Jablonski, Soonkyo Jung, Blake Fleischer, Tzu-Hsueh Huang, Yen-Cheng Chen, Aida Demissie, and Joe Richardson for help and support. To our younger students Baijie, Yi-Han, and Alex, best of luck in the future. I'm sure the lab is in good hands.

I would also like to thank Prof. Maged Henary and his grad students Eric, Matt, and Tyler at Georgia State for collaborative assistance in synthesizing organic dyes for me to test and helping research move forward. Drs. Jeff Petty and Kyril Solntsev have also helped me with experiments in lab and interpretation of results. Thank you also to Profs. Joe Perry,

Andrew Lyon, Robert Whetten, Angus Wilkinson, and Christine Payne for guidance in research and in the classroom.

Thank you to all of my friends outside of lab: Khanh Do, Mauricio Gutierrez, Aaron McKee, Quaovi Sodji, Hiro Ichikawa, Sean Ryno, Ryan Josefsberg, Jeannie Yom, and everyone else along the way as we got through the emotional difficulties of grad school and into real life. To my girlfriend Hillary, my parents, and my sister Lizz, thank you for all of the love and support over the years.

TABLE OF CONTENTS

ACKNOWLEDGMENTS.....	iii
LIST OF TABLES.....	viii
LIST OF FIGURES.....	x
LIST OF SYMBOLS AND ABBREVIATIONS	xvii
SUMMARY	xx
CHAPTER 1 INTRODUCTION	1
1.1 Motivation	1
1.2 Fluorescence Microscopy	3
1.3 Fluorescent Labels	6
1.4 Cyanine Dyes	11
1.5 Fluorescent Protein Chromophore	14
1.6 Optical Modulation	16
1.7 Organization of Thesis	25
CHAPTER 2 EXPERIMENTAL AND THEORETICAL METHODOLOGY	26
2.1 Sample preparation	26
2.2 Bulk Characterization	27
2.3 Fluorescence Microscopy	29
2.4 Time Correlated Single Photon Counting	32
2.5 Fluorescence Correlation Spectroscopy	34
2.6 Optical Modulation	36
2.7 Density Functional Theory	42

CHAPTER 3 CYANINE DYE MODULATION EXPERIMENTS.....	45
3.1 Introduction	45
3.2 Cyanine Photophysics	46
3.3 Cyanine Modulation	49
3.4 Cyanine Enhancement and On & Off Times	52
3.5 Conclusion	58
CHAPTER 4 CYANINE MECHANISM OF MODULATION AND SYNTHETIC FEEDBACK.....	60
4.1 Introduction	60
4.2 Cyanine Theory: Electronic Energies and Photoisomerization	61
4.3 Experimental dark state energy	66
4.4 Calculated photoisomer ground state energies	68
4.5 Calculated photoisomer excited state energies	71
4.6 Theoretical Predictions	72
4.7 Testing Properties of New Cyanine Variants	74
4.8 Solution additives for manipulation of photophysics	77
4.9 Conclusions	80
CHAPTER 5 OPTICALLY ACTIVATED DELAYED FLUORESCENCE	82
5.1 Introduction	82
5.2 Cy5 Experimental Results	85
5.3 Merocyanine 540 Experimental Results	86
5.4 Triplet State Lifetime Modifications	89
5.5 Conclusions	93

CHAPTER 6 PROTEIN-CHROMOPHORE BINDING MODULATION	94
6.1 Introduction	94
6.2 Fluorescence Modulation of Protein-Binding Chromophores	97
6.3 Time Trace Analysis of HSA-complex Photophysics	101
6.4 Fluorescence Phase Advance	104
6.5 Conclusions & Future Work	106
CHAPTER 7 CONCLUSIONS AND FUTURE WORK	108
APPENDIX A: EXTRA MODULATION DATA	110
APPENDIX B: SECONDARY INDUCED FLUORESCENCE	112
APPENDIX C: ADDITIONAL DENSITY FUNCTIONAL THEORY CALCULATIONS.....	121
APPENDIX D: DENSITY FUNCTIONAL THEORY CALCULATION INPUT	123
APPENDIX E: NUMERICAL SIMULATIONS OF PHOTOPHYSICS	125
APPENDIX F: COPYRIGHT PERMISSIONS	130
REFERENCES	140

LIST OF TABLES

Table 2.1.	Summary of lasers and their characteristics used in this research.	30
Table 3.1.	Summary of experimental results including enhancement and on and off times for Cy5 derivatives. R ¹ and R ² positions are as shown in Figure 3.5. For τ_{on} and τ_{off} measurements, the primary and secondary laser intensities were 350 and 640 W/cm ² , respectively.	53
Table 3.2.	FCS data for Cy5 compounds. The first values listed are for primary only and the second are for dual laser excitation. The decrease in dark state fraction after secondary laser co-illumination shows that the dark state is effectively depleted by the secondary laser.	56
Table 4.1.	Summary of ground state DFT computational results: Cis23-Trans and cis12-Trans refer to the energy differences between the ground states of the different cis-photoisomers (as labeled in Figure 4.5) and the all-trans ground states. (Note: Due to short lifetimes, E65 and Cy7 exhibited insufficient dark state buildup to determine experimental cis-trans values.) E _a is the activation energy obtained by Arrhenius calculations using the experimental k_{off}° and setting A = 10 ¹² s ⁻¹	70
Table 4.2.	Ground to excited state transition wavelengths calculated by TDDFT.	72
Table 4.3.	Calculated energies comparing cis and all trans ground states for structures with substituents at “o,” “m,” and “p” positions. All data are in eV units.	74
Table 4.4.	Summary of new cyanine dye photophysical properties.	76
Table 4.5.	Summary of additive effects on Cy5 modulation depth and photophysics. Experiments were conducted in water, Cy5 concentrations were ~1-10 nM while additive concentrations were approximately 100 mM.	78
Table 5.1.	Photophysical OADF properties of Merocyanine 540.	91
Table 6.1	Summary of HSA binding compounds fluorescence modulation. Modulation depth generally increases while characteristic frequency decreases upon binding. k_{dark} was obtained by fitting to the frequency domain lifetime equation and extrapolating to zero primary intensity (explained in section 3.3).	99
Table 6.2.	Concentration dependence of HSA on fluorescence modulation. HSA concentration varies while chromophore concentration stays constant at approximately 5 μM . Laser intensities were approximately 1.4 kW/cm ² and 5 kW/cm ² for 476 nm primary and 561 nm secondary excitation, respectively.	101

Table A1.	SAFIRE fluorescence enhancement data for other cyanine derivatives. .	110
Table C1.	Energy differences between the Cis01 isomer and all trans ground states.	121
Table C2.	Energy differences for asymmetric molecules.	122

LIST OF FIGURES

Figure 1.1.	a) Jablonski diagram showing the different types of energy levels present in a typical molecule. b) Jablonski diagram showing the visible transitions between electronic and vibrational states corresponding to different absorption and emission wavelengths. Large energy differences correspond to lower wavelength radiation, and vice versa.	4
Figure 1.2.	A fluorescence microscope diagram. In this case a light source is filtered for green light, which is used to excite the sample and subsequent red fluorescence transmitted for detection.	5
Figure 1.3.	An illustration of fluorescence imaging by wavelength from UV to visible to NIR. At short UV wavelengths, light does not travel as deeply due to absorption and scattering, and high autofluorescence occurs, obscuring any fluorophore signal. However at longer wavelengths absorption, scattering, and autofluorescence is diminished.	9
Figure 1.4.	Example of pentamethine cyanine with indole side groups.	11
Figure 1.5.	Potential energy diagram representing cyanine photoisomerization. The all trans ground state is the lowest energy level and from there excitation to a higher electronic state can occur, followed by either decay to the ground state by internal conversion or fluorescence or photoisomerization to a cis-photoisomer state, where it can reverse photoisomerize to the all trans ground state.	13
Figure 1.6.	Structure of GFP chromophore.	14
Figure 1.7.	Locked GFP chromophore variants.	15
Figure 1.8.	Schematic of photophysical processes of ortho-hydroxy fluorescent protein chromophore.	16
Figure 1.9.	Top: Jablonski diagram describing a typical three electronic state system. Bottom: Schematic fractional populations of S_0 , S_1 , and T_1 as a function of time.	17
Figure 1.10.	Fluorescence time trace of a rose bengal solution modulated at 10 Hz. ..	19
Figure 1.11.	Demonstration of Cy5 modulation. When Cy5, which is capable of secondary modulation at 710 nm, is paired with Texas Red (not modulatable), only the Cy5 signal is recovered upon demodulation.	22
Figure 1.12.	After embedding Cy5 into a tissue mimicking phantom, secondary modulation allows for modulated fluorescence recovery, which allows for stronger signal and greater imaging depth.	23

Figure 1.13.	(A) Fluorescence modulation of blue fluorescent protein (modBFP/H148K) where the primary laser is held constant while the secondary laser is modulated by an external square waveform. The dark state population is at a minimum at the fluorescence maximum and at a maximum at the fluorescence minimum. (B) Fluorescence time trace of modBFP/H148K modulated at 13 Hz with the inset showing the fast Fourier Transform with corresponding peaks at the appropriate frequencies. (C) Analysis of fluorescence modulation with a charge-coupled device (CCD) camera detector. Upon demodulation, the image becomes more clear as there is less interference by background fluorescence.	24
Figure 2.1.	The synthesis of cyanine compounds used.	26
Figure 2.2.	Fluorescence microscope setup with dual laser excitation. In this diagram a blue primary laser and red secondary laser are aligned and used to excite a sample which fluoresces green. A dichroic filter is used to reflect blue and red light while allowing green to pass through. A bandpass filter is used to further ensure that only fluorescence transmits through to the detector.	31
Figure 2.3.	Schematic of TCSPC.	33
Figure 2.4.	Illustration of FCS process. (a) A fluorescent molecule diffusing through the focal volume, (b) an increase in fluorescence is observed as the molecule passes through the focal volume, (c) the FCS autocorrelation function, (d) schematic of the fluorescence as the time lag (τ) in the autocorrelation is applied, (e) the overlap after time lag τ between the original fluorescence fluctuation and the time lagged fluctuation. The overlap decreases as the time lag increases.	35
Figure 2.5.	EOM devices: Conoptics model 350 EOM driven by model 25D driver.	37
Figure 2.6.	Basic optical modulation setup in the case of dual laser excitation with secondary modulation. Primary and secondary lasers are aligned into an inverted microscope. The secondary laser is modulated with an EOM and a function generator applies an external waveform which controls the modulation. The lasers are directed through an objective and are focused into the sample. Fluorescence from the sample is collected via the objective and directed through the microscope to the detector, where it is recorded by a counting board and analyzed by computer software.	38
Figure 2.7.	Plot of modulation depth vs modulation frequency governed by the equation $m = A / \sqrt{1 + (2\pi\nu\tau)^2}$ where $A = 0.5$ and $\tau = 300 \mu\text{s}$. The	

	modulation depth is at a maximum at low modulation frequency and decays to near zero by 100 kHz.	39
Figure 2.8.	Simulation of photophysics using Cy5 parameters with square wave modulation. On top, modulation at 2 kHz, on bottom: modulation at 15 kHz. At 2 kHz modulation a clear decay is observed while at 15 kHz it is comparatively flattened out because the dark state does not have time to adequately recovery with such a short period between excitation pulses.	41
Figure 2.9.	Top: Cy5 photophysics simulation with primary only square wave modulation at 4 kHz. Bottom: Simulation with primary on, then primary off and secondary on, then primary on again with secondary off. The initial fluorescence is higher when there is secondary laser pre-illumination, this can be used to estimate the dark state thermal population.	42
Figure 3.1.	Modulation frequency scans of Cy5 with 633 nm primary excitation and 710 nm secondary excitation. In A) the primary laser intensity is 1.8 kW/cm ² while in B) it is 7.7 kW/cm ² . The secondary is held constant at 12 kW/cm ² . In this example, going from lower to higher primary intensity the modulation depth decreases, the characteristic frequency ($k_{on} + k_{off}^0$) increases, and both the on and off times decrease. What this suggests is that at higher primary intensity Cy5 photoisomerizes more quickly but is also excited out of the dark state, leading to higher characteristic frequency but lower modulation depth. It is therefore possible to control modulation depth and frequency with laser intensity based on molecular photophysics.	45
Figure 3.2.	Illustration of kinetics of cyanine photophysical processes. ${}_0^1N$, ${}_1^1N$, and ${}_1^3N$ refer to the all trans isomer ground state, singlet excited state, and lowest triplet state, respectively. ${}_0^1P$, ${}_1^1P$, and ${}_1^3P$ refer to the photoisomer ground state, singlet excited state, and lowest triplet state, respectively. k_{ISC} and k_T refer to intersystem crossing to triplet and decay from triplet rates while k_{perp} represents photoisomerization and k_{PN} back photoisomerization. σ signifies absorption cross section and I_{exc} laser excitation intensity. Photoisomerization (possibly over multiple bonds) can occur, along with intersystem crossing to triplet states, which occur in both trans and cis photoisomers. All of these processes occur on similar timescales, with triplet transitions occurring about ten times faster than photoisomerization.	48
Figure 3.3.	A) Cy5 derivative MHI97 (See Table 3.1) modulation depth as a function of modulation frequency and fit to equation 1. Data were collected for 1	

	second at each modulation frequency. B) MHI97 characteristic frequency as a function of primary intensity and the line to which it fits.	51
Figure 3.4.	Fluorescence traces showing ground state recovery for MHI106 using different primary laser off periods, T_{off} . Using an electro-optic modulator, the primary laser is turned on for 500 μs and off for A) 300 μs , B) 100 μs , C) 50 μs , and D) 20 μs . Laser spot size was expanded 300 μm^2 , to increase diffusion timescales to $\sim 10\text{ms}$, such that it does not interfere with the modulation timescales. For each panel, data were collected for 20 seconds and modulation cycle averages are taken and ratios of initial to final intensities within the average primary illumination period, T_{on} , as a function of T_{off} are fit to equation 3.	52
Figure 3.5.	General structure of Cy5 analogs. Modifications were incorporated as alkyl substitutions at the heterocyclic nitrogens (R^1) and halogen incorporation on the <i>meso</i> position of the polymethine bridge (R^2).	53
Figure 3.6.	FCS data for cyanine compounds with single and dual laser excitation. The autocorrelation data are shown with the fits to the FCS formula overlapped. Exp refers to experimental data while Theo signifies fit to the FCS formula.	58
Figure 4.1.	Calculated (CS INDO) potential energy vs twisting coordinate for the 2-3 and 3-4 <i>cis</i> isomers of a pentamethine cyanine with nitrogen atoms at both ends (structures shown in diagram).	63
Figure 4.2.	Pentamethine molecule used in the experimental and theoretical study by Baraldi et al.	64
Figure 4.3.	Pentamethine cyanine and rotation scheme used in this study.	65
Figure 4.4.	Optical recovery of thermally populated dark states. Primary-only induced fluorescence from MHI97 with (black) and without (red) secondary laser pre-illumination. The increased fluorescence with secondary-only pre-illumination relative to no secondary pre-illumination generates higher initial fluorescence intensity by optically recovering molecules from the thermally populated dark state.	67
Figure 4.5.	All-trans isomers of A) Cy5, B) Cy5.5, C) Cy7, D) Merocyanine 540 numbered to show isomerization possibilities. When <i>cis</i> isomers are described, the numbers refer to the bonds between carbon atoms. For example, <i>cis</i> 23 refers to the bond between the 2 and 3 labeled carbon atoms.	69
Figure 4.6.	Theoretical cyanine structures tested using density functional theory. Structure A has a <i>cis</i> 23-Trans energy of 0.137 eV, structure B has a <i>cis</i> 23-	

	Trans energy of 0.134 eV, and structure C has a cis23-Trans energy of 1.779 eV.	73
Figure 4.7.	Cy5-like structure with substituents labeled at “o,” “m,” and “p” positions.	74
Figure 4.8.	New cyanine dyes. MDL-45 contains a phenyl substituent on the polymethine bridge, while T-81 and TRC-84 contain substituents on the indole side groups. SP-2-28 and ZK-311 both contain benzothiazole side groups.	76
Figure 5.1.	Jablonski diagrams illustrating fluorescence recovery pathways via dark state recovery. In the case of a photoisomer, both thermal relaxation and secondary excitation return the dark state to the fluorescent ground state, but in the case of a triplet dark state the excited fluorescence state is recovered, allowing for subsequent fluorescence.	84
Figure 5.2.	Cy5 fluorescence with pulsed primary (647 nm) excitation with and without constant secondary (710 nm) excitation. Left: Pulsed primary with no secondary laser. The peak height is 1680 counts, and the decay is 1 ns. Right: Pulsed primary excitation with constant secondary excitation. In this case the peak height is 2085 counts and the decay is also 1 ns. ...	85
Figure 5.3.	Modulated fluorescence of Merocyanine 540 in water. A) modulated primary excitation (543 nm, 600 W/cm ²), B) modulated primary plus constant secondary co-illumination (637 nm, 10 kW/cm ²), showing elimination of fluorescence decay due to lack of dark state build up. C) modulated primary excitation (50 W/cm ²), D) Alternating modulated primary and secondary (140 kW/cm ²) excitation, causing greater fluorescence decay due to photoisomer depopulation to the ground state. Fluorescence intensity is significant between primary pulses due to high intensity secondary bleed through.	87
Figure 5.4.	Merocyanine 540 fluorescence in aqueous solution using 532 nm pulsed excitation (rep rate 10 kHz) with and without secondary (637 nm) co-illumination. Optically activated delayed fluorescence is observed when the secondary laser is present, presumably due to a repumping of the excited bright state. A) Pulsed primary with and without secondary illumination. With the addition of the secondary laser a slight upconversion tail is observed at the end of the pulse. B) Pulsed primary plus secondary with ~1 ns time resolution, showing OADF more clearly. C) Secondary power dependence of fluorescence decay. Higher power (or intensity due to constant spot size) shortens the observed timescale due to faster depletion of dark state.	88
Figure 5.5.	A) Pulsed-CW data for Merocyanine 540 in water after nitrogen purging. The secondary fluorescence is much longer lived. B) Secondary power	

	dependence with N ₂ gas. The dark state lifetime is 16.1 μ s. C) Pulsed-CW data for Merocyanine 540 in PVA. D) Secondary power dependence in PVA. The dark state lifetime is 45.5 μ s.	90
Figure 6.1.	Fluorescence activation by binding to HSA. The protein-binding molecule is by itself weakly fluorescent, but becomes much brighter upon encapsulation by the binding pocket of the protein.	95
Figure 6.2.	Different GFP chromophore derivatives and their fluorescence increase upon binding to HSA.	96
Figure 6.3.	Two laser data for the HSA-chromophore complex in which the primary laser is constant and secondary laser is modulated. In the image on the left the modulation depth is recorded over many modulation frequencies while in the image on the right a fluorescence intensity time trace is take over the modulation cycle.	100
Figure 6.4.	Top: Fluorescence time trace of HSA-chromophore complex with only primary illumination modulated at 0.5 Hz showing bi-exponential decay behavior (476 nm, ~340 W/cm ²). Bottom: Time traces of HSA-chromophore complex beginning with primary only excitation and later a constant fluorescence bump due to secondary laser turn on. Bottom left: Lower primary intensity (100 W/cm ²), Bottom right: Higher primary intensity (600 W/cm ²).	103
Figure 6.5.	HSA-chromophore complex fluorescence with square wave (left) and sinusoidal (right) excitation. With square wave excitation a decay due to dark state behavior is clearly seen, and with sinusoidal excitation a slight phase advance can be observed.	104
Figure 6.6.	Comparison of phase advance with different laser intensity and modulation conditions. A) 1 Hz sine wave modulated primary at 1 kW/cm ² . B) 100 Hz sine wave modulated primary at 1 kW/cm ² . C) 1 Hz sine wave modulated primary at 1 kW/cm ² , plus constant secondary at 100 kW/cm ² . D) 1 Hz sine wave modulated primary at 13 kW/cm ²	105
Figure B1.	Comparison of secondary fluorescence between MHI-97 (left) and MHI-106 (right). With excitation laser intensity and concentration held constant, MHI-97 has much greater secondary fluorescence.	112
Figure B2.	A) Cy5 fluorescence decay with pulsed primary excitation. B) Fluorescence decay with pulsed primary and secondary excitation. C) Fluorescence decay peaks with secondary only excitation. D) Concurrent primary and secondary excitation, zoomed into secondary fluorescence peaks. Upon dual excitation the primary fluorescence peak increases by ~15%, the same as the bulk fluorescence enhancement, while the secondary fluorescence peaks are unchanged.	114

Figure B3.	UV-vis absorption spectrum in visible-NIR region. There is a red-shift in the fluorescence from E27 to MHI97, from low to high modulation depth compounds.	115
Figure B4.	MHI-97 secondary fluorescence (670 nm emission and 710 nm excitation) with varying solvent refractive index, from ethanol (1.36), to propanol (1.39), dichloromethane (1.44), and pyridine (1.51). Increasing refractive index correlates with increasing secondary fluorescence. ...	116
Figure B5.	UV-vis absorption of MHI-97 with varying solvent. With increasing refractive index: ethanol (1.36), propanol (1.39), DMSO (1.48), and quinoline (1.63) the maximum absorption appears to shift to higher wavelength.	117
Figure B6.	Left: MHI-97 Fluorescence excitation scan from 690-800 nm with emission held constant at 665 nm. Right: Fluorescence emission from 600-700 nm with 710 and 730 nm excitation, the maxima of which correspond to the excitation scan value observed on the left.	118
Figure B7.	Left: UV-vis absorption of MHI-97 at high concentration (~100 μ M). Zoomed in, one can observe that the absorbance at 710 nm is 0.02, while the absorbance at 590 nm is 1.04. Right: The fluorescence emission of the same sample at 590 and 710 nm excitation.	119

LIST OF SYMBOLS AND ABBREVIATIONS

ϵ	Extinction coefficient
Φ	Quantum yield
σ	Absorption cross section
τ_c	Characteristic time
τ_{on}	On time
τ_{off}	Off time
ν_c	Characteristic frequency
ν_{mod}	Modulation frequency
I_F	Fluorescence intensity
k_{exc}	Excitation rate
k_{fl}	Fluorescence rate
k_{on}	On rate
k_{off}	Off rate
D	Dark state
N	Refractive Index
S_0	Ground state
S_1	Excited State
T_1	Lowest triplet state
A	Absorbance
APD	Avalanche photodiode
B3LYP	Beck, three-parameter, Lee-Yang-Parr
BSA	Bovine serum albumin
BFP	Blue fluorescent protein
BME	Beta-mercaptoethanol
BODIPY	Borondipyrromethane
CCD	Charge coupled device
CW	Continuous wave
DFT	Density Functional Theory

DMSO	Dimethylsulfoxide
ECP	Effective core potential
EOM	Electro-optic modulator
ESIPT	Excited state intramolecular proton transfer
eV	electronvolt
FCS	Fluorescence correlation spectroscopy
FFT	Fast Fourier Transform
FRET	Fluorescence (or Förster) resonance energy transfer
FP	Fluorescent protein
GFP	Green fluorescent protein
GGA	Generalized gradient approximation
HSA	Human serum albumin
INDO	Intermediate neglect of differential overlap
IR	Infrared
IRF	Instrument response function
ISC	Intersystem crossing
kDa	Kilodalton
KD*P	Potassium Dideuterium Phosphate
LANL2DZ	Los Alamos National Lab ECP plus double zeta
LDA	Local density approximation
M	Molar (moles/liter)
NA	Numerical aperture
ND	Neutral Density
OD	Optical density
OLID	Optical lock-in detection
OPO	Optical parametric oscillator
p-HBDI	p-hydroxybenzylidene-imidazolidinone
PAMAM	Poly(amidoamine)
PBS	Phosphate buffered saline

PDT	Photodynamic therapy
PMT	Photomultiplier tube
PVA	Polyvinyl alcohol
PCM	Polarizable continuum model
QD	Quantum dot
SAFIRE	Synchronously amplified fluorescence image recovery
SNR	Signal to noise ratio
TCSPC	Time-correlated single photon counting
TD-DFT	Time dependent-density functional theory
TMR	Tetramethylrhodamine
UV-vis	Ultraviolet-visible spectroscopy

SUMMARY

Fluorescence microscopy is an established technique in chemical and biological imaging, allowing signal of interest from fluorescent molecules to be detected over background. However, autofluorescent background and finite imaging depth limit signal to noise in traditional fluorescence imaging. Amplitude modulation is one way to increase signal to noise, and by modulation and subsequent demodulation of fluorescent signal, but not background, allows for greater signal to noise as well as imaging depth. The properties of nonfluorescent dark states allow for application of modulation by controlling fluorescence signal intensity. This has been demonstrated previously by work from the Dickson Lab using triplet, photoisomer, and electron transfer dark states. In the work contained in this thesis commercial and synthesized cyanine molecules were studied in depth, investigating dark state photophysics, applying new modulation techniques and theoretical insights to better understand the mechanism of modulation and how to improve fluorescence modulation utilizing dark state photophysics.

First, new pentamethine cyanine derivatives were tested experimentally using single and dual laser modulation techniques to determine fluorescence enhancement and photophysical dark state kinetics. Application of these techniques showed that derivatives with longer alkyl chain substituents had greater fluorescence enhancement (modulation depth) as well as longer on and off times (longer lived dark states). Molecules with short alkyl chains and halogen substituents on the polymethine bridge exhibited lower modulation depth and shorter on and off times. In the case of these cyanine dyes, increased fluorescence enhancement is correlated with longer-lived dark states, while cyanines with

shorter-lived dark states show less enhancement. Longer dark state lifetimes allow for greater dark state buildup leading to greater fluorescence recovery, whereas shorter dark state lifetimes yield less fluorescence recovery. Commercial cyanines Cy5.5 and Cy7 show less modulation depth than Cy5, while Merocyanine 540 is comparable.

By investigating the mechanism of modulation using experimental and theoretical methods we can determine energetics of the photoisomer dark states as well the photoisomer responsible for the fluorescence modulation. By using dual laser modulation, thermal dark state population can be estimated and used to calculate the dark state-ground state energy difference via the Boltzmann distribution. This is compared to Density Functional Theory calculations of the all trans ground state and various cis photoisomers, showing that isomerization about the middle of the polymethine bridge is most likely responsible for the modulatable dark state, with other states possibly playing a minor role.

Next, new cyanines were synthesized and tested. No improvements in enhancement were observed, but different substituents can affect modulation frequency and water solubility. In another direction, triplet quenchers and enhancers were found to affect modulation depth without a clear relationship with modulation timescales. It appears that triplet quenchers increase fluorescence enhancement while triplet enhancers decrease modulation depth. It could be that triplet state populations are affected but photoisomerization timescales are not. An anomalous red-shifted fluorescence excitation effect was observed, and appears to be anti-Stokes fluorescence, which is incapable of modulation. Lastly and most importantly, Merocyanine 540 was studied and found to have both red-shifted photoisomer and triplet absorptions. Experiments show that photoisomer dark states recover the fluorescent ground state upon dark state recovery while triplet dark

states transition to the fluorescent excited state and subsequently fluoresce. This effect allows for optically activated delayed fluorescence and can be utilized for fluorescence recovery by a red-shifted excitation source. The triplet state depends on O₂ concentration, so removing molecular oxygen using nitrogen gas, an enzymatic oxygen scavenging system, or by immobilizing in a polymer film extend triplet lifetimes.

Finally, a protein-binding chromophore was studied using fluorescence modulation. This molecule is an analog of the green fluorescent protein and binds to human serum albumin. Upon binding, the chromophore goes from nonfluorescent in solution to brightly fluorescent with ~40% modulation depth upon longer wavelength secondary co-illumination. Modulation depth increases with increasing concentration, an effect not seen in cyanines which can possibly be attributed to binding affecting the modulation. Analysis of modulation timescales shows two or more components, which could possibly be photoisomerization, binding/unbinding, or photobleaching. Additionally, the fluorescence decay is very steep, making dark state behavior strongly apparent and allowing for time or frequency domain modulation applications as this decay is modulation or intensity dependent. More work needs to be done to completely understand the modulation timescales, but overall this protein-binding fluorophore shows promise in binding activated modulation applications.

CHAPTER 1

INTRODUCTION

1.1 Motivation

The observation of structures smaller than the human eye can detect has long allowed for the development of new science. Before modern microscopes, people did not know what made up matter, if it was smooth and continuous or comprised of discrete particles. Experimental and theoretical breakthroughs in this area have revolutionized many areas of science, especially fields such as chemistry, physics, biology and materials science. By seeing smaller than is possible with the unaided eye, new structures are revealed and one learns more about the components that make up the world. Modern imaging techniques such as electron microscopy (EM), scanning probe microscopy, optical coherence tomography (OCT), magnetic resonance imaging (MRI), magnetoencephalography (MEG), and fluorescence microscopy have all enabled researchers to visualize previously unresolved physical structures.¹⁻¹⁰

Fluorescence microscopy is an invaluable technique in biology and spectroscopy, used in such applications as flow cytometry, medical diagnostics, DNA sequencing, forensics, and genetic analysis.^{1-2, 11-13} By utilizing a strong signal from fluorescent molecules of interest, one can detect emitted light and discriminate from nonfluorescent background, allowing visualization of fluorescent and fluorescently-labeled objects, making it a highly selective and sensitive technique. Fluorescence can also provide information regarding molecular properties, such as electronic states, and can be used to

probe solvent environment and solution behavior, kinetics, energy transfer, nonlinear optics, sensing, and other scientific applications.

To further improve fluorescence signal strength and selectivity over background, optical modulation based on molecular photophysics has been utilized. In bulk samples, fluorescence can be controlled to increase or decrease based on whether or not molecules are in a bright or dim state. Specifically certain molecules, such as cyanine or xanthene dyes, in addition to absorbing light and emitting fluorescence they can undergo photoisomerization or intersystem crossing to yield a non-fluorescent dark state with a red-shifted transient absorption, which can be reverted back to the fluorescent bright state by secondary laser co-illumination. This secondary laser can be modulated, causing modulated fluorescence signal to be detected, allowing for greater image recovery due to enhanced signal to noise (SNR) ratio and imaging depth. By varying laser power and modulation frequencies and observing changing modulation depth one can determine the photophysical rates of the process. With this information, one obtains insight into how this process works and the effects of structural and environmental changes.

This work focuses on applying previous research, in particular Cy5 modulation,¹⁴ to new cyanine dyes, and looking closely at certain structural modifications to see how they affect dark state kinetics and energetics. Initially, high modulation depth was considered most desirable, but other characteristics such as modulation frequency and optically delayed fluorescence have emerged as potential improvements to imaging. Single and dual laser modulation experiments were combined with density functional theory (DFT) calculations to elucidate photophysical kinetics and mechanism. From there, these techniques can be applied to other systems such as small molecule protein-binding

chromophores, additives can be applied to modulatable systems to affect photophysics, and new techniques introduced in the literature (particularly phase advance modulation) can be applied to systems we have already studied and understand in order to offer new imaging modalities.

1.2 Fluorescence Microscopy

Fluorescence occurs when a molecule absorbs and then re-emits light. After excitation, some of the energy from the initial photon is lost to vibrational relaxation or other processes, causing the emitted light to be longer in wavelength than the initially absorbed light. To explain this mechanism further, a molecule is most often in (or near) its ground state, the lowest electronic energy level. From there it can be excited to higher rotational, vibrational, or electronic levels. In the case of visible light fluorescence microscopy, transitions mainly occur between electronic levels, which are spaced several electron volts apart. Between these energy levels lie smaller spaced rotational and vibrational energy levels. As depicted in Figure 1.1, upon absorption of light, a molecule is excited to a higher electronic state as well as a higher vibrational and/or rotational state. Vibrational and/or rotational relaxation occurs, and an electronic transition back to the ground state can occur by radiative emission. Furthermore, transitions to different electronic manifolds or other states can occur, such as intersystem crossing to a triplet state, photoisomerization, or charge transfer. The characteristics of these processes are illustrated in the figure below.

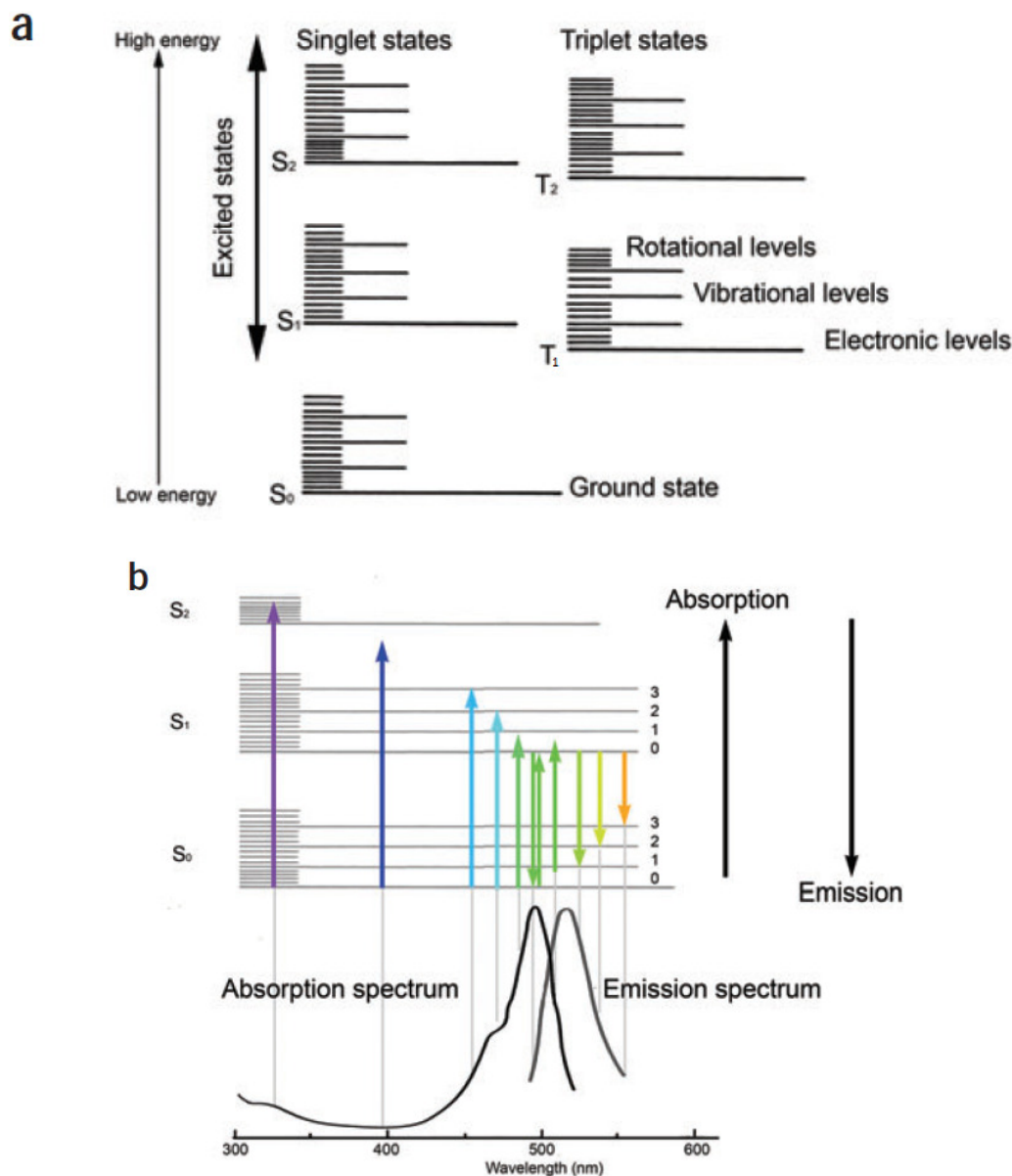


Figure 1.1. a) Jablonski diagram showing the different types of energy levels present in a typical molecule. b) Jablonski diagram showing the visible transitions between electronic and vibrational states corresponding to different absorption and emission wavelengths. Large energy differences correspond to lower wavelength radiation, and vice versa.¹¹

With two separate wavelength ranges for molecular absorption and emission, fluorescence can be utilized in a microscope by using a dichroic mirror to reflect the excitation light to the sample with fluorescence being transmitted through to an eyepiece or detector. A schematic is shown in the figure below.

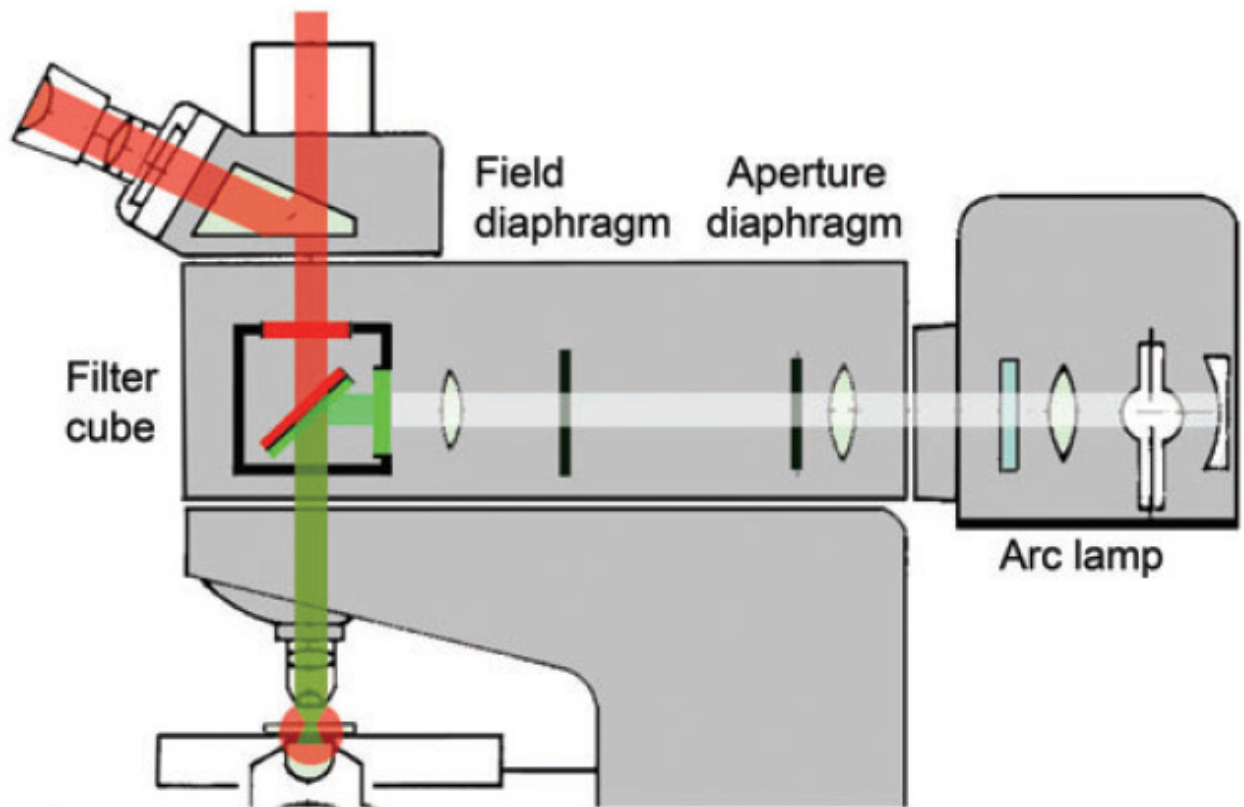


Figure 1.2. A fluorescence microscope diagram. In this case a light source is filtered for green light, which is used to excite the sample and subsequent red fluorescence transmitted for detection.¹¹

A lamp or laser is often used as an excitation source. A lamp (often a mercury or xenon arc lamp) offers white light illumination which often is filtered with a dichroic for the wavelength range of interest. A laser delivers intense, coherent, typically monochromatic radiation which is focused into the microscope. From there, light is reflected by the dichroic filter and focused onto the sample with an objective, which also collects and magnifies the red-shifted fluorescence and transmits it back through the dichroic filter to the detector. The detector is typically a charge-coupled device (CCD) camera which can be used to obtain an image, or a photomultiplier tube (PMT) or avalanche photodiode (APD) which can be used for fast time resolution when dealing with

fluorescence lifetime measurements of high modulation frequency experiments. The resolution for a microscope image is typically about half the wavelength used, but advancements have been made in the field of super-resolution microscopy, allowing one to achieve a ~10-fold improved spatial resolution.¹⁵⁻¹⁹

1.3 Fluorescent labels

Good fluorescent labels exhibit high oscillator strengths and emit brightly (moderate to high fluorescence quantum yield). Other characteristics such as solubility, small size, and membrane permeability factor in as well. Chemical conjugation is also important, as probes must also be able to be attached to species of interest. For fluorophores to be useful in biological applications dyes must also not be harmful in biological environments. Many different types of molecules have been utilized for this purpose ranging from metal nanoclusters, inorganic quantum dots, fluorescent proteins, and organic dyes. These classes of molecules have very different properties ranging from molecular structure, brightness, photostability, and cytotoxicity.

Metal nanoclusters, in particular gold and silver, have been explored as fluorophores.²⁰⁻²⁵ Metal clusters behave similarly to multielectron atoms with discrete transitions that can be tuned through the visible and near infrared with cluster size. Metal nanoclusters must be prepared within a scaffold when in solution, otherwise the clusters will aggregate to form larger, non-emissive nanoparticles. Gold nanoclusters have been prepared with poly(amidoamine) (PAMAM) dendrimers²¹ while silver nanoclusters are encapsulated within DNA scaffolds.²⁴ Metal nanoclusters generally have high luminescence, good photostability, and significant two photon absorption.²⁶

Quantum dots are fluorescent, inorganic semiconductor nanoparticles that have also been utilized in biomedical imaging.²⁷⁻²⁹ Similar to metal nanoclusters, quantum dots are nanoparticle chromophores with size-dependent physical and chemical properties. QDs are often made of semiconductor materials such as CdSe, CdTe, or PbS and can range in size from 1 to 30 nm. At small radii, properties deviate from bulk to molecular behavior due to quantum confinement. As semiconductor materials can be toxic, QDs used in biological imaging often have outer shells such as ZnS to prevent cytotoxic material such as cadmium from harming biological environments. The advantageous properties of QDs include photostability, broad absorption (increasing at short wavelength), narrow fluorescence emission, large extinction coefficients (100,000 to 1,000,000 M⁻¹ cm⁻¹), and significant luminescent quantum yields (0.1-0.9).²⁸ Disadvantages include large, bulky size, potential toxicity in biological systems, aggregation, multivalency, and long-lived fluorescence and multiexponential decay behavior that obscures time-resolved fluorescence measurements.

Fluorescent proteins (FPs) have long been utilized in cellular imaging. FPs most often consist of a visible light absorbing chromophore contained within a β -barrel protein structure.³⁰⁻³¹ They are generally bio-compatible, can be expressed in cells, and are optimized for optical properties such as brightness and photoswitching.³²⁻³⁶ FPs extend through the entire visible wavelength range, from blue through red. FPs have shown to be also capable of photoswitching, possibly due to photoisomerization or excited state intramolecular proton transfer.^{1, 34-38} The green fluorescent protein (GFP) was discovered by Shimomura and colleagues when studying the *Aequorea* jellyfish, noticing that after purification the protein in solution fluoresced green under sunlight illumination.³⁹ Since then, GFP, its chromophore, and structural variants have been studied experimentally and

theoretically, focusing on photochemistry and structural dynamics. GFP is stable up to 65° C with a broad pH range of 5.5 to 12, and its chromophore is easily synthesized, making it an ideal choice to image in biological systems.³⁰ GFP consists of a p-hydroxybenzylidene-imidazolidinone chromophore hydrogen bonded within a beta-barrel structure, has absorption maxima around 398 and 483 nm, and emits fluorescence at 508 nm.⁴⁰ Other GFP variants have been developed, including analogs with improved brightness and improved pH resistance, as well as blue,³⁴ cyan, and yellow fluorescent proteins.⁴¹ Further efforts with proteins from coral reefs gave rise to red fluorescent proteins such as “DsRed” from the *Discosoma* species.⁴²

Organic dyes also show promise in biomedical imaging, due to their small size, high molecular brightness, chemically tunable properties, and ease of synthesis. Organic dyes are also a good choice for biological imaging due to low toxicity, as compared to many inorganic fluorophores. The optical transitions of organic dyes typically originate from electronic transitions which are delocalized over the molecule (π -conjugation), or from intramolecular charge transfer.²⁸ The optical properties of organic dyes can also be fine-tuned using design strategies. For example, a cyanine dye with a longer polymethine chain will typically have a longer wavelength absorption. A small π -conjugated organic molecule such as benzene absorbs in the UV, while a longer cyanine dye such as indocyanine green (a heptamethine cyanine) absorbs in the NIR. NIR fluorescence from approximately 650-900 nm is critically important because in that optical range there is minimal scattering and autofluorescence as well as maximum light penetration of organ tissue, making NIR fluorophores highly desirable in biomedical imaging applications.^{2, 4, 13, 43-47} Figure 1.3 below illustrates fluorescence imaging by wavelength, showing that the

NIR range has the greatest photon penetration and the least absorption, scattering, and autofluorescence. Smaller chromophore organic dyes absorb and emit at lower wavelengths, while larger chromophores fluoresce in the NIR.

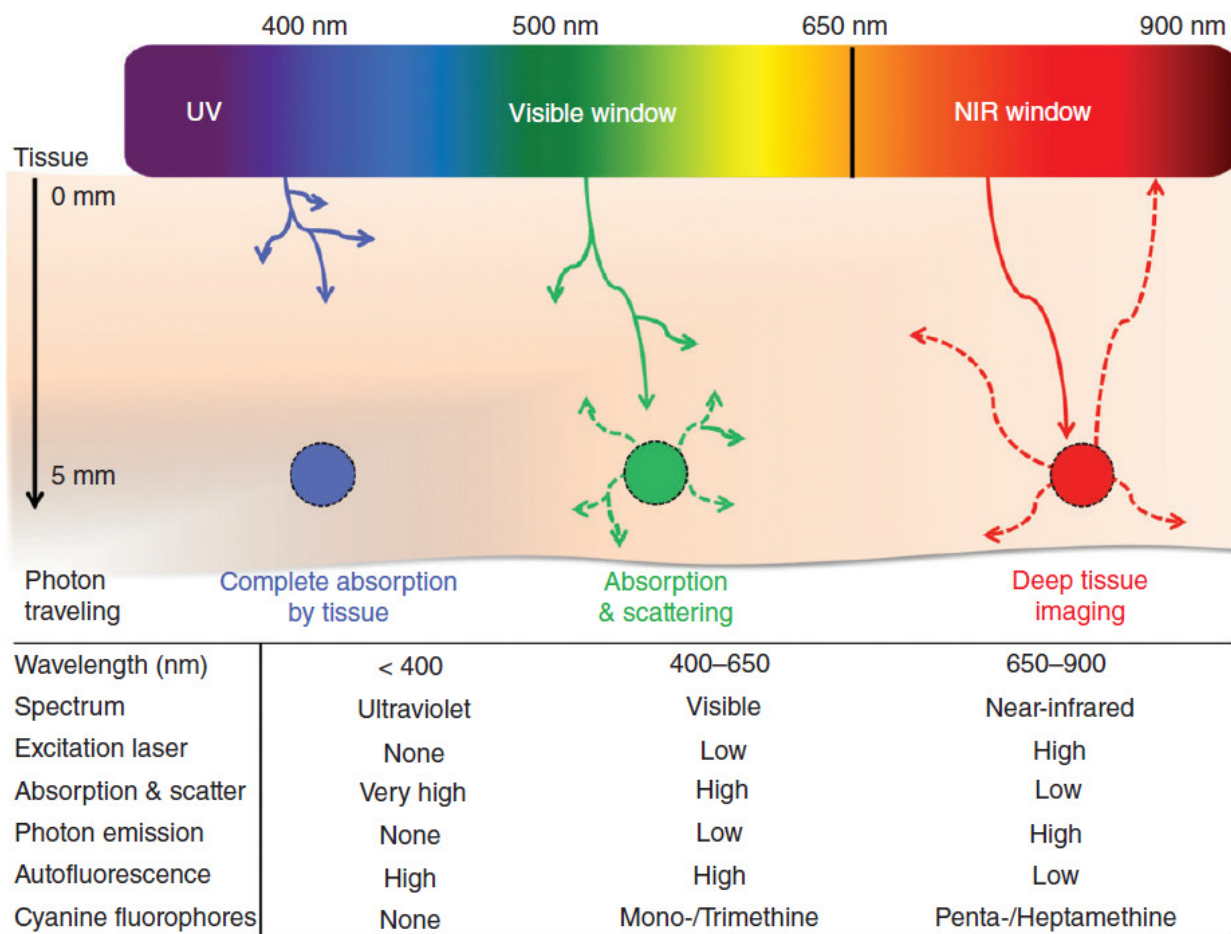


Figure 1.3. An illustration of fluorescence imaging by wavelength from UV to visible to NIR. At short UV wavelengths, light does not travel as deeply due to absorption and scattering, and high autofluorescence occurs, obscuring any fluorophore signal. However at longer wavelengths absorption, scattering, and autofluorescence is diminished.⁴⁷

Generally, four types of dyes used for NIR fluorescence imaging include cyanines, phthalocyanines and porphyrins, Squaraines, and BODIPY dyes.^{13, 28-29, 45} Cyanine dyes are small organic molecules consisting of two aromatic heterocycles linked by a

polymethine bridge. Cyanines utilize electronic π -conjugation and absorb and emit light in the visible and near-infrared range.^{13, 45, 48} Cyanines have high extinction coefficients, moderate fluorescent quantum yields, allow for conjugation in biological systems, and due to the π bonding in the central polymethine bridge, can photoisomerize.^{14, 20, 49-57} Since they are of significant importance in this thesis, cyanines will be discussed in extensive detail in the following section. Phthalocyanines and porphyrins are cyclic aromatic compounds consisting of four bridged pyrrole subunits linked by their nitrogen atoms. The π electrons are delocalized throughout the molecule.⁴⁵ In addition to visible and NIR fluorescence imaging, porphyrins have proven useful in photodynamic therapy (PDT) applications since they can be taken up in tumors and effectively generate singlet oxygen (toxic to cells) when excited by light.⁵⁸⁻⁶⁰ Photochemically, this occurs when the singlet excited state of the fluorophore undergoes intersystem crossing to the triplet state and then the triplet state reacts with ground state (triplet) molecular oxygen to generate singlet oxygen. Singlet oxygen can then generate reactive oxygen species, which cause DNA and cell damage. Squaraine dyes have a unique four-membered central ring and exhibit intense NIR fluorescence. They have been conjugated to bovine serum albumin (BSA) and are soluble in aqueous environments.⁶¹ Lastly, BODIPY (borondipyrromethane) dyes are another class of organic fluorophores which absorb and fluoresce in the visible range (or NIR with appropriate substituents). They offer strong absorption and fluorescence as well as excellent photostability and tunable wavelengths.⁶²

1.4 Cyanine Dyes

As mentioned in the previous section, cyanine dyes are popular in optical applications including lasers, photovoltaics, and solar cells, nonlinear optics, and biological imaging. Cyanines generally consist of two nitrogen containing side groups linked by a π -conjugated polymethine bridge, which typically ranges from three to seven carbon atoms. Although typically drawn with different possible resonance structures (with one terminal nitrogen having a positive charge), cyanines have symmetric electronic states. The π conjugation allows for a one-dimensional metallic state model to describe the electronic properties. The most common side groups include indole, quinoline, benzoxazole, and benzothiazole.^{48, 54, 63} These heterocyclic side groups are needed for stability, while other modifications such as sulfonate groups, for example, are added when solubility in water is required.⁴⁸ An example of this structure is shown below.

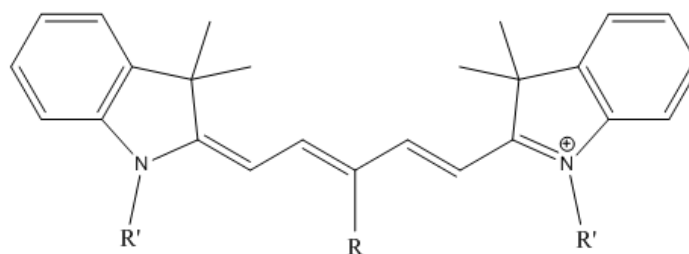


Figure 1.4. Example of pentamethine cyanine with indole side groups.

These molecules are most often thermodynamically stable in an all-trans ground state, but can undergo photoisomerization from an excited state to a metastable nonfluorescent cis-isomer state. Unless water-soluble modifications are made to the aromatic side groups, cyanines undergo aggregation in aqueous and biological environments to form dimers or

more complex H- and J-aggregates due to strong intermolecular forces. This effect can cause spectral and photophysical changes, and has biological application when dimers intercalate in DNA or bind to proteins.⁴⁸

Cyanines have been in use since photographic applications in the mid-nineteenth century, and recently have become popular as the fields of single molecule spectroscopy and super resolution microscopy have emerged.^{15-16, 18, 64-65} Applications involving cyanine dyes include semiconductor materials, optical disks, solar energy, laser materials, photosynthesis, nonlinear optics, as well as biological imaging.^{63, 66-69}

In addition to high molecular absorption coefficients and fluorescence quantum yields, cyanines can transition to other states from electronically singlet excited states. One important transient state is the triplet, which limits the photostability of cyanines in imaging applications. This limitation is due the susceptibility of the triplet state to photobleaching or other photochemical transitions. Researchers can inhibit and exploit this effect, for example by removing oxygen with an oxygen scavenging system.^{65, 70-74} The triplet state has been characterized by transient absorption⁵³ and phosphorescence experiments.⁷⁵ Photoisomerization is another possible transition from a singlet excited state. Since the polymethine bridge contains a chain of carbon atoms connected by alternating single and double bonds (π conjugation), rotations about those bonds are possible. After excitation to a higher electronic state, π conjugation disruption, followed by bond twisting to a metastable photoisomer state can occur.

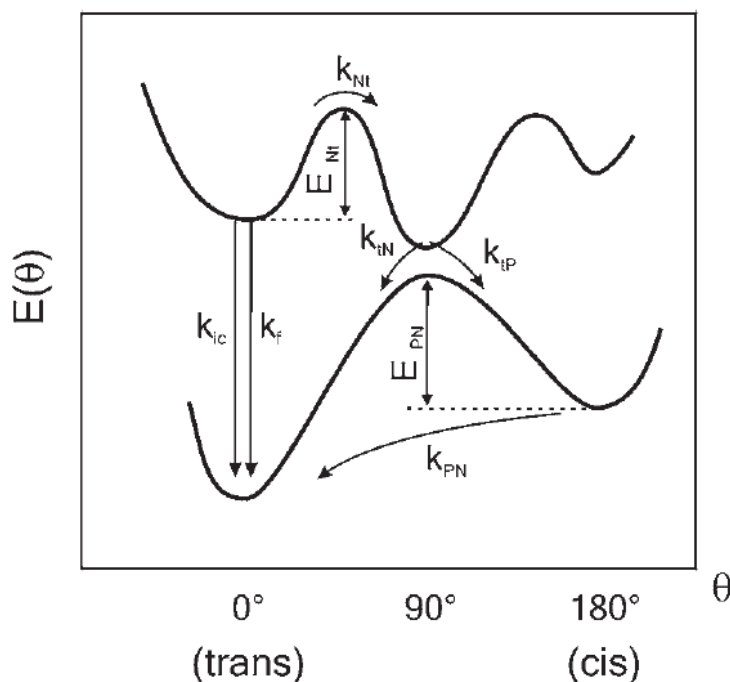


Figure 1.5. Potential energy diagram representing cyanine photoisomerization. The all trans ground state is the lowest energy level and from there excitation to a higher electronic state can occur, followed by either decay to the ground state by internal conversion or fluorescence or photoisomerization to a cis-photoisomer state, where it can reverse photoisomerize to the all trans ground state.⁴⁸

Cyanine photoisomerization has been studied by many experimental and theoretical techniques including FCS, transient absorption, DFT, and INDO (Intermediate Neglect of Differential Overlap).^{48, 53-55, 57, 76-82} It has been shown that Cy3 and Cy7 have short-lived photoisomer states, on the range of several microseconds, while Cy5 and Merocyanine 540 have longer lived photoisomer states, on the order of 100 μ s.^{54, 83-86} As triplet state yields and lifetimes are affected by the presence of heavy atoms or triplet quenchers, photoisomer photophysics can be affected by changing solution viscosity or environment (solution vs immobilized). One strategy to study this phenomenon in cyanines is to relate kinetics to energetics. Ground state energies can be determined for all possible isomers and then compared to experimentally determined energies and timescales.

1.5 Fluorescent protein chromophore

The chromophore of GFP itself, p-hydroxybenzylidene-imidazolidinone (p-HBDI), has been studied for other potential applications, including protein binding,³³ fluorescence imaging,⁸⁷ light-emitting diodes,⁸⁸ and the study of excited state intramolecular proton transfer (ESIPT).^{38, 89} The p-HBDI structure is shown below.

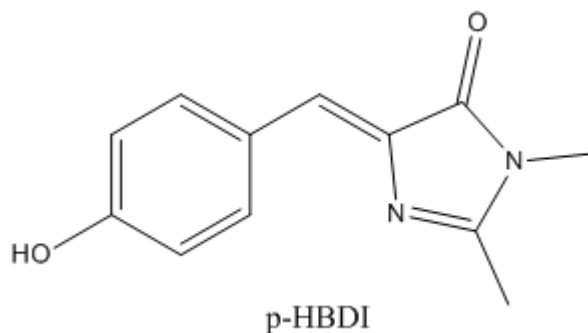


Figure 1.6. Structure of GFP chromophore.

The interesting properties are due in part to the chromophore structure and how it is affected by its structure and environment. For example, when the chromophore is inside the beta barrel structure of GFP, non-radiative relaxation is suppressed due to inhibition of torsional motion.⁸⁸ Conversely, in solution nonradiative pathways are more kinetically favored, and as a result the quantum yield is much lower. One way to increase the quantum yield of this structure is to lock the chromophore, as has been done by Baranov et al.⁸⁹ This is detailed in the figure below. The original p-HOBDI structure has a quantum yield of $\sim 10^{-4}$ while the p-HOBDI-BF₂ structure improves the quantum yield to 0.73.

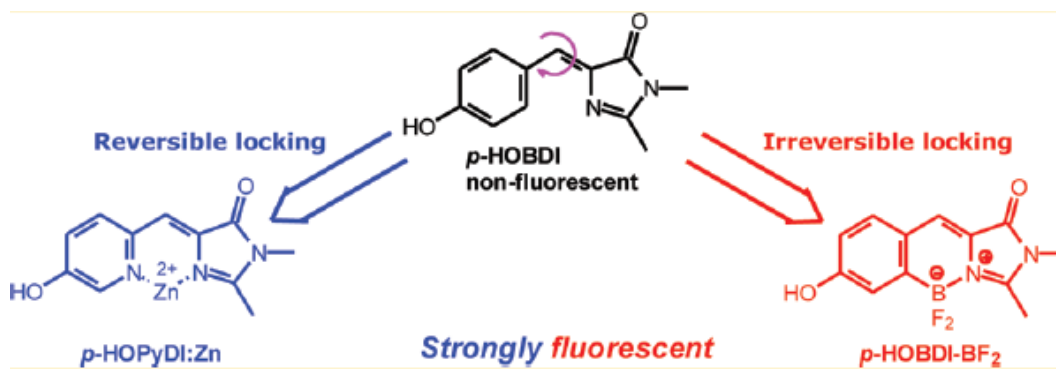


Figure 1.7. Locked GFP chromophore variants.⁸⁹

Another way to partially lock this structure is to move the hydroxy group to the ortho position on the aryl ring. By doing this, a hydrogen bond can form between the oxygen, hydrogen, and nitrogen which stabilizes the structure and improves quantum yield.³⁷ This ortho-hydroxy structure allows the study of a proton transfer cycle of the protein chromophore. After absorption in the UV (~385 nm), the chromophore undergoes a rapid ESIPT process (<25 fs), then emits 605 nm fluorescence or undergoes internal conversion before returning to the ground state (deprotonation and recombination can occur as well).³⁸

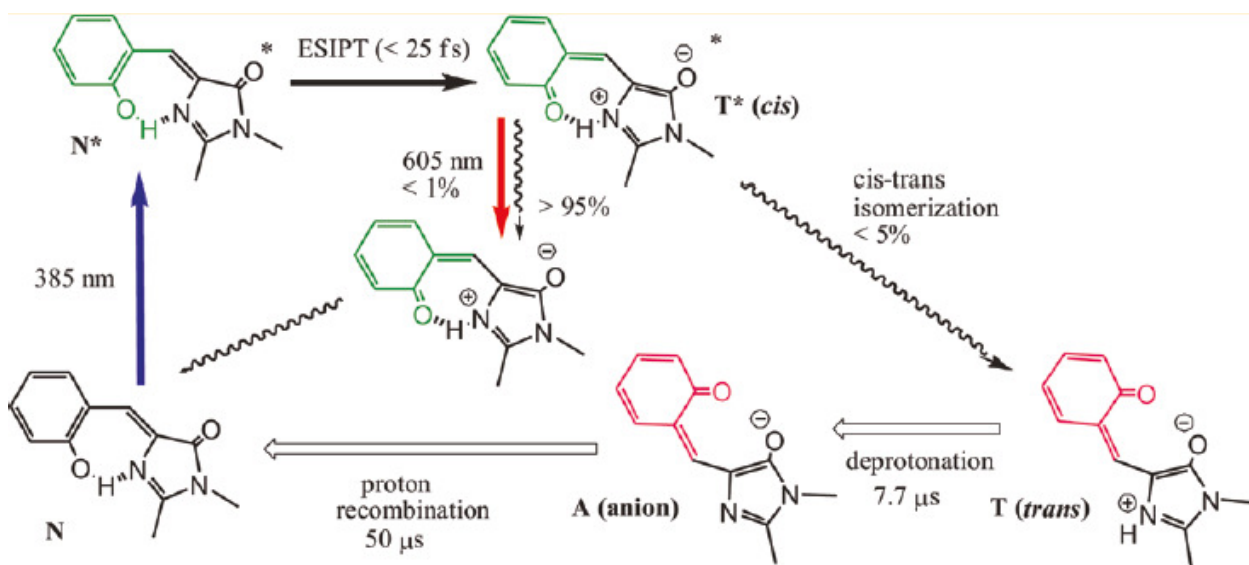


Figure 1.8. Schematic of photophysical processes of ortho-hydroxy fluorescent protein chromophore.³⁸

Other structural variations were shown to affect absorption wavelength, molar absorptivity, pKa, and fluorescence lifetime.⁸⁷ In addition, external influences affect chromophore behavior. GFP chromophore variants can bind to different proteins such as human serum albumin (HSA) and beta-lactoglobulin, increasing the fluorescence quantum yield in a “fluorescence turn on” effect, and different analogs can be used as RNA and pH sensors.⁹⁰ Bile salts, such as sodium cholate, also have this effect which could be useful for studying trafficking of fat-soluble transport in biological systems.⁹¹

1.6 Optical Modulation

By varying light intensity, or by switching lasers on and off, one can utilize transient dark state kinetics for improving imaging methodology, particularly increasing signal to noise to diminish background. The most common transient state is the triplet, populated when molecules undergo intersystem crossing from the singlet to triplet manifold from the excited singlet state. The molecule will stay in the triplet state for a short

(typically μs) time and then return to the ground state singlet state by reverse intersystem crossing, phosphorescence, or other methods of relaxation. If the triplet state is sufficiently populated and long-lived, detected fluorescence will decrease due to increased population in the nonfluorescent triplet state. This effect can be used with modulation techniques, one example being single laser modulation.⁹²⁻⁹³ Due to the effects of triplet states in generating singlet oxygen, this is especially useful in PDT applications in biological systems.⁹⁴⁻⁹⁵ Details of this photophysical process and experimental implementation are shown in Figure 1.9.

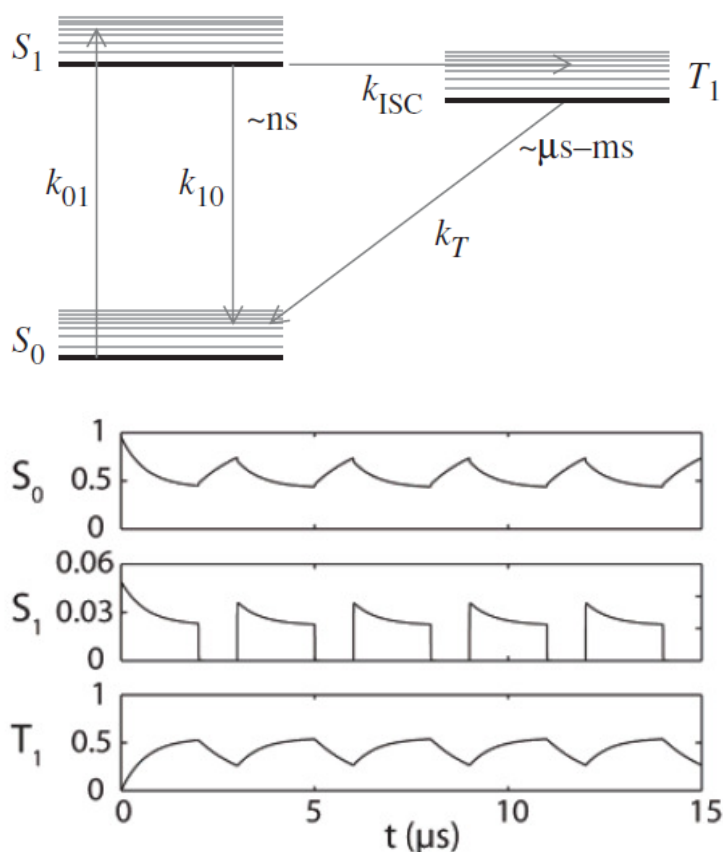


Figure 1.9. Top: Jablonski diagram describing a typical three electronic state system. Bottom: Schematic fractional populations of S_0 , S_1 , and T_1 as a function of time.⁹²

At room temperature most molecules populate S_0 , the ground singlet state, and upon laser excitation ground state molecules transition up to the excited singlet state, S_1 . From there they can relax radiatively (fluorescence) or non-radiatively (internal conversion) back to S_0 . This $S_1 \rightarrow S_0$ transition occurs on the nanosecond timescale. From S_1 , molecules can also intersystem cross to the lowest triplet state, T_1 . Depending on the molecular triplet lifetime and environment, molecules can stay in T_1 for the order of microseconds to milliseconds after which they will decay to S_0 . While in T_1 molecules cannot fluoresce, and this will manifest as a decrease in fluorescence. The kinetics of this process are governed equation 1.1 below.

$$\frac{d}{dt} \begin{pmatrix} S_0(\vec{r},t) \\ S_1(\vec{r},t) \\ T_1(\vec{r},t) \end{pmatrix} = \begin{bmatrix} -k_{01}(\vec{r},t) & k_{10} & k_T \\ k_{01}(\vec{r},t) & -(k_{ISC} + k_{10}) & 0 \\ 0 & k_{ISC} & -k_T \end{bmatrix} \begin{pmatrix} S_0(\vec{r},t) \\ S_1(\vec{r},t) \\ T_1(\vec{r},t) \end{pmatrix} \quad \text{Equation 1.1}$$

This equation can be solved numerically,⁵⁷ which will be explained in Appendix E. The behavior of the S_0 , S_1 , and T_1 populations is shown graphically in Figure 1.9 for square wave amplitude modulated single laser excitation. For the duration of the excitation pulse, a fluorescence decay is observed due to dark state population build up. From Figure 1.9, the S_1 population is used as a surrogate for the fluorescence. After an off period the sample is excited again and fluorescence again begins at a higher level before decaying. The reason for the initial increase is that the molecules in the triplet state have relaxed during the laser off period. When the sample is excited, the population of the S_0 state starts at unity and then decreases as the T_1 population builds up. When the laser is off, the dark state decays

so the S_0 population begins to recover while the T_1 population decreases. This model can be generalized to other systems with dark states, such as the photoisomerized states in cyanine dyes.

Similar to transient state imaging, Synchronously Amplified Fluorescence Image Recovery (SAFIRE) also utilizes triplet (or other dark) states in molecules but uses a constant intensity primary laser with a modulated secondary laser. In a study of the xanthene dyes Rose Bengal, Eosin Y, and Erythrosin B,⁹⁶ the fluorescence inducing primary laser was constant in intensity while the secondary laser, which optically depopulates the triplet dark state by exciting a $T_1 \rightarrow T_n$ transition, was modulated leading to modulated fluorescence. These fluorophores are all similar in structure to fluorescein except that they have the heavy atoms present on the π conjugated rings, which increases the yield of the triplet states (up to 98% in the case of Rose Bengal).

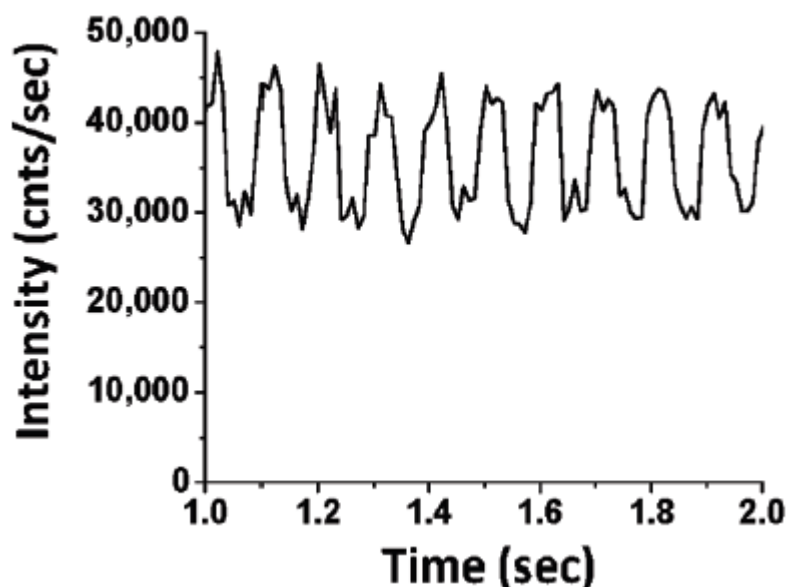


Figure 1.10. Fluorescence time trace of a rose bengal solution modulated at 10 Hz.⁹⁶

In this modulation scheme, the secondary laser is typically longer in wavelength and lower in energy than is the primary laser. Lower energy secondary co-illumination allows for minimal secondary interference since longer wavelength light produces no additional background fluorescence in the higher energy fluorescence window. Shorter wavelength (higher energy) modulated secondary laser schemes are also possible in optical switching applications, but can potentially induce additional autofluorescence. In either case, the criteria for successful modulation are a naturally decaying dark state, dark state absorption sufficiently shifted away from the primary absorption and fluorescence, and large forward and reverse action cross sections which enable efficient switching between bright and dark states. The maximum relative enhancement factor is determined by $\tau_{\text{off}}^0/\tau_{\text{on}}$, or the dark state lifetime divided by the bright state lifetime, a factor that can potentially increase the fluorescence many times.^{20, 96}

Many of the fluorophores discussed earlier in this chapter can be optically modulated. Silver nanoclusters encapsulated in single-stranded DNA have been shown to exhibit visible to NIR fluorescence, which is modulatable by longer wavelength secondary co-illumination. The ssDNA sequence determines the photophysical properties such as emission wavelength, lifetime, quantum yield, and absorbance. Transient absorption and fluorescence correlation spectroscopy studies, along with other Ag nanocluster research, lead researchers to believe that a charge-separated dark state is the modulatable state.²⁰ Fluorescence Resonance Energy Transfer (FRET) pairs can also be used by using a secondary laser to saturate the acceptor, allowing one to manipulate and modulate higher energy donor fluorescence. Fluorescein and tetramethylrhodamine (TMR), as well as Cy3 and Cy5 are FRET pairs that have been utilized for this effect.⁹⁷ Organic fluorophores have

also exhibited modulation, generally through triplet or photoisomer effects. Fluorescein and rhodamine derivatives with heavy atom modifications, such as Rose Bengal, have high triplet yields which allow for significant dark state population. When the dark state has a red-shifted transient absorption, fluorescence can be modulated. Another type of modulatable organic fluorophore is the cyanine dye. As mentioned above, π -conjugated carbon chains lead to photoisomerization possibilities and if the state is sufficiently well-populated and long-lived it can offer >50% modulation depth in the case of pentamethine derivatives.⁹⁸ Cy5 in particular has been studied thoroughly and demonstrated to be capable of long wavelength modulation due to its red-shifted photoisomer transient absorption.¹⁴ By scanning secondary modulation frequency and fitting to a frequency domain lifetime equation (method described in detail in chapter 3), the characteristic modulation frequency was measured to be ~10-20 kHz, dependent on primary excitation intensity. By using SAFIRE imaging with Cy5 one can discriminate signal from background fluorescence. Cy5 fluorescence modulation was shown to be recoverable from a Texas Red background, since Texas Red exhibits fluorescence from 594 nm excitation but does not have a dark state that can be excited at 710 nm.

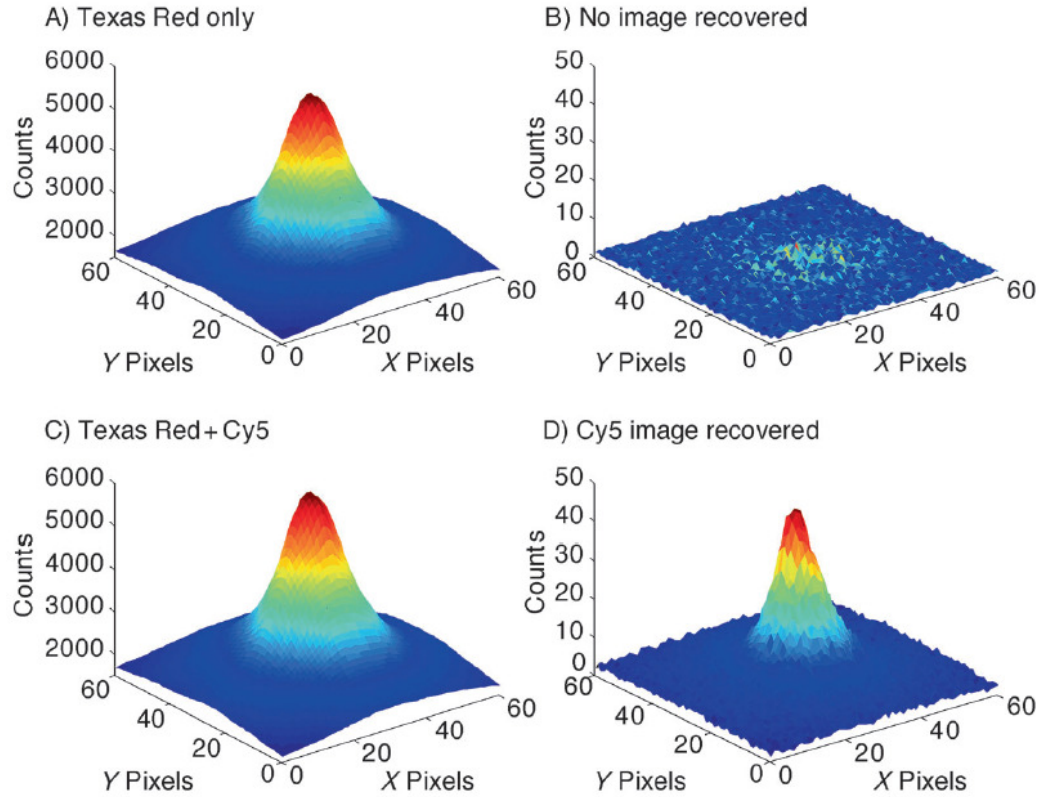


Figure 1.11. Demonstration of Cy5 modulation. When Cy5, which is capable of secondary modulation at 710 nm, is paired with Texas Red (not modulatable), only the Cy5 signal is recovered upon demodulation.¹⁴

Cy5 modulation offers the potential to be used in medical imaging applications where fluorescence modulation allows for higher signal to noise and greater imaging depth. One example is tissue mimicking phantoms.⁵⁶ With conventional fluorescence imaging, signal can only be recovered from 1-2 mm imaging depths, mostly limited by scattering and absorption of signal. Tissue mimicking phantoms were constructed from polystyrene beads, talc-France perfume powder, and Texas red fluorophores embedded in sodium alginate, which was cross-linked in calcium chloride aqueous solution. These tissue mimicking phantoms had optical properties closely matching human skin tissue. Experimentally, low intensity of light is desirable to prevent tissue burns and low

fluorophore concentration is necessary to avoid toxicity. In this work, using ~140 nM Cy5 and primary and secondary lasers at 0.29 kW/cm² and 5.9 kW/cm², respectively, signal was recovered up to 6 mm, with a possibility of eventually achieving 1 cm.

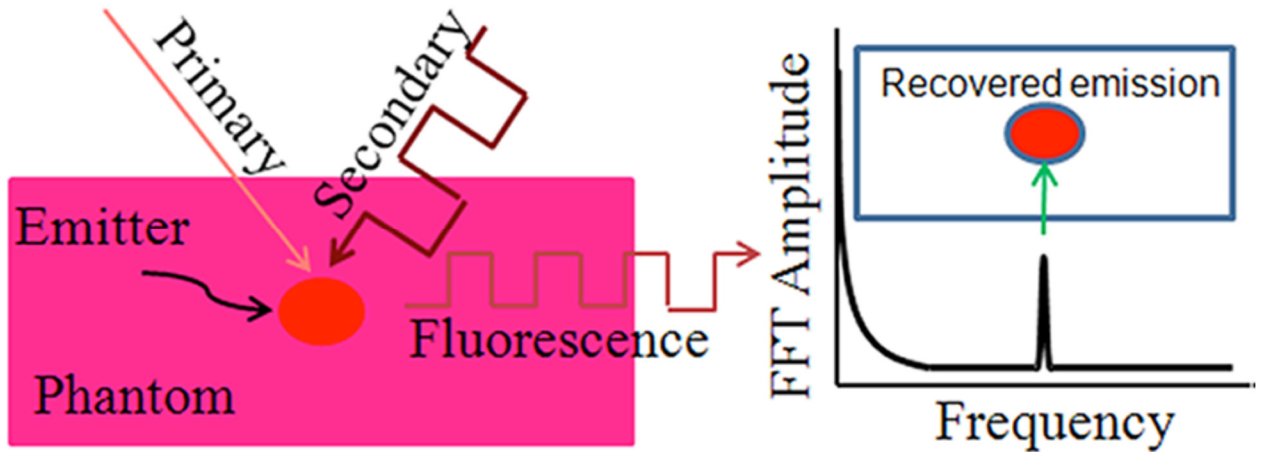


Figure 1.12. After embedding Cy5 into a tissue mimicking phantom, secondary modulation allows for modulated fluorescence recovery, which allows for stronger signal and greater imaging depth.

Fluorescent proteins have also been shown to exhibit fluorescence modulation across the full range of the visible spectrum.^{34,36} Fluorescent proteins offer excellent biological compatibility, making them ideal for cellular imaging. The fluorescent proteins studied so far typically utilize a photoisomerized dark state, though an excited-state proton transfer could also be involved. Also, the fluorescent protein chromophore environment influences the photophysical properties which can alter modulation wavelength and increase fluorescence enhancement. By expressing these fluorescent proteins capable of long wavelength modulation in cells, one obtains a greater signal to noise image after demodulation. This is depicted in Figure 1.13.

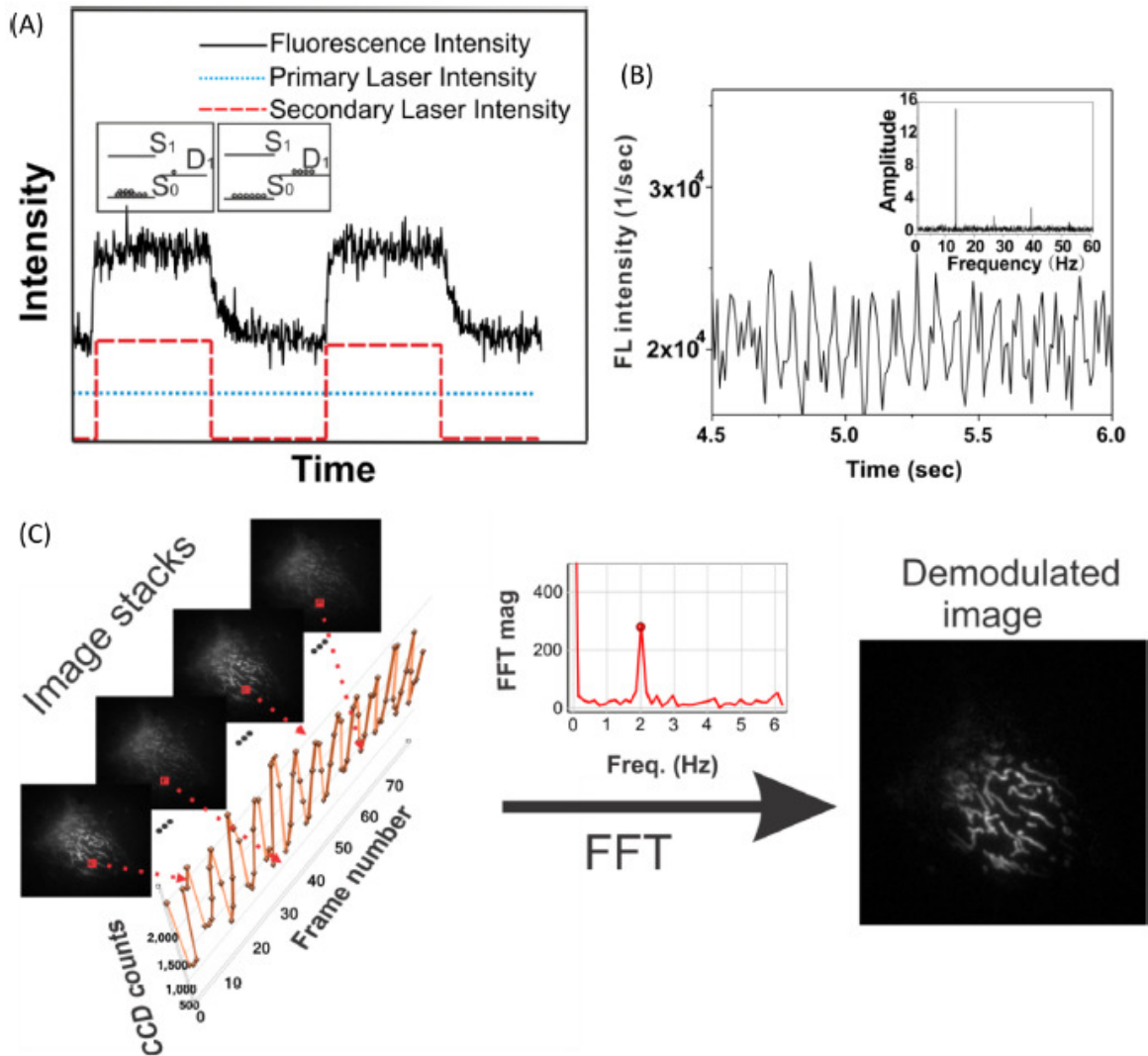


Figure 1.13. (A) Fluorescence modulation of blue fluorescent protein (modBFP/H148K) where the primary laser is held constant while the secondary laser is modulated by an external square waveform. The dark state population is at a minimum at the fluorescence maximum and at a maximum at the fluorescence minimum. (B) Fluorescence time trace of modBFP/H148K modulated at 13 Hz with the inset showing the fast Fourier Transform with corresponding peaks at the appropriate frequencies. (C) Analysis of fluorescence modulation with a charge-coupled device (CCD) camera detector. Upon demodulation, the image becomes more clear as there is less interference by background fluorescence.²⁰

1.7 Organization of Thesis

The research in this thesis builds on seminal work in the Dickson Lab studying optical modulation of fluorescence, based on transitions into and out of nonfluorescent (dark) photophysical states. The dark states used for this technique include triplet, photoisomer, and charge-transfer states, among other possibilities.²⁰ Chapter 2 explains all of the experimental methods used in this work, including modulation techniques and time-resolved fluorescence microscopy, as well as computational density functional theory methods. In chapter 3, newly synthesized Cy5 analogues were tested to explore the question of how molecular structural variants affect fluorescence enhancement and modulation timescales by performing fluorescence modulation experiments. To probe more deeply into the mechanistic details to study isomer energetics and back-isomerization kinetics, in chapter 4 experimental and theoretical methods were utilized to study cyanine photoisomerization in depth, focusing on the fluorescence modulation application. Chapter 5 explores a modulation scheme, optically activated delayed fluorescence. It is possible that with the appropriate dark state, the secondary laser can induce delayed, background free fluorescence. In OADF a triplet dark state is used to generate delayed fluorescence due to reverse intersystem crossing back to the fluorescent excited state. Finally, in chapter 6 a fluorescent protein-binding chromophore is studied to characterize fluorescence modulation in relation to binding as well as photoisomerization. Different timescales and a different process, along with biological relevance, make this system intriguing for future study.

CHAPTER 2

EXPERIMENTAL AND THEORETICAL METHODOLOGY

2.1 Sample preparation

Cyanine dye fluorescence experiments were conducted in solution, while HSA-bound chromophores were studied in immobilized environments. Cyanine dyes were either purchased commercially (Lumiprobe and GE Biosciences) or synthesized by our collaborators in the Maged Henary lab at Georgia State University. The details are explained in the supporting information in our publication,⁹⁸ but the general scheme utilized by the Henary lab is depicted in the figure below.

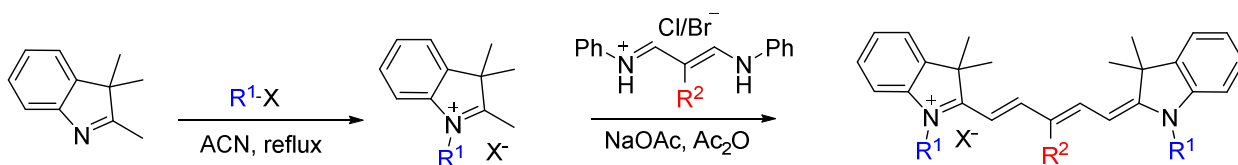


Figure 2.1. The synthesis of cyanine compounds used.⁹⁸

Cyanines consisting of a polymethine bridge with indole side groups are not water soluble and need to be dissolved in a less polar solvent such as DMSO to prevent aggregation. However, cyanine dyes can become soluble in water when functional groups such as sulfonate and carboxylic acid are added. For absorbance and fluorescence measurements, micromolar concentrations were used, while for time correlated single photon counting fluorescence measurements nanomolar concentrations were used.

The HSA-binding chromophores were provided by the Tolbert lab, as described in their publication.³³ Samples were prepared by first dissolving the chromophore in ethanol, then adding to a stock solution of HSA (Sigma-Aldrich) in PBS buffer. Since long timescales were observed for photophysical modulation, immobilization in a low gelling temperature agarose gel (Sigma-Aldrich) was needed to limit diffusion out of the focal volume. Thus the HSA-chromophore complex was added to a 1% w/v agarose solution.

2.2 Bulk characterization

To characterize the bulk properties of the fluorophores studied, such as molar absorptivity or extinction coefficient (ϵ), concentration, and fluorescence quantum yield (ϕ), the experimental techniques used involved Ultraviolet-visible (UV-vis) spectroscopy and fluorimetry to determine molecular absorption (extinction coefficient) and fluorescence emission (quantum yield). To determine molar absorptivity and concentration, measurements were conducted with a Shimadzu UV-2401 PC spectrophotometer. Samples were contained in a glass or quartz cuvette. Beer's law was utilized to characterize absorption, stating that $A = \epsilon bc$, where A is the absorbance measured, ϵ is the extinction coefficient, b is the cell path length (typically 1 cm), and c is the concentration (units of M or moles/liter). Absorbance is related to the amount of light that passes through the sample $A = -\log_{10}(T)$ where T (transmittance) is the fraction of light passing through the sample. The extinction coefficient is a fixed molecular parameter that relates to the transition probability of the molecule and typically has units of $M^{-1} \text{ cm}^{-1}$. In this sort of experiment, one measures absorbance and knows the cell path length, leaving ϵ and c as the two possible unknown variables. In this work, ϵ is either known from

published work, allowing one to solve for c , or if ϵ is unknown then concentration can be determined by dissolving a known amount of sample into solution (typically molecular weight is known) or by doing a Fluorescence Correlation Spectroscopy (FCS) measurement which determines the average number of molecules in the focal volume.

To measure fluorescence properties, in particular fluorescence quantum yield, fluorimetry is the desirable measurement. Fluorescence measurements were conducted with a Photon Technology International (PTI) Quanta Master 40, equipped with a xenon arc lamp as excitation source and a photomultiplier tube as detector. The most basic fluorimetry experiments are emission scans, which are performed by selecting an excitation wavelength and emission wavelength range and then exciting the sample and detecting fluorescence emission. Other setups are possible, such as excitation scans where the emission wavelength is constant and the excitation wavelength range is scanned. Fluorimetry experiments are useful to determine excitation and emission wavelength maxima, and can also be used to determine molecular properties such as fluorescence quantum yield, the fraction of photons emitted compared to photons absorbed. To calculate this, one measures the absorbance and fluorescence emission of a known reference and unknown sample and uses the formula¹²

$$Q = Q_R \frac{I}{I_R} \frac{OD_R}{OD} \frac{n^2}{n_R^2}$$

Equation 2.1

Where Q is the fluorescence quantum yield of the unknown, I is the integrated fluorescence emission, OD is the absorbance, and n is the solvent index of refraction. R denotes a property of the reference, compared to the unknown.

2.3 Fluorescence Microscopy

All fluorescence based microscopy experiments were performed using Olympus IX-70 or IX-71 inverted fluorescence microscopes in which a certain excitation wavelength illuminates the sample while only the fluorescence wavelength is collected and observed by the detector. Excitation sources were most often lasers, although mercury lamps (Olympus U-LH100G, 100 W) were occasionally used. Lasers are particularly useful because they are coherent radiation that can be focused to a tight spot with the capability of power attenuation by neutral density (ND) filters. This allows for manipulation of excitation intensity, which is important for controlling molecular photophysics such as fluorescence emission and dark state transition frequency. With either lamp or laser excitation, dichroic filters were used to select a specific wavelength range and filter out any undesirable excitation wavelengths. Many different types of lasers were used including Argon ion, He-Ne, diode, and Ti:sapphire lasers. These wavelengths spanned the visible and NIR and were operated in continuous wave (CW) or pulsed modes. In CW mode the intensity is constant while in pulsed mode ns to fs width pulses are used at repetition rates in the kHz to MHz range. Laser pulses are useful in lifetime measurements, where a pulse excites a sample and fluorescence is collected afterward allowing a fluorescence decay to be constructed and a fluorescence lifetime can be measured. Pulsed mode can also be used when constant excitation of the fluorophore is undesirable, for instance if the laser also depletes the dark state, or if a higher peak intensity is needed. In two-photon absorption, for example, a very high intensity is needed to maximize transition probability. Repetition rate can also be controlled, and when very high (MHz) allows for a pseudo-CW effect (relative to molecular dark state photophysics). When the rep rate is considerably lower, a large

temporal spacing between pulses occurs so that the molecule is excited and then can relax before subsequent excitation. A low rep rate is also useful in photoacoustic applications since that system needs to be repeatedly excited and relaxed to generate photoacoustic waves.⁹⁹⁻¹⁰¹ With pulsed diodes the rep rate is controlled by the laser driver (internally or externally), but when using the Ti:Sapphire or optical parametric oscillator (OPO) the rep rate is determined by cavity length, so a “pulse-picking” setup is used involving an EOM and synchronous countdown system to modulate down to a certain rep rate.

Table 2.1. Summary of lasers and their characteristics used in this research.

Laser & type	Wavelength (nm)
Diode (Thorlabs, fiber-coupled CW)	405, 450, 515, 637, 705, 800, 830
Diode (Picoquant, pulsed ps)	372, 467, 647
Argon ion (Coherent, CW)	457, 476, 488, 496, 515
He-Ne (Melles-Griot, JDS Uniphase, CW)	543, 594, 633
Solid-state Sapphire (Coherent, CW)	561
Ti:Sapphire (Coherent Mira 900, CW or pulsed ps or fs, 80 MHz)	Tunable 700-1000
Optical Parametric Oscillator (APE Berlin, pumped by mode-locked Ti:Sapphire in ps or fs, frequency doubled)	~515-690

For two-laser experiments, primary and secondary excitation beams were spatially overlapped in x, y, and z dimensions in the microscope after combining on a dichroic mirror. Collimation of lasers was utilized with magnifying lens pairs as needed. Appropriate band-pass filters blocked the primary and secondary excitation wavelengths to only let the desired fluorescence signals reach the detector. When necessary to

distinguish timescales comparable to those of diffusion ($\sim\mu\text{s}$), a defocusing lens was used to increase the laser spot size, shifting diffusion-based fluctuations to much longer timescales ($\sim\text{ms}$). Excitation light was directed toward the sample using a dichroic having a nearly complete reflectance of the excitation light (at both primary and secondary excitation) while being transparent to fluorescence emission. A water immersion objective (Olympus 60x, NA 1.20) was used to focus light onto the sample, contained in solution and prepared on 22.5 mm x 22.5 mm glass coverslips (Fisher) with thicknesses of .15 mm. All solution data were acquired by focusing $\sim 30\ \mu\text{m}$ into solution. When testing immobilized samples an oil objective (Olympus 60x, NA 1.45) was used due to the higher numerical aperture which allowed for a wider field of view. Emission from the sample was collected with the same objective and directed to either a CCD camera (Andor iXon) attached to a trinocular head or to the side port of the microscope. The CCD camera is used for beam alignment since it is sensitive and allows for visualization of the beam in the x, y, and z dimensions. This is also safer than using the eyepiece, which in the case of high intensity light could harm an observer's eyes.

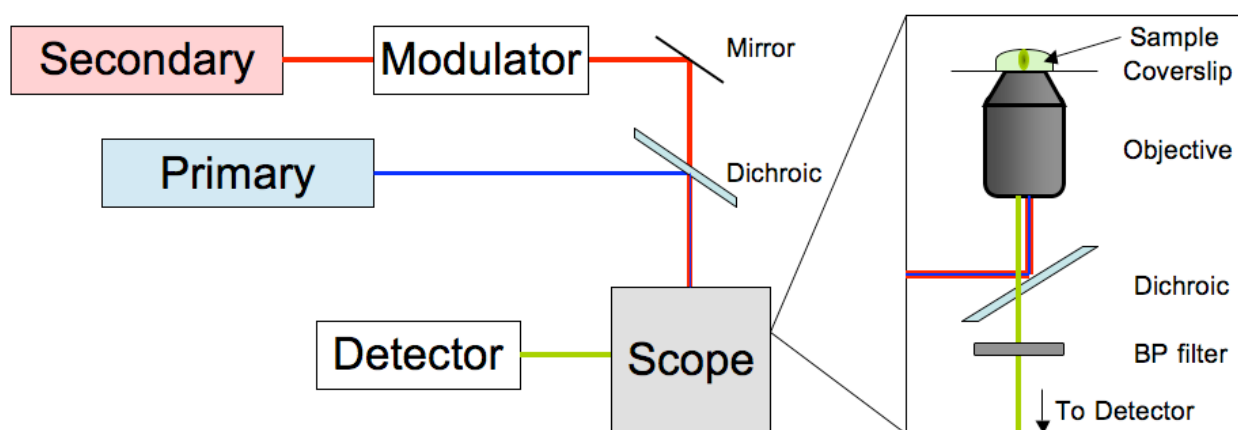


Figure 2.2. Fluorescence microscope setup with dual laser excitation. In this diagram a blue primary laser and red secondary laser are aligned and used to excite a sample which

fluoresces green. A dichroic filter is used to reflect blue and red light while allowing green to pass through. A bandpass filter is used to further ensure that only fluorescence transmits through to the detector.

Most often, the CCD is mounted on a trinocular head on the top of the microscope so that the side port can be used with an APD or PMT for single photon counting detection. In this setup, fluorescence signal sent to the side port was collected in a confocal arrangement with a 100 μm multimode fiber serving as the pinhole and directing the emission to a photon-counting avalanche photodiode (APD, Perkin-Elmer). Intensity trajectories were recorded using a Becker-Hickl SPC-630 or Time Harp single photon counting board to time-stamp individual photon arrival times.

2.4 Time Correlated Single Photon Counting

Time Correlated Single Photon Counting (TCSPC) is a technique used to record the timing of individual photons with high precision and picosecond resolution, making it useful in many fluorescence applications including time-resolved spectroscopy and single molecule methods.¹⁰²⁻¹⁰⁴ This is typically accomplished with a detector capable of highly sensitive (low light level) detection and picosecond time response, typically an avalanche photodiode (APD) or photomultiplier tube (PMT). Upon detection of a photon, an electronic signal is generated and sent to a photon counting module (Becker-Hickl SP630 or Time Harp counting board) which uses an external sync source as a mechanism to time stamp individual photon arrival. The start signal is initiated by the detection of the incident photon and the stop signal is caused by the next sync pulse. From there, a histogram can be built up of the timing between the sync and the photon with resolution on a picosecond time scale, allowing for a fluorescence decay measurement to determine fluorescence

lifetime. This is referred to as the microtime and is shown schematically in the figure below.

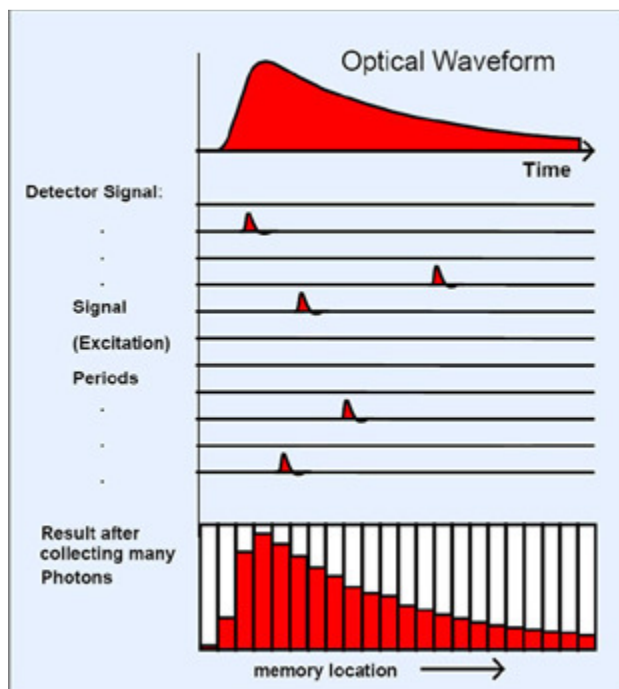


Figure 2.3. Schematic of TCSPC.¹⁰⁵

A macrotime also exists in which the photon timing from the beginning to the end of the experimental data set is recorded giving rise to a time trace where each photon is stamped with the total elapsed experimental time. This can be useful when looking at bulk properties or when performing slower modulation frequency experiments. When utilizing the instrument response function (IRF) for deconvolution of the detected fluorescence signal, one can detect a signal down to the APD or PMT resolution limit (~300 ps).

Additionally, TCSPC can be performed using an Edinburgh Instruments Lifespec-ps system equipped with a Hamamatsu multi-channel photomultiplier tube detector, allowing resolution down to ~25 ps. In this setup a sample is contained within a cuvette,

and a monochromator is used to filter out all wavelengths except for the fluorescence. Picoquant laser diodes (repetition rate ~2-40 MHz) were used as excitation sources, driven by a Sepia II laser driver system.

2.5 Fluorescence Correlation Spectroscopy

Fluorescence Correlation Spectroscopy (FCS) is a microscopy technique which utilizes fluorescence fluctuations to determine molecular properties and dynamics such as diffusion into and out of the focal volume, average concentration, chemical reaction rates, and singlet-triplet dynamics.^{12, 106-110} The experimental setup is straightforward: a laser excitation source is used with a fluorescent microscope, a low concentration (nM to pM) fluorescent sample is used so that only a few molecules are in the focal volume at a time (although up to μM samples have been demonstrated as well¹¹¹), and fluorescence is collected by an APD, PMT, or CCD and read using a counting board installed in a computer. From there a fluorescence time trace is recorded and an autocorrelation is performed to determine fluorescence fluctuations in the signal. Fluorescence fluctuations can be due to diffusion, triplet or other dark state processes, chemical reactions, or other transient processes. In this research, diffusion and dark state processes were studied so the resulting autocorrelation was fitted to the formula below.¹²

$$G(\tau) = G(0) \frac{(1 - F + Fe^{-\tau/\tau_T})}{(1 - F)} \frac{1}{(1 + (\tau/\tau_{D,i})) (1 + a^{-2}(\tau/\tau_{D,i}))^{1/2}} \quad \text{Equation 2.2}$$

In this equation τ represents the delay time, $G(0)$ is the correlation amplitude at time zero, F is the dark state fraction, τ_T represents the dark state (often triplet) timescale, τ_D is the diffusion time, and a is the ratio of axial to radial e^{-2} radius of the measurement volume.

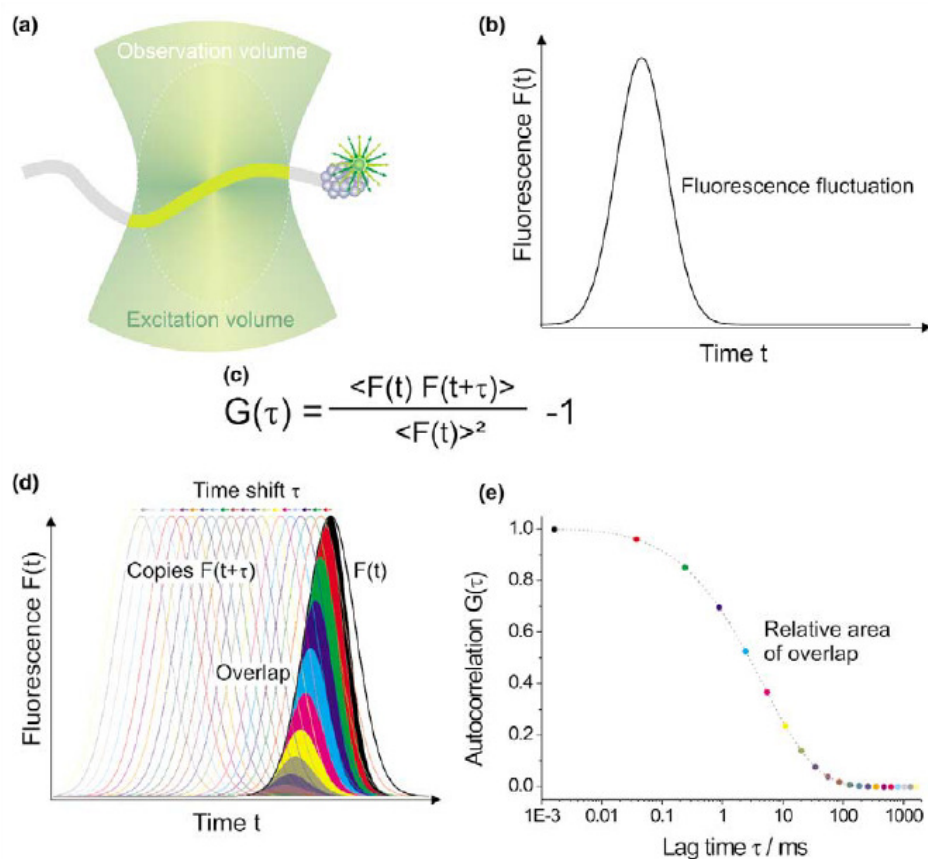


Figure 2.4. Illustration of FCS process. (a) A fluorescent molecule diffusing through the focal volume, (b) an increase in fluorescence is observed as the molecule passes through the focal volume, (c) the FCS autocorrelation function, (d) schematic of the fluorescence as the time lag (τ) in the autocorrelation is applied, (e) the overlap after time lag τ between the original fluorescence fluctuation and the time lagged fluctuation. The overlap decreases as the time lag increases.¹⁰⁶

In this work, FCS is used to observe single molecule behavior in solution, looking in particular at diffusion times and dark state times. It is useful to determine those two different fluctuation timescales and if they affect each other. For example, in the case of cyanines the dark state fluctuation time is close to the diffusion time and FCS is able to show this. FCS also calculates dark state fraction, which is useful in determining how

primary laser intensity affects the dark state population and how the presence of a secondary laser depletes the dark state.

2.6 Optical Modulation

In this work many modulation techniques were used, typically involving electro-optic modulators (EOMs) with one or two lasers. The EOMs used in this research were typically Conoptics model 350 series with a Potassium Dideuterium Phosphate (KD*P) crystal as the electro-optic media (wavelength 240 to 1100 nm). These types of EOMs are intensity modulators with a polarizer aligned to the crystal axis. To use an EOM, light is first passed through an alignment tube which is adjusted in position (horizontal, vertical, diagonal) until >90% of laser power is transmitted through. Then the EOM is placed in the holder and connected to a driver which provides a voltage to control the electro-optic switching. A function generator provides the voltage waveform that drives the EOM driver. Square and sine waves are commonly used, and in the case of square waves it is possible to modify the pulse length and the time between pulses. The EOMs used in this work can typically modulate up to 30 MHz. As mentioned earlier in the fluorescence microscopy section, when paired with a synchronous countdown the EOM can also act as a pulse selection system to control the rep rate of a pulsed laser, for example a Ti:Sapphire laser. The EOM and driver are shown in the figure below.



Figure 2.5. EOM devices: Conoptics model 350 EOM driven by model 25D driver.¹¹²

The EOM modulated the intensity of the secondary laser in dual laser experiments, or primary laser in the case of single laser experiments. Fluorescence time traces were recorded on CCD cameras or counting boards utilizing the TCSPC method and time binned at least 2.2 times faster than the highest modulation frequency. Data were processed by Fast Fourier Transform (FFT) of each time correlated single photon counting fluorescence intensity time trace. The corresponding FFT peak amplitude at each modulation frequency was divided by the DC peak amplitude and corrected as necessary for the proper adjustment ($4/\pi$ term needed for square wave) to calculate modulation depth. An illustration of this process is shown in the figure below.

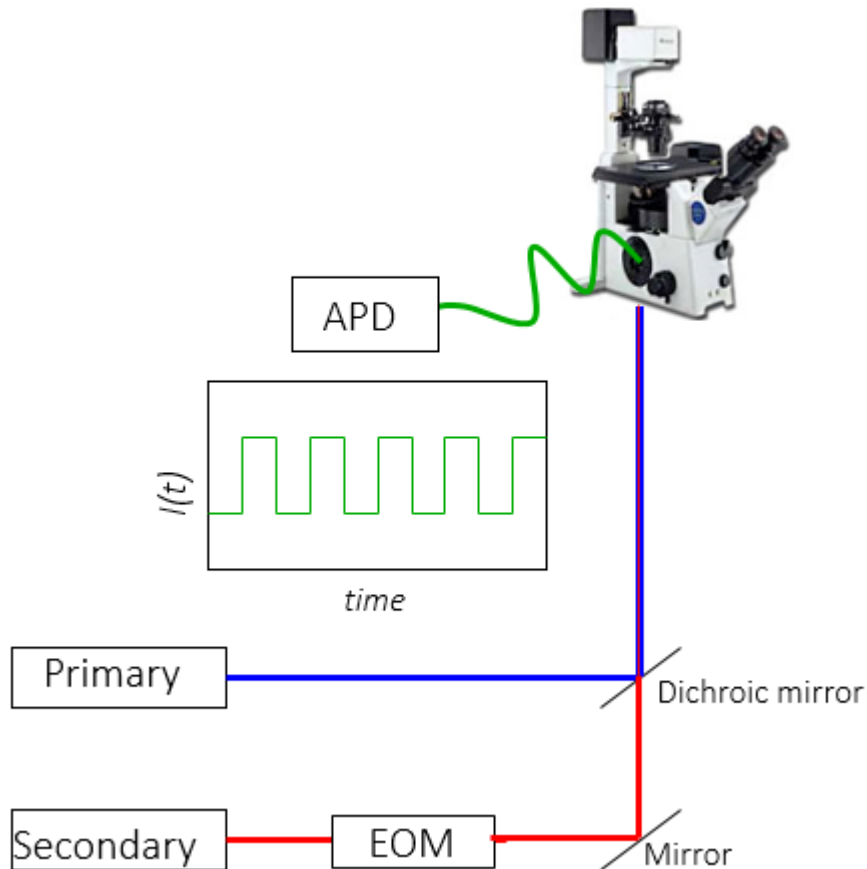


Figure 2.6. Basic optical modulation setup in the case of dual laser excitation with secondary modulation. Primary and secondary lasers are aligned into an inverted microscope. The secondary laser is modulated with an EOM and a function generator applies an external waveform which controls the modulation. The lasers are directed through an objective and are focused into the sample. Fluorescence from the sample is collected via the objective and directed through the microscope to the detector, where it is recorded by a counting board and analyzed by computer software.

There are several modulation schemes applied to fluorescence microscopy in this research. The first one used was a two laser setup where the primary laser is constant and the secondary is modulated with a square (or sine) waveform at 50% duty cycle. The modulation begins at a low frequency (generally 1 Hz) and continues until the modulation depth has reached near zero. In this work this method is often referred to as a frequency

scan because the modulation depth is recorded at each modulation frequency over a range of modulation frequencies and fit to the frequency domain lifetime equation to get τ , the lifetime of the dark state.¹² m refers to modulation depth, A is the modulation amplitude at zero modulation frequency, and ν refers to modulation frequency.

$$m = A / \sqrt{1 + (2\pi\nu\tau)^2} \quad \text{Equation 2.3}$$

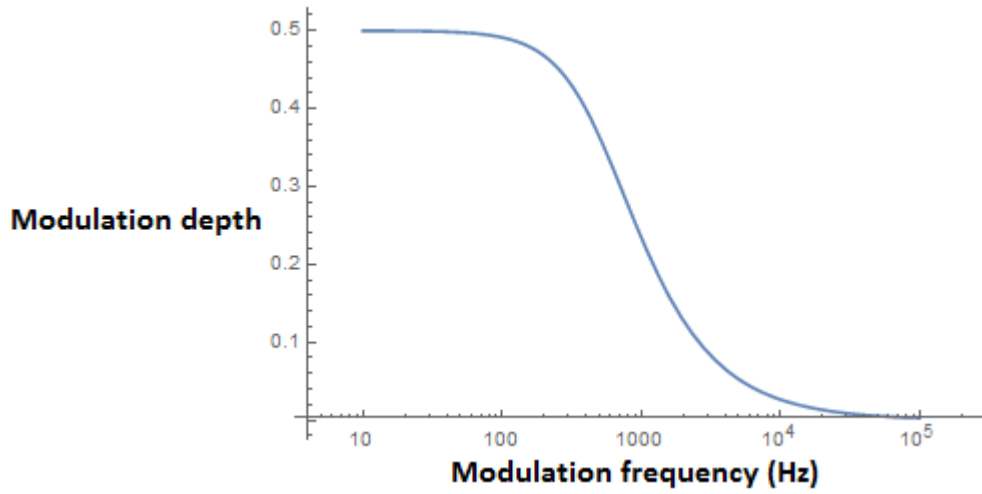


Figure 2.7. Plot of modulation depth vs modulation frequency governed by the equation $m = A / \sqrt{1 + (2\pi\nu\tau)^2}$ where $A = 0.5$ and $\tau = 300 \mu\text{s}$. The modulation depth is at a maximum at low modulation frequency and decays to near zero by 100 kHz.

The dark state lifetime is dependent on the rate of entering the dark state and the decay out of the dark state. The rate into the dark state is primary laser dependent, so varying the power of that laser can be used to uncouple the dark state dynamics. This is explained in specific detail in chapter 3.

Another modulation scheme is one laser modulation. Using this method one modulates with a square wave pulse and varies the time between pulses. When there is a large temporal distance between pulses, a significant fluorescence decay is observed

corresponding to a noticeable dark state population buildup. When the time between pulses is decreased, the dark state does not have enough time to fully decay between excitation pulses so the decay begins to disappear and the fluorescence pulses appear more flat. One can measure the drop off from the initial to final pulse values and fit to

$$\frac{n_B(t)}{n_{tot}} = 1 - \frac{\tau_{off}^o}{\tau_{on} + \tau_{off}^o} e^{\frac{-T_{off}}{\tau_{off}^o}} \quad \text{Equation 2.4}$$

in order to fit for the natural dark state lifetime, τ_{off}^o . In equation 2.4, n_B represents the number of molecules in the bright state, while n_{tot} is the total number of molecules. τ_{on} and τ_{off}^o represent the photophysical on and off times, and T_{off} is the off period between primary laser pulses.

One laser modulation can be modeled by a numerical simulation. This is explained in Appendix E, in which a first order differential equation is solved by matrix exponentiation with given photophysical kinetic rates. This allows one to monitor fluorescence (S_1 population) over time, taking into account modulation effects.

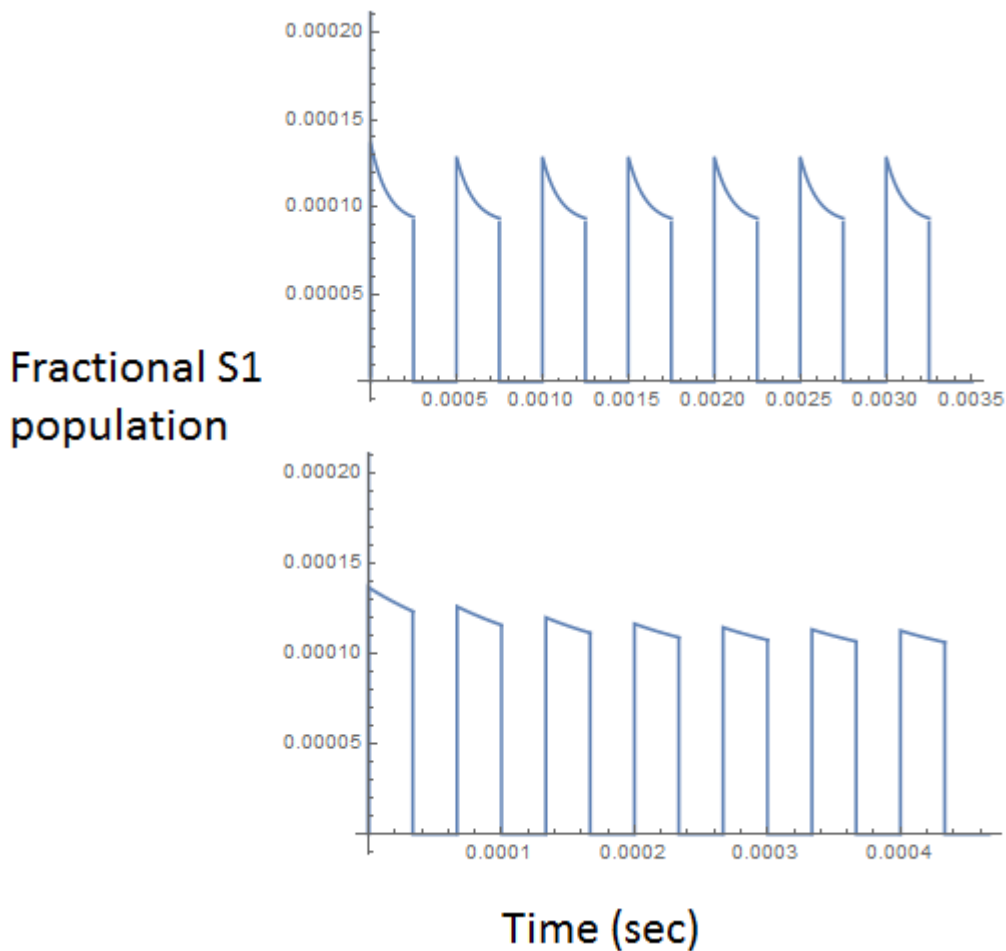


Figure 2.8. Simulation of photophysics using Cy5 parameters with square wave modulation. On top: modulation at 2 kHz, on bottom: modulation at 15 kHz. At 2 kHz modulation a clear decay is observed while at 15 kHz it is comparatively flattened out because the dark state does not have time to adequately recovery with such a short period between excitation pulses.

It is also possible to use a dual laser modulation scheme to probe dark state thermal population. Similar to one laser modulation, the primary laser is modulated with a square wave pulse, but in this experiment a square wave secondary laser pulse illuminates the sample while the primary laser is off. This is used to completely depopulate the dark state. By comparing the initial fluorescence values with and without secondary pre-illumination one can determine the dark state population by using a Boltzmann distribution.

Fractional S1
population

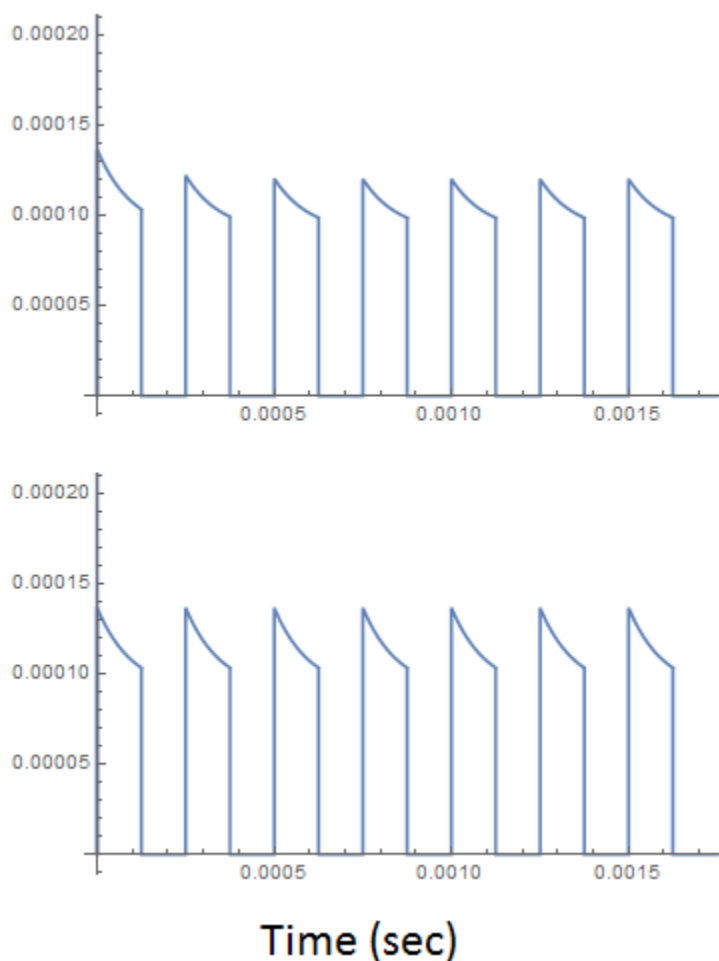


Figure 2.9. Top: Cy5 photophysics simulation with primary only square wave modulation at 4 kHz. Bottom: Simulation with primary on, then primary off and secondary on, then primary on again with secondary off. The initial fluorescence is higher when there is secondary laser pre-illumination, this can be used to estimate the dark state thermal population.

2.7 Density Functional Theory

Density functional theory (DFT) is an electronic structure method that is based on electron density rather than the wave function. For many years it was used in solid-state physics but is more recently popular in theoretical chemistry.¹¹³⁻¹¹⁴ DFT is unique in its approach since the other widely used methods, including Hartree-Fock, perturbation

theory, coupled cluster, and configuration interaction, all use the many electron wave function as opposed to the density. The basis of DFT comes from the Hohenberg-Kohn theorems,¹¹⁵ the first of which shows that the ground state electronic energy only depend on electron density, reducing the many body problem from 3N spatial coordinates to 3 spatial coordinates by using electron density functionals. From there, the Kohn-Sham equations¹¹⁶ introduce orbitals to the system making it a problem of non-interacting electrons moving in an effective potential. That leaves the electron exchange and correlation interactions as the difficulty in solving by this method. The local-density approximations (LDA) are used to estimate that the functional depends only on the value of electronic density at each point in space, but since they assume that the density is the same everywhere, generalized gradient approximations (GGA) are used which add an exchange functional with a term depending on the gradient to the LDA energies. Hybrid functionals such as B3LYP (Becke, three-parameter, Lee-Yang-Parr)¹¹⁷ utilize LDA and GGA to develop an exchange-correlation functional by mixing Hartree-Fock exchange into the DFT functional. DFT has become widely popular in the fields of chemistry and materials science to model molecular and solid-state properties. It can give fairly accurate results without being too computationally expensive.

In this work, DFT calculations were used to optimize ground state energies and calculate ground state and excited energies. In this case of this research, commercially available cyanine dyes as well as cyanines with structural modifications synthesized by our collaborators were modeled using DFT. Molecules not yet synthesized were also able to be modeled this way. By doing this, any theoretical molecules that showed promising DFT results we could encourage our collaborators to synthesize. In addition, different

isomerization possibilities were explored by manually rotating around different bonds in the polymethine bridge in the ball and stick model in Avogadro. By comparing these results to experimental calculations, one gains insight into mechanistic possibilities of the photoisomerization observed responsible for dark state behavior.

To perform electronic structure calculations, molecules were first drawn in the program Avogadro¹¹⁸ using a ball and stick model for atoms and chemical bonds. Then a classical force field optimization can be done to optimize the geometry prior to the electronic structure calculation. After molecule design in Avogadro, a script is created and exported which can be read by Gaussian. This script specifies the job name, memory and processors needed, type of calculation to be performed, molecular charge and spin, and the molecular geometry in three-dimensional atomic coordinates. When the computational job is submitted to a cluster for calculation, it is performed using Gaussian 09.¹¹⁹ Most commonly, DFT calculations performed in this work used Becke's three-parameter hybrid density function in combination with the Lee-Yang-Parr correlation functional (B3LYP) and the effective core potential (ECP) basis set Los Alamos ECP plus double zeta (LanL2DZ). Ground state geometries of Cy5 and its synthesized derivatives were optimized and the energy levels calculated, and frequencies were calculated to ensure that the geometry was at a minimum point in energy. Next, time-dependent density functional theory (TDDFT) was used to calculate transition energies for the geometry optimized ground states. The polarizable continuum model (PCM) was applied for ground state geometry optimizations and excited state absorption spectra calculations to determine the solvation effects of DMSO, as applied in experimental conditions.^{51-52, 55, 120-121}

CHAPTER 3

CYANINE DYE MODULATION EXPERIMENTS

3.1 Introduction

Previously, Cy5 was studied using SAFIRE.¹⁴ As mentioned in the first chapter (section 1.6: Optical Modulation), Cy5 fluorescence modulation had been successfully applied in imaging applications such as discrimination from fluorescent background with Texas Red and fluorescent signal recovery from tissue mimicking phantoms that absorb and scatter light.⁵⁶ Cy5 is a red/NIR fluorophore with a red-shifted transient absorption, and in these experiments it is excited by a 594 or 633 nm He-Ne laser. Fluorescence was collected from 660-690 nm, and a 710 nm laser was used as a secondary laser to excite the dark state and recover fluorescence. Modulation depths up to ~50% were achieved, and modulation drops off to near zero by 100 kHz modulation frequency. An illustration of this characterization method is depicted below.

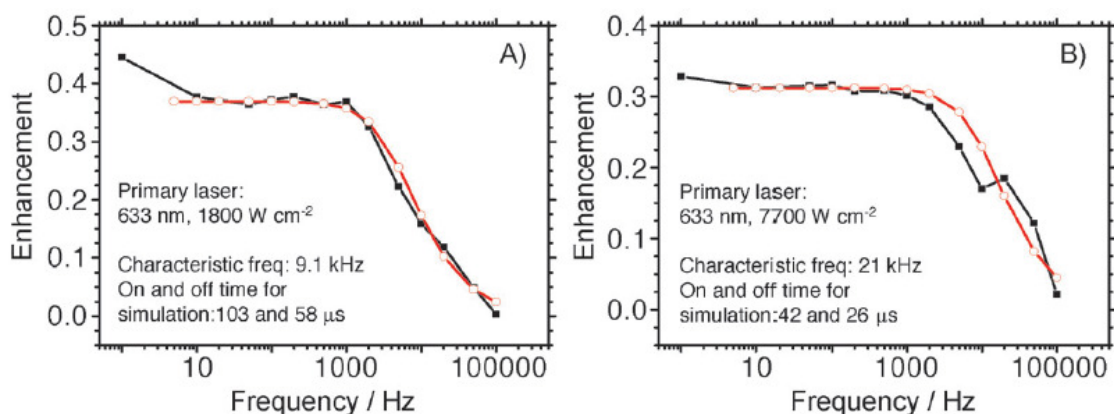


Figure 3.1. Modulation frequency scans of Cy5 with 633 nm primary excitation and 710 nm secondary excitation. In A) the primary laser intensity is 1.8 kW/cm² while in B) it is 7.7 kW/cm². The secondary is held constant at 12 kW/cm². In this example, going from lower to higher primary intensity the modulation depth decreases, the characteristic

frequency ($k_{\text{on}} + k_{\text{off}}^0$) increases, and both the on and off times decrease. What this suggests is that at higher primary intensity Cy5 photoisomerizes more quickly but is also excited out of the dark state, leading to higher characteristic frequency but lower modulation depth. It is therefore possible to control modulation depth and frequency with laser intensity based on molecular photophysics.

Given the imaging success seen with Cy5, one can wonder whether structurally similar molecules will change or alter modulation depth and on and off times. Based on previous research, it seems that different structural modifications have an impact on photophysics regarding fluorescence quantum yield and photoisomerization.^{47, 54, 122-124} Professor Maged Henary's lab at Georgia State University specializes in organic synthesis and works on cyanine dyes, and they were willing to let us borrow compounds to test, with future goals being synthetic design for new molecules. Their previous work has shown that modifying structure can affect photophysical properties such as absorption wavelength, extinction coefficient, and quantum yield. Therefore, it is reasonable to believe that dark state photophysics could also be affected by structural modifications, particularly those affecting isomerization and intersystem crossing and that this could lead to interesting advances in SAFIRE. In this section, new cyanine compounds are introduced, experimental methods (dual and single laser modulation) used to investigate dark state modulation are described, the resulting data is presented, and the next steps in the research are outlined.

3.2 Cyanine photophysics

The photophysics of Cy5 have been thoroughly studied using fluorescence correlation spectroscopy (FCS)⁵⁷ and transient absorption,⁵³ leading to the observation of multiple dark states, including photoisomers and triplet levels. FCS experiments and simulations suggest a diffusion time around 170 μs and on and off times of ~ 70 and ~ 90 μs , respectively,

making it necessary to discriminate photophysics from diffusion. Transient absorption spectra show two peaks, one at 625 nm and another at 690 nm. The peak at 625 nm has a lifetime of 35 μ s while the 690 nm peak is fit to a bi-exponential with timescales at 150 μ s and 5.8 μ s. To confirm intersystem crossing, one can add ethyl iodide to the solution, which increases the triplet yield due to a heavy atom spin-orbit coupling effect. Upon addition of ethyl iodide, the 625 nm peak and faster timescale at 690 nm become more pronounced, suggesting that they are the triplet peaks in the transient absorption spectrum. The 625 nm peak is ascribed the trans-triplet while the shorter-lived 690 nm peak is ascribed to the cis-triplet absorption.⁵³ A phosphorescence peak is also observed at 840 nm which has been described as cis-phosphorescence.⁷⁵ For Cy5, the cis-photoisomer absorption is red-shifted by \sim 45 nm, yielding a transient absorption at 690 nm with a lifetime of 150 μ s.⁵³ The relatively long cis-Cy5 lifetime enables significant buildup of this dark state under even low steady-state excitation. Excitation of cis-Cy5 in its absorption band, however, photoreverts the Cy5 to the trans state and recovers fluorescence with enhancements of up to 50%.¹⁴ A schematic of these photophysical processes is shown below.

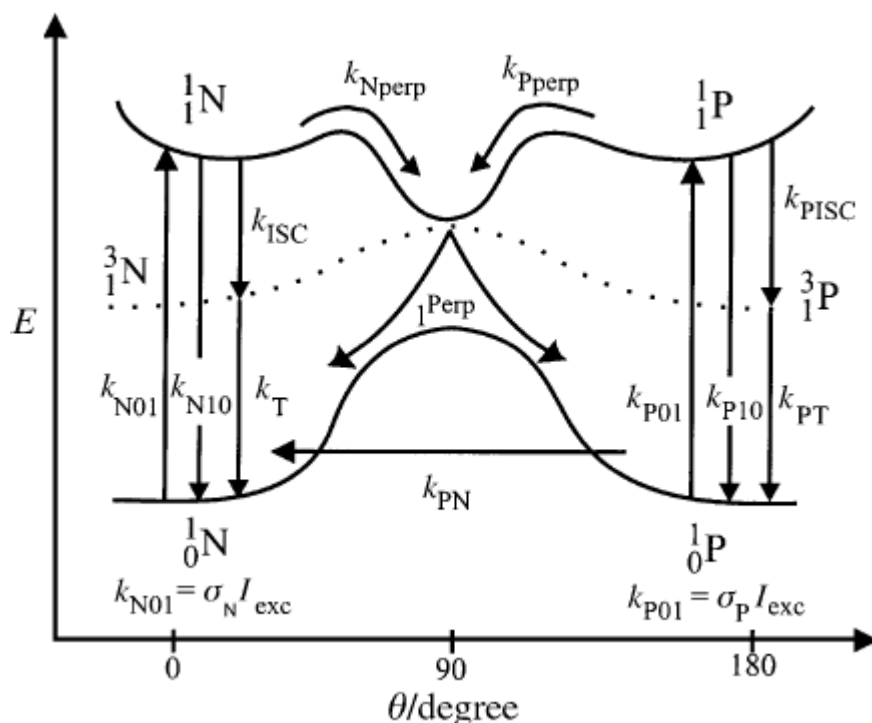


Figure 3.2. Illustration of kinetics of cyanine photophysical processes. 1_0N , 1_1N , and 3_1N refer to the all trans isomer ground state, singlet excited state, and lowest triplet state, respectively. 1_0P , 1_1P , and 3_1P refer to the photoisomer ground state, singlet excited state, and lowest triplet state, respectively. k_{ISC} and k_T refer to intersystem crossing to triplet and decay from triplet rates while k_{perp} represents photoisomerization and k_{PN} back photoisomerization. σ signifies absorption cross section and I_{exc} laser excitation intensity. Photoisomerization (possibly over multiple bonds) can occur, along with intersystem crossing to triplet states, which occur in both trans and cis photoisomers. All of these processes occur on similar timescales, with triplet transitions occurring about ten times faster than photoisomerization.⁸⁴

When all of this is considered, Cy5 can be a difficult molecule to study because many timescales are close together. Diffusion often occurs on a $\sim 100 \mu s$ timescale, isomerization is typically ~ 10 - $100 \mu s$, and intersystem crossing is fastest, often around $1 \mu s$ or faster. This makes it difficult to separate out different photophysical processes, and observed modulation could be a result of multiple effects. Based on the modulation timescales, coupled with the energetic properties of these dark states, we believe that our approach of fluorescence excitation combined with secondary laser co-illumination on-resonance with

the transient absorption dynamically modulates the Cy5 fluorescence intensity via optical depopulation of primarily the photoisomerized dark state, with other states playing a smaller role.

3.3 Cyanine modulation

Using Synchronously Amplified Fluorescence Intensity Recovery (SAFIRE)⁹⁶ we can modulate the long-wavelength secondary laser to modulate the cis vs. trans-Cy5 ground state populations, thereby modulating collected fluorescence and enhancing signal to noise. Such fluorescence recovery from high background was demonstrated for the commercially available parent Cy5 in solution¹⁴ and buried within tissue mimicking phantoms.⁵⁶ To understand and improve detection sensitivity, we studied cyanine structural variants (synthesized by the Henary lab) and utilized optical modulation methods as a screening tool to assess how variations in cyanine structure affect modulatability and, therefore, signal recovery in high background fluorescence experiments. Our specific emphasis is on understanding the bright state and dark state photophysics to enhance and tailor optically recovered ground state populations.

Cyanine photophysics and dark state recovery kinetics were investigated under single and dual laser excitation. Compounds were dissolved in DMSO to about 1 nM concentration for the appropriate signal intensity. At this concentrations the sample was dilute enough to exclude aggregation effects. Coexcitation with a 594 nm primary and 710 nm square-wave-modulated secondary laser was used for synchronously amplified fluorescence intensity recovery (SAFIRE). This dual laser method uses the primary excitation to produce fluorescence and populate the dark state, while the much lower

energy secondary laser depopulates the nonfluorescent dark state, shifting the population to the bright state faster than the dark state would naturally decay. By modulating this secondary laser, we directly modulate Cy5 fluorescence, shifting its signal to a unique detection frequency, where there is little to no background. At sufficiently high modulation frequencies, the system has insufficient time to establish steady-state populations, meaning that measurements of modulation depth, m , vs modulation frequency, ν , report on the time to establish dark and bright manifold steady state populations, and is given by equation 2.3. When a specific timescale exists, fitting frequency-dependent modulation depth curves to equation 3.1 enables extraction of the characteristic time, τ_c . When a good fit to a single characteristic time, τ_c , is not possible, one can specify the time at which the modulation depth drops by half to extract a characteristic time.¹⁴ Changing with primary laser intensity, the inverse of τ_c is the characteristic frequency, or rate $k_c = k_{on} + k_{off}^\circ$, where

$$k_{on} = \frac{\sigma_{abs} * I_{pri}}{h\nu} \Phi_D$$

(σ_{abs} is the absorption cross section, I_{pri} is the primary laser intensity, and Φ_D is the dark state quantum yield) and k_{off}° is the natural dark state decay rate constant.³⁴ The parameters k_{on} and k_{off}° (or their inverses τ_{on} and τ_{off}°) can be used to determine the rates at which molecules enter and exit the dark state, allowing one to determine fluorescence enhancement,²²

$$Enh = \frac{\tau_{off}^\circ - \tau_{off}}{\tau_{on} + \tau_{off}} \quad \text{Equation 3.1}$$

in which τ_{off} is the dark state lifetime with the secondary laser on. The data in Figure 3.3A demonstrate this process, showing a diminishing modulation depth with increasing

modulation frequency, and the fitted characteristic frequencies at varying primary power are used to extract on and off times (Figure 3.3B).

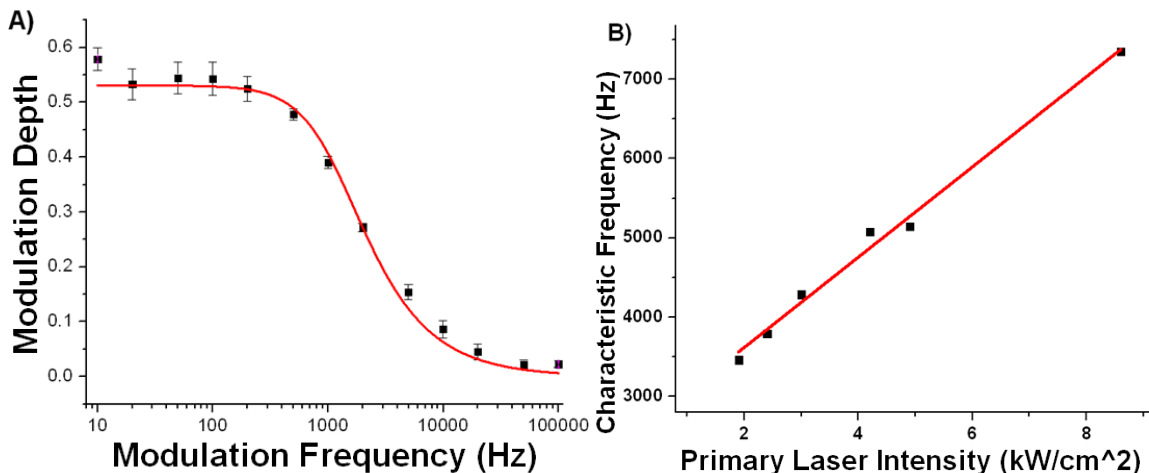


Figure 3.3. A) Cy5 derivative MHI97 (See Table 3.1) modulation depth as a function of modulation frequency and fit to equation 2.2. Data were collected for 1 second at each modulation frequency. B) MHI97 characteristic frequency as a function of primary intensity and the line to which it fits.

At low modulation depths (<15%), extracting accurate photophysical parameters can be difficult from modulation depth vs. frequency curves. Instead, by achieving steady state dark state population through extended primary illumination,⁹⁵ thermal recovery from the dark state occurs upon rapidly turning the primary laser off. By varying the primary illumination off period, T_{off} , the fraction of molecules in the bright state, n_B/n_{tot} will recover to a degree that depends on the natural off time, τ_{off}^0 according to equation 2.3. By fitting the experimentally determined fraction of molecules in the bright state as a function of the laser off period we can determine the natural dark state decay rate. This process is illustrated in Figure 3.4 where Figure 3.4A shows a large intensity drop off with 300 μs between laser pulses, Figure 3.4B demonstrates less drop off with 100 μs between pulses, in Figure 3.4C there is even less decay with 50 μs between pulses, and finally in Figure 3.4D the intensity drop is the least significant. This shows that the longer the laser off

period, the greater the recovery from the dark state, which yields a higher initial fluorescence intensity when the primary laser is turned back on.

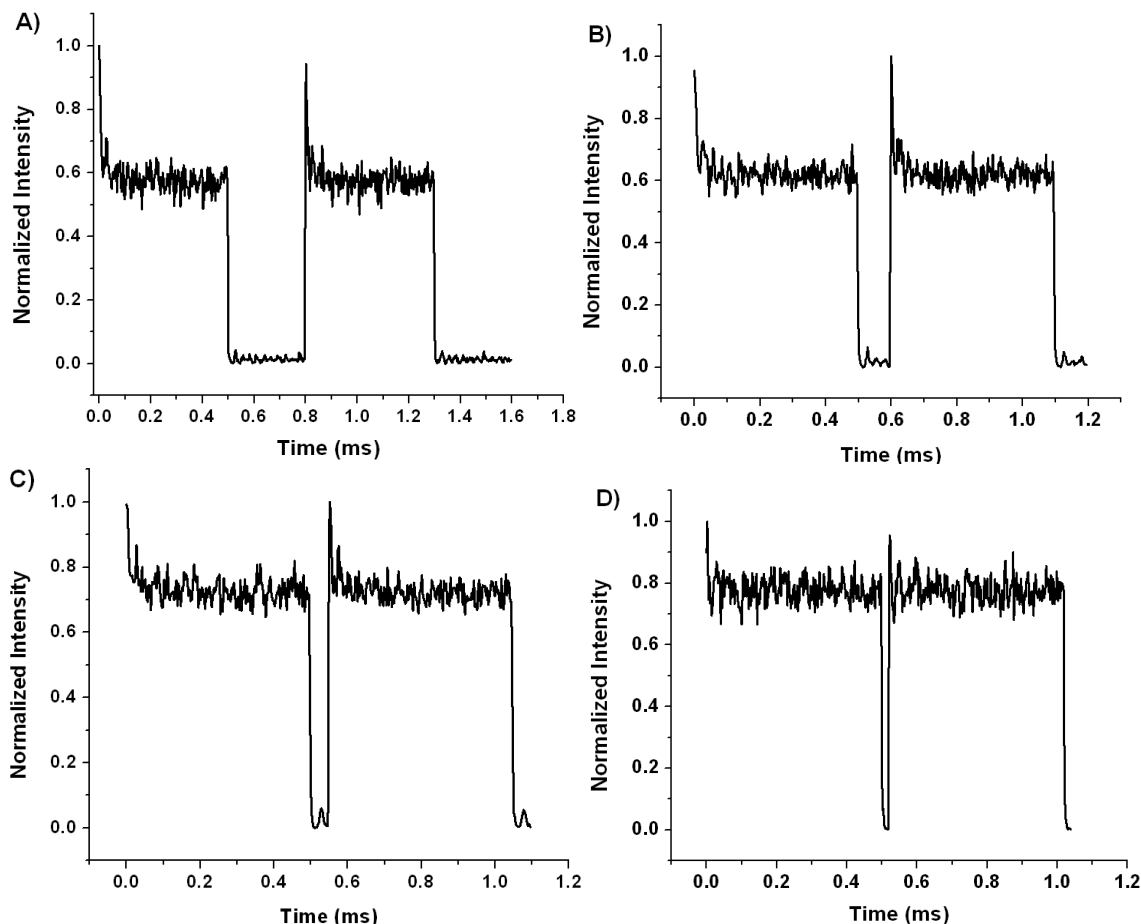


Figure 3.4. Fluorescence traces showing ground state recovery for MHI106 using different primary laser off periods, T_{off} . Using an electro-optic modulator, the primary laser is turned on for 500 μs and off for A) 300 μs , B) 100 μs , C) 50 μs , and D) 20 μs . Laser spot size was expanded 300 μm^2 , to increase diffusion timescales to $\sim 10\text{ms}$, such that it does not interfere with the modulation timescales. For each panel, data were collected for 20 seconds and modulation cycle averages are taken and ratios of initial to final intensities within the average primary illumination period, T_{on} , as a function of T_{off} are fit to equation 2.3.

3.4 Cyanine Enhancement and On & Off times

The synthesized cyanines studied have the general structure below.

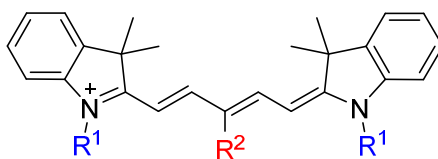


Figure 3.5. General structure of Cy5 analogs. Modifications were incorporated as alkyl substitutions at the heterocyclic nitrogens (R^1) and halogen incorporation on the *meso* position of the polymethine bridge (R^2).

Even with the seemingly minor structural changes to Cy5 indicated in Figure 3.5, modulation depth and photophysical parameters are strongly affected by slight substituent changes. Using modulation frequency dependence and bright state recovery methods (Figures 3.3 & 3.4), photophysical on and off times were extracted (Table 3.1). Overall, with the Cy5 derivatives, modulation depth increases with alkyl chain length and decreases with increasing halogen mass.

Table 3.1. Summary of experimental results including enhancement and on and off times for Cy5 derivatives in DMSO at 298 K. Concentrations were approximately 1 nM. R^1 and R^2 positions are as shown in Figure 3.5. For τ_{on} and τ_{off} measurements, the primary and secondary laser intensities were 350 and 640 W/cm², respectively.

Dye	R^1	R^2	Mod depth	τ_{off}^0 (μ s)	τ_{off} (μ s)	τ_{on} (μ s)	Φ_D
Cy5			50% (± 4)	73(± 7)	20(± 3)	88(± 9)	.011(± 0.002)
MHI84	CH ₃	H	40% (± 2)	87(± 4)	25(± 2)	130(± 8)	.0077(± 0.001)
LO4	CH ₂ CH ₃	H	50% (± 4)	130(± 3)	40(± 3)	140(± 7)	.0072(± 0.001)
MHI97	(CH ₂) ₃ CH ₃	H	58% (± 2)	210(± 8)	40(± 5)	250(± 11)	.004($\pm 5 \times 10^{-4}$)
MHI106	CH ₃	Cl	28% (± 3)	60(± 8)	45(± 7)	10(± 3)	.10(± 0.007)
E27	CH ₃	Br	13% (± 1)	25(± 3)	20(± 3)	7(± 2)	.14(± 0.01)
E63	CH ₂ CH ₂ OAc	Cl	20% (± 1)	50(± 5)	37(± 4)	25(± 3)	.040(± 0.003)
E65	CH ₂ CH ₂ OAc	Br	7% (± 2)	12(± 3)	10(± 2)	7(± 2)	.14(± 0.009)
Cy5.5			12% (± 2)	140(± 11)	118(± 10)	100(± 3)	.012(± 0.002)
Cy7			15% (± 3)	16(± 3)	13(± 3)	6(± 2)	.21(± 0.01)
Merocyanine 540			40% (± 3)	216(± 15)	123(± 10)	110(± 11)	.016(± 0.001)

The fluorescence enhancement of Cy5 is due to optical depopulation of a dark state, and derivatives' modulation depth generally increases with increasing alkyl chain length and decreases with increasing halogen atomic mass at the central carbon. Despite the added bulk to the polymethine chain, halogens seem to shorten the on and off times, while long alkyl chains appear to slow the forward and back-isomerization processes. The photophysical rates into and out of the dark state control the steady state dark state population. The larger the achievable steady-state dark state population, the larger the possible enhancement upon complete depopulation through secondary illumination. MHI97, for example, exhibits the highest enhancement and is the slowest to photoisomerize, but because the dark state is long-lived, a high modulation depth is recorded. On the other hand, halogenated E27 and E65 rapidly photoisomerize, but also back-photoisomerize very quickly, leading to low dark state buildup and low overall modulation depths. All of the Cy5 variants have similar secondary-induced τ_{off} values, minimizing its impact with these derivatives. Thus, within this family of Cy5-like compounds, structural modifications that increase the ratio of $\tau_{\text{off}}^{\circ}$ to τ_{on} for a given primary excitation intensity have the greatest effect on overall enhancement. Through such optical control of emission with tailorable on and off times, applications in super-resolution imaging may also become possible at faster timescales,^{16, 65, 125-128} possibly coupled with the improved sensitivity afforded by modulation-based SAFIRE.²⁰

Interestingly, Cy5.5 has photophysical on and off times similar to the best Cy5 derivatives, but shows much lower enhancement. While R1 and R2 substitutions showed the same trend as with Cy5, the lower modulation depths precluded full photophysical characterization, except for commercial Cy5.5. In contrast to Cy5, the low enhancement

appears to arise from inefficient dark state depletion – an interpretation corroborated by FCS data which show a higher dark state population for Cy5.5 than for Cy5 when both primary and secondary lasers are on.

The ~100 μ s natural dark state lifetimes suggest that a ground state process such as photoisomerization leads to the modulatable metastable dark state, as suggested previously for commercially available Cy5.¹⁴ Considering the range of cyanines studied, increased conjugation length appears negatively correlated with dark state buildup. Merocyanine 540, for example, exhibits a relatively high modulation depth due to its long-lived dark state and fast forward photoisomerization rate, but its dark state is less efficiently depleted by the secondary laser, causing the modulation depth to not be as high as Cy5 and some of its related analogues. Cy7 exhibits a short-lived dark state, similar to the brominated Cy5 derivatives, and therefore does not offer as much fluorescence recovery as the Cy5 compounds or Merocyanine 540. When Cy7 isomerization is chemically prevented around the central double bond as in Fig. 5, however, isomerization is forced to occur around other bonds, likely limiting accessible photoisomers to increase photoreversible dark state populations and modulation depth.

FCS experiments were also performed with primary only and dual laser continuous excitation to observe dark state timescales. It appears that the dark state lifetimes shorten while dark state fractional populations decrease when both lasers illuminate the sample, however diffusion, photoisomer, and triplet time scales tend to blend when they are so close in magnitude. The autocorrelation data were fit to the equation 3.2

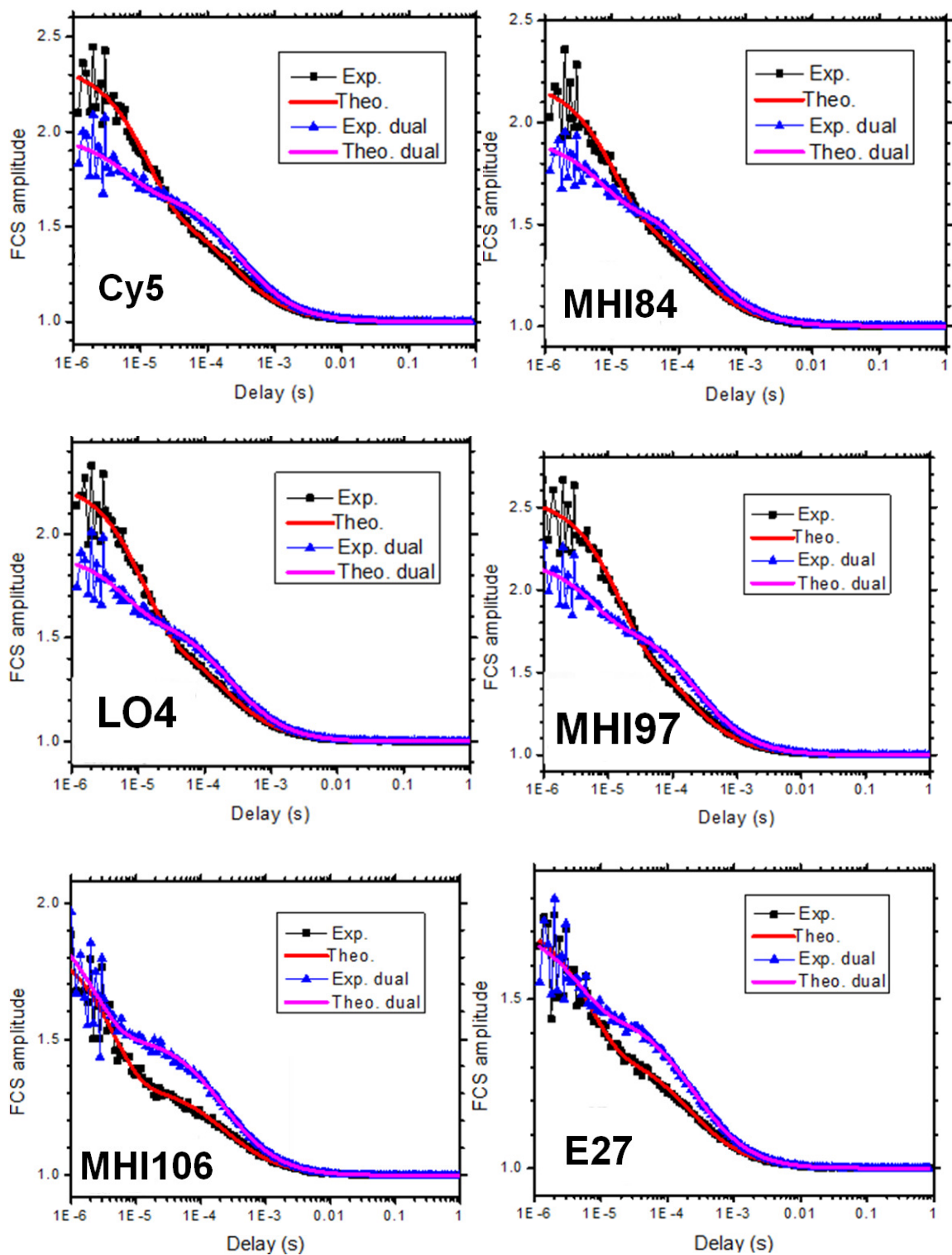
$$G(\tau) = \frac{1}{\langle N \rangle} \frac{1 - F + Fe^{-\tau/\tau_{Dark}}}{1 - F} \frac{1}{(1 + (\tau/\tau_{diff})) (1 + a^{-2}(\tau/\tau_{diff}))^{1/2}} \quad \text{Equation 3.2}$$

where $\langle N \rangle$ is the average number of particles in the focal volume, F is the fraction of molecules in the dark state, τ_{Dark} is the dark state relaxation time (or inverse characteristic frequency), τ_{diff} is the characteristic diffusion residence time, and $a = \omega_z/\omega_{xy}$ is the ratio of axial to radial e^{-2} radii of the measurement volume.¹² The FCS data and fits are shown in Figure 3.6 and the results are summarized in Table 3.2.

In these FCS data the main items of interest are dark state fraction, diffusion time, and dark state time. Dark state fraction decreases upon secondary illumination, as expected. The secondary laser also seems to decrease the dark state time while increasing the diffusion time. The dark state time decreases as expected due to secondary laser depletion while the diffusion time becomes more distinguished from the dark state timescale.

Table 3.2. FCS data for Cy5 compounds. Samples were approximately 100 pM, in DMSO at 298 K. The first values listed are for primary only and the second are for dual laser excitation. The decrease in dark state fraction after secondary laser co-illumination shows that the dark state is effectively depleted by the secondary laser.

Molecule	$\langle N \rangle$	Diffusion time (μs)	Dark state fraction	Dark state time (μs)
Cy5	1.65 / 1.42	222 / 284	0.55 / 0.28	13.5 / 6.00
MHI84	1.73 / 1.60	163 / 213	0.52 / 0.32	11.0 / 6.35
LO4	1.87 / 1.63	180 / 228	0.58 / 0.33	12.7 / 6.40
MHI97	1.38 / 1.24	157 / 228	0.54 / 0.32	15.2 / 5.76
MHI106	3.02 / 1.94	234 / 223	0.61 / 0.47	4.64 / 2.31
E27	2.84 / 2.14	203 / 240	0.52 / 0.35	6.95 / 4.55
E63	1.97 / 1.24	259 / 228	0.61 / 0.32	7.36 / 5.76
E65	2.16 / 1.20	278 / 246	0.48 / 0.26	7.03 / 4.23
Cy5.5	6.89 / 7.83	2820 / 2350	0.319 / 0.276	183 / 137



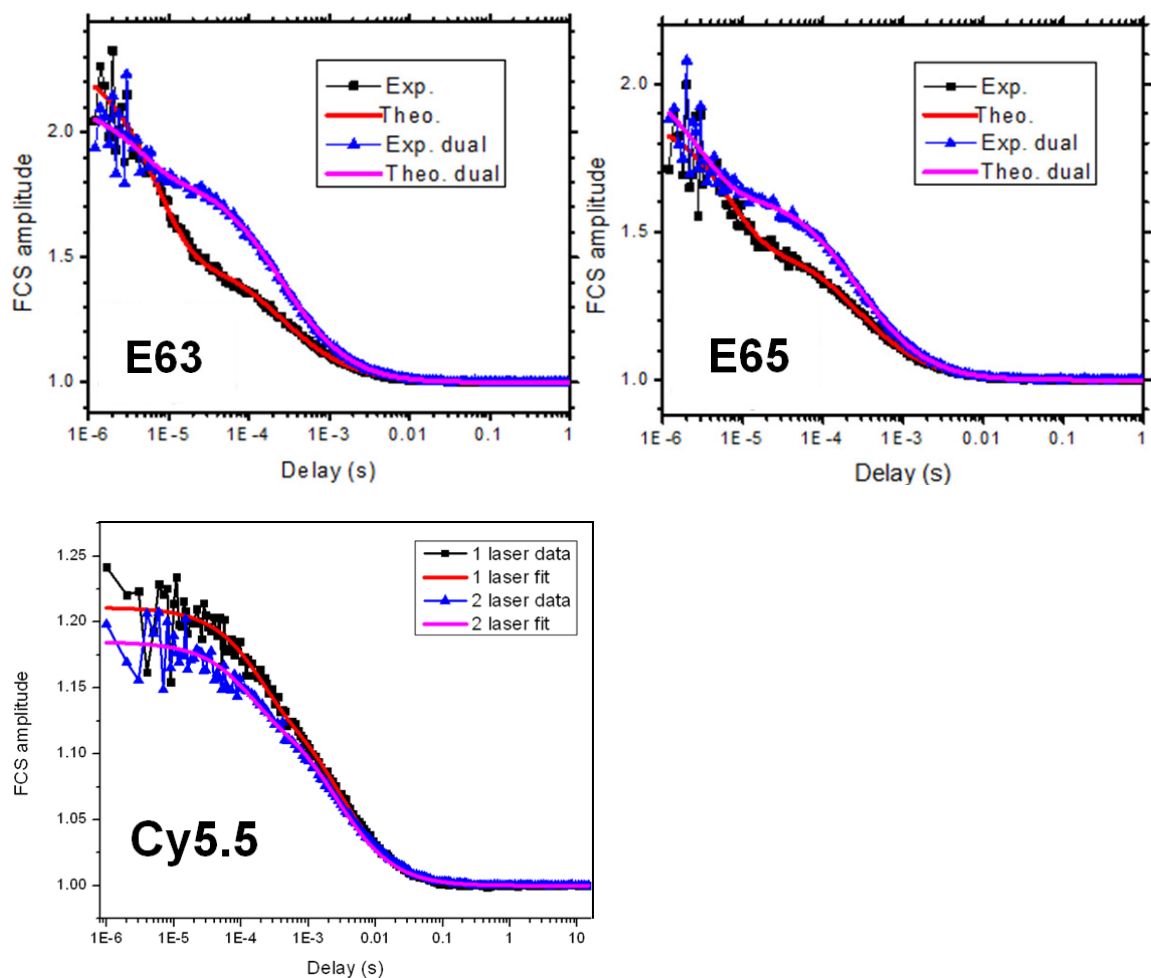


Figure 3.6. FCS data for cyanine compounds with single and dual laser excitation. The autocorrelation data are shown with the fits to the FCS formula overlapped. Exp refers to experimental data while Theo signifies fit to the FCS formula (Equation 3.2).

3.5 Conclusions

Following previous work on Cy5 modulation, single and dual laser techniques were extended to synthetic variants of the Cy5 structure and other commercial cyanine dyes. The main experiments conducted involved dual laser modulation, with a primary laser on resonance with molecular absorption and a red-shifted secondary laser to excite a transient dark state. Modulation depth and photophysical on and off times were determined by performing square wave modulation with an EOM by varying modulation frequency and

primary laser intensity, and also single laser modulation using square wave pulses but varying the time between pulses. From these results, it can be inferred that a short on time and long off time are desirable for maximum enhancement, though faster characteristic frequencies could be desirable in certain applications.

Among the commercially available cyanines, Cy5 showed the greatest fluorescence enhancement. Adding an extra phenyl ring to the indole, as is the case with Cy5.5, decreased enhancement. A trimethine bridge (Cy3) showed no enhancement and a heptamethine bridge (Cy7) showed less enhancement due to shorter lived dark states. This relationship held among the synthetic variants. Those similar to commercial Cy5 (pentamethine chain with indole side groups) showed the greatest amount of modulation depth. Among the Cy5-like dyes, longer alkyl chains on the side group nitrogen atoms increased modulation depth, while increasing halogen mass on the polymethine bridge decreased modulation depth. Further analysis of timescales revealed that longer alkyl chains increased photophysical on and off times, while increasing halogen mass decreased on and off times. Longer off times allow for greater dark state buildup, and greater fluorescence recovery upon secondary illumination of the transient dark state.

Going further, it would be worth thinking more about the cyanine mechanism of modulation, in particular isomerization pathways that could be explored with experimental and theoretical investigations. Different modulation experiments can explore the energetics of the dark state, and these data can be compared to theoretical calculations, leading to insight about which photoisomers play a role. Furthermore, synthetic design parameters can be tested to figure out how to modify future fluorophores for use in SAFIRE.

CHAPTER 4

CYANINE MECHANISM OF MODULATION AND SYNTHETIC FEEDBACK

4.1 Introduction

From experimental modulation data one obtains fluorescence enhancement as well as kinetic data from on and off times. Knowing that photoisomerization is likely responsible for the fluorescence modulation, more research was needed to understand the energies of these photoisomer states. Experiments with alternating primary and secondary lasers were used to probe the dark state thermal population, and by using a Boltzmann distribution analysis dark state energy levels were obtained. Next, by employing density functional theory, energy levels of different cyanine isomers were calculated and compared to experimental results. This analysis allowed for determination of which photoisomer was likely responsible for modulation. Even further corroboration came in the form of TD-DFT calculations of excited state energies, showing which photoisomers have red-shifted absorptions. Using these methods, theoretical calculations were carried out for future molecules that could potentially be synthesized. This way our synthetic collaborators have feedback to create new dyes for testing.

After studying cyanine fluorescence and dark state photophysics by experimental and theoretical methods and determining how different photophysical parameters can improve or limit fluorescence modulation, one can expand on this method to look at different molecules and different sample environments. Given the interesting findings on cyanine photophysics (especially Cy5 variants), more dyes were synthesized and more experiments planned. While none of the newer dyes have exceeded previously observed modulation

depth (~58%), new relationships between molecular structure and photophysics have been explored. In addition, it appears that solution additives (triplet quenchers and enhancers) affect the modulation depth, with triplet quenchers increasing and triplet enhancers decreasing fluorescence enhancement.

4.2 Cyanine theory: electronic energies and photoisomerization

Since cyanine photoisomerization appears to be largely responsible for the observed modulation due to dark states, it is useful to investigate the electronic structure of the chromophore. In previous literature, analyses involving semi-empirical and DFT theoretical methods and spectroscopic experimental methods provide insight into molecular and photoisomer energetics and kinetics.^{52, 55, 76, 81} Because the cyanine chromophore consists of a π -conjugated polymethine bridge, the simplest way to model cyanine electronic structure is with the particle in a box model or the Hückel molecular orbital method. In a π -conjugated system electrons are considered to be de-localized and can travel as if they were in a one-dimensional box.¹²⁹ Therefore, the electrons can be

described by the particle in a box wavefunction $\psi(x) = \sqrt{\frac{2}{L}} \sin(\frac{n\pi x}{L})$ and energy levels

$E = \frac{n^2 h^2}{8mL^2}$ where L is the length of the box and n is a positive integer quantum number. In

the case of a pentamethine cyanine with nitrogen atoms at both ends (one positively charged and one neutral) there are six π electrons, so in accordance with the Pauli exclusion principle only two electrons can populate an energy level, meaning that the bottom three are filled. This means that the highest occupied molecular orbital (HOMO) can be

described by $\psi(x) = \sqrt{\frac{2}{L}} \sin(\frac{3\pi x}{L})$ while the lowest unoccupied molecular orbital (LUMO) is described by $\psi(x) = \sqrt{\frac{2}{L}} \sin(\frac{4\pi x}{L})$. This can help one visualize the wavefunctions. In particular, the nodes are useful because they represent regions of zero particle probability where bond breaking and isomerization is more likely. In addition, excited state transition energy can be approximated by using the formula $\Delta E = E_4 - E_3 = (4^2 - 3^2)h^2/8mL^2$ where h is the Planck constant and m is the mass of an electron. L is approximated as 150 pm for each of the six bonds. By plugging in one gets an answer of 3.09 eV, corresponding to a 401 nm transition wavelength. This is not far from literature TDDFT values.¹³⁰

To use the Hückel method to model the polymethine system,¹³¹ one can set up and solve the appropriate secular determinant, but the general formula for linear polyenes is $\Delta E = -4\beta \sin(\frac{\pi}{2(n+1)})$ where the Hückel parameter β is approximately -70.4 kcal/mol and n is the number of π electrons in the molecule. By plugging in $n = 6$, in the case of the pentamethine cyanine considered previously, one gets a transition energy of 2.69 eV which corresponds to a wavelength of 461 nm, similar to the result using the particle in a box model considering the rough approximations of the method.

Going further with the same model molecule (two nitrogen atoms with five carbon atoms between them and π conjugation consisting of six π electrons), qualitative molecular orbital (Hückel) results can be coupled to semi-empirical results, such as those obtained by the CS INDO (Conformation Spectra Intermediate Neglect of Differential Overlap) technique. CS INDO is used to calculate potential energy surfaces (energy barriers) for S_0 , S_1 , and T_1 energy levels as a function of bond twisting angle. This diagram is shown in the

figure below. From these results by Momicchioli et al.,⁵⁵ one can conclude that upon excitation from the all trans ground state the molecule (among other relaxation pathways) likely twists perpendicular to an S_1 potential minimum and relaxes to the S_0 maximum, where it can end up either in the cis photoisomer ground state or all trans ground state. One can also note that the energy barriers from all trans to 2-3 cis are higher than the energy barrier to 3-4 cis in both the S_0 (ground) and S_1 (excited) states.

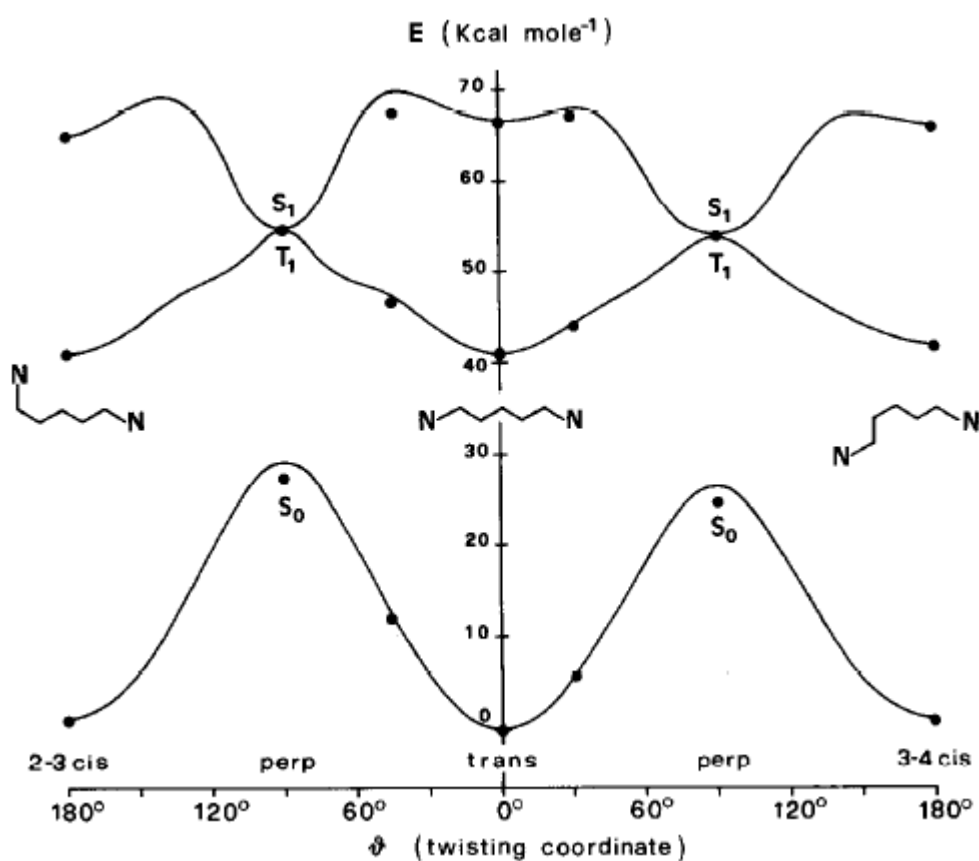


Figure 4.1. Calculated (CS INDO) potential energy vs twisting coordinate for the 2-3 and 3-4 cis isomers of a pentamethine cyanine with nitrogen atoms at both ends (structures shown in diagram).⁵⁵

In another study by Baraldi et al.,⁵² focusing on the pentamethine cyanine chromophore, it was concluded that visible irradiation in the visible range gave rise to a

planar cis photoisomer at the middle of the polymethine bridge. By measuring fluorescence quantum yields and lifetimes while varying temperature and solvent viscosity (using the Arrhenius rate equation), they could explore excited state relaxation channels and kinetics of thermal back-isomerization of the photoisomerization while coupling these results to semi-empirical (CS INDO CI) calculations of trans and cis isomers. The aim in this study was to use both experimental and theoretical methods to look at relative energies and potential energy barriers describing the trans-cis isomerization energetics and kinetics of the process.

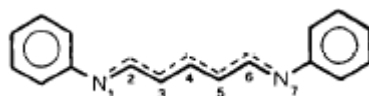


Figure 4.2. Pentamethine molecule used in the experimental and theoretical study by Baraldi et al.⁵²

From the experimental data, the pentamethine isomer around the center of the bridge (3-4 cis as defined in Figure 4.2) had a larger energy barrier than the isomer around the bond furthest from the center (65.7 vs 59.4 kJ/mol). The computational results of the energy barriers were 68.1 kJ/mol for 1-2 cis, 93.8 kJ/mol for 2-3 cis, and 82.3 kJ/mol for 3-4 cis. This means that the isomer closest to the edge of the bridge had the lowest energy barrier, and the center most isomer (3-4) had the second lowest energy barrier, while the 2-3 cis had the highest energy barrier. This agrees with the DFT results in our work (discussed later this section).

It is also necessary to look at energy levels in addition to kinetics and energy barrier considerations. In one study⁸¹ DFT and time dependent DFT were used to study all of the different possible isomers by rotating the C-C bonds of the polymethine chain. The DFT

method used in this work was B3LYP/6-31g* and geometries were optimized and ground state energies calculated, then the optimized geometries were used to calculate excited state transition energies. A pentamethine cyanine with indole side groups, similar to commercially available Cy5 was studied and rotations were made around each C-C bond systematically to explore all of the different isomerization possibilities.

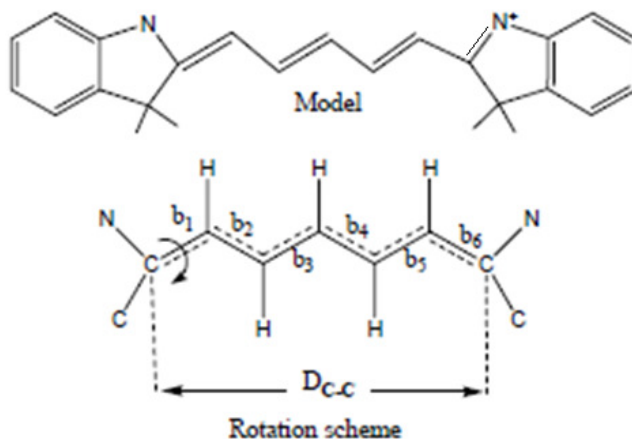


Figure 4.3. Pentamethine cyanine and rotation scheme used in this study.⁸¹

When comparing the energetics of the different isomers, there are many different possibilities, but since experimentally we expect a metastable dark state with a red-shifted transient absorption, we can pay special attention to theoretical data that fit these criteria. As it turns out, DFT predicts that the all trans ground state is the most stable state and all other isomers are higher in energy. The lowest energy isomer is simply one indole end group rotated relative to the other, with the polymethine chain unchanged. However, TD-DFT does not predict a large red-shift for the excitation of this isomer, meaning that when it occurs it is likely re-excited by the primary laser. The next three lowest energy isomers are rotations around the b₁, b₂, and b₃ bonds, all of which have energies around .15 eV

greater than the ground state, and two of the three have red-shifted excitation energies. All other isomers have energies more than .22 eV greater than the ground state. Thus, these less stable isomers are likely too short-lived to give rise to the observed >100 μ s dark state.

Armed with all of this information, we now have a simple model of electronic structure (particle in a box and Hückel), information on isomerization energy barriers based on experimental Arrhenius data and semi-empirical computational methods, and data regarding isomer ground and excited state energy levels. Now we can apply this information and these methods to study the cyanines in this work.

4.3 Experimental dark state energy

To probe the ground state energy differences between modulatable dark and bright states, we conducted dual laser experiments in which one laser was turned on while the other was turned off, and then vice versa. The idea was to pre-illuminate fluorophores with the secondary laser to remove molecules from the dark state as much as possible, and compare initial fluorescence intensity of molecules with and without secondary pre-illumination. This method is used to probe dark state thermal population. Figure 4.4 depicts the results of this experiment. The relative initial fluorescence intensities with and without secondary pre-illumination are used to determine the energy difference between the trans and photoreversible cis isomers involved in modulation. Assuming the dark state is completely depleted upon secondary laser pre-illumination, a Boltzmann distribution ($n_i/n_j = \text{Exp}(-\Delta E_{ij}/k_B T)$) enables experimental trans-cis energy differences for all cyanine derivatives to be determined (Table 4.1). Theoretical energetic degeneracies are ignored, but could potentially play a factor. A defocusing lens to expand the laser spot from $\sim 1 \mu\text{m}^2$

to $\sim 300 \mu\text{m}^2$ was used to prevent diffusion in and out of the focal volume from affecting results. The results obtained seem to agree with experiment. The relatively low energy difference between bright and dark states further supports the idea that a photoisomer, and not the much higher energy triplet level, is the experimentally modulatable dark state.

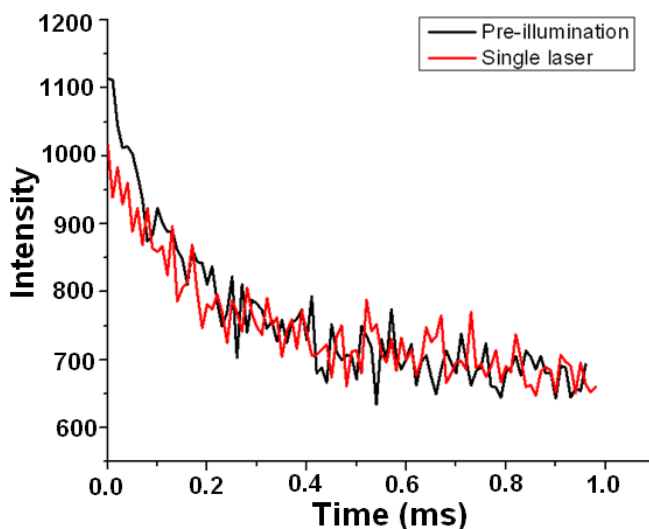


Figure 4.4. Optical recovery of thermally populated dark states. Primary-only induced fluorescence from MHI97 with (black) and without (red) secondary laser pre-illumination. The increased fluorescence with secondary-only pre-illumination relative to no secondary pre-illumination generates higher initial fluorescence intensity by optically recovering molecules from the thermally populated dark state.

Although the timescales and pre-illumination experiments suggest that photoisomerization and back isomerization give rise to optical modulation, photoisomerization can potentially occur about any of the bonds along the cyanine polymethine chain (Figure 4.5A-D for Cy5, Cy5.5, Cy7 and Merocyanine 540, respectively). Because of this, theoretical insight into different photoisomer possibilities and their energies could help us understand what is going on at the molecular level. These experimental energies are compared to theoretical photoisomer energies in table 4.1 in the next section.

4.4 Calculated photoisomer ground state energies

To gain further insight into the isomerization mechanism, density functional calculations were employed to compare ground and excited state energies of the different possible isomers. The B3LYP functional and LanL2DZ basis set were used, taking into account DMSO solvation with the polarizable continuum model (PCM), analogous to previous Cy5 calculations.^{51,81} The results of these calculations were compared to previous literature results, as well as our experimental results to ensure consistency. Exact details of this procedure are described in Appendix D. Geometry optimizations and ground state energy calculations were performed on the all-trans and each of the various cis-photoisomers, and TDDFT was used to calculate vertical excitation energies. Experimental and calculated cis-trans energy differences are compared in Table 4.1. Arrhenius-extracted activation energies for cis to trans regeneration of the bright manifold are also given as calculated from the experimentally derived rate constants for dark state decay, k_{off}^0 .

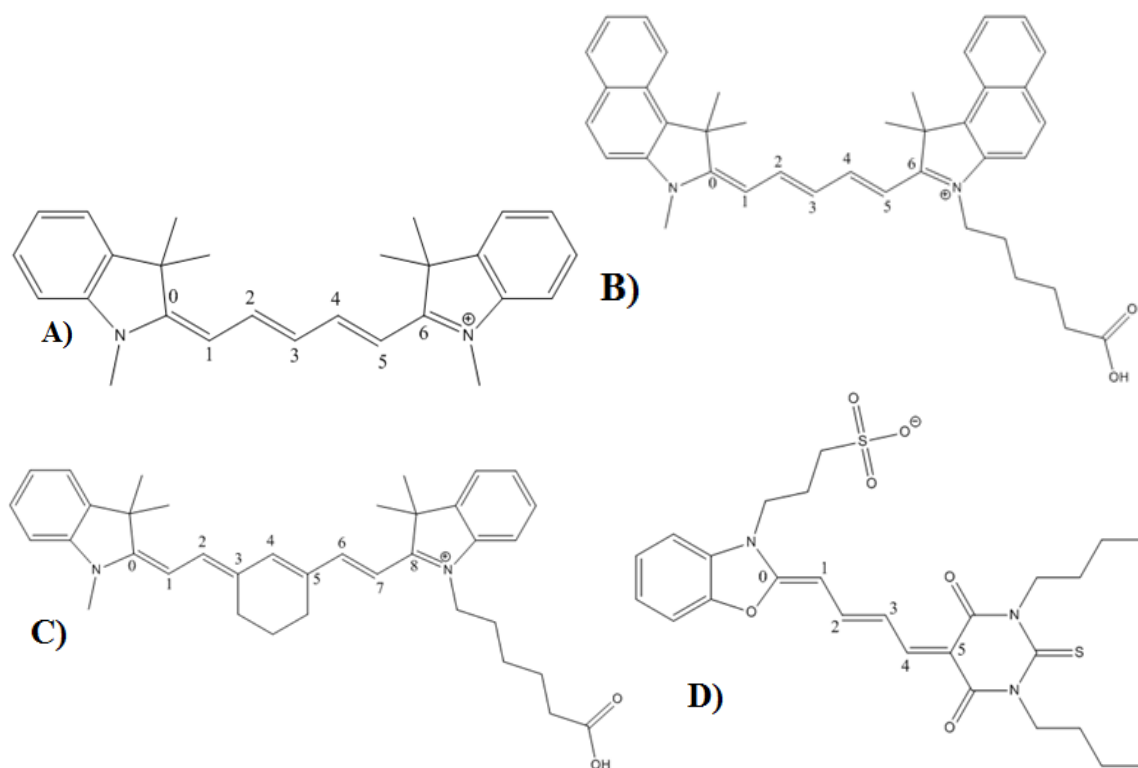


Figure 4.5. All-trans isomers of A) Cy5, B) Cy5.5, C) Cy7, D) Merocyanine 540 numbered to show isomerization possibilities. When cis isomers are described, the numbers refer to the bonds between carbon atoms. For example, cis23 refers to the bond between the 2 and 3 labeled carbon atoms.

Table 4.1. Summary of ground state DFT computational results: Cis23-Trans and cis12-Trans refer to the energy differences between the ground states of the different cis-photoisomers (as labeled in Figure 4.5) and the all-trans ground states. (Note: Due to short lifetimes, E65 and Cy7 exhibited insufficient dark state buildup to determine experimental cis-trans values.) E_a is the activation energy obtained by Arrhenius calculations using the experimental k_{off}° and setting $A = 10^{12} \text{ s}^{-1}$.⁷⁷

	Cis23-Trans (eV)	Cis12-Trans (eV)	Exp Cis-Trans (eV)	E_a (eV)
Cy5	.1345	.3091	.0757(\pm .01)	.465(\pm .04)
MHI84	.1366	.3087	.0592(\pm .008)	.470(\pm .03)
LO4	.1366	.3157	.0505(\pm .007)	.480(\pm .01)
MHI97	.09528	.2758	.0419(\pm .007)	.492(\pm .04)
MHI106	.1608	.7520	.0905(\pm .02)	.460(\pm .05)
E27	.1621	.8439	.0732(\pm .008)	.438(\pm .05)
E63	.1593	.9554	.0762(\pm .009)	.455(\pm .05)
E65	.1488	1.212		.419(\pm .06)
Cy5.5	.1349	.3033	.110(\pm .012)	.482(\pm .04)
Cy7	.2086	.7661		.426(\pm .07)
Merocyanine 540	.2985	.1628	.0540(\pm .008)	.493(\pm .04)

Comparing the DFT and experimental energy differences between cis and trans, the modulatable dark states of all cyanines other than Merocyanine 540 appear to result from isomerization around the 2-3 carbon-carbon bond. For Merocyanine, isomerization appears to occur about the 1-2 bond. The 2-3 cis isomer (and 1-2 cis for Merocyanine 540) and trans isomer energy difference is in fair agreement (\sim factor of 2) with the experimentally obtained values, while the 1-2 isomer (and 2-3 for Merocyanine) is higher in energy, and much higher in the halogenated compounds. Cis01 isomers have small energy differences compared to trans isomers and do not change much with substituents. When also taking into consideration the lack of a red-shifted transition energy, these isomers are less likely give rise to fluorescence recovery. Cis isomers other than 01, 12, and 23 are not considered for symmetric molecules, but extra data including cis01 isomers and asymmetric commercial dyes are included in Appendix B.

The combination of ground vs. dark state thermal populations, natural dark state lifetimes, and density functional theory calculations enable improved understandings of cis and trans photoisomer energy differences. Relative calculated energy differences are compared with experimental values to lend insight into which isomers are likely to give rise to the modulatable dark states for each cyanine derivative. It appears that the halogenated compounds have a larger energy difference between cis and trans isomers, a fact that could explain lower the activation barrier and observed higher reverse photoisomerization rates. On the other hand, DFT suggests that compounds with longer alkyl chains have smaller energy differences separating isomers, corroborating the observed larger activation energies and longer $\tau_{\text{off}}^{\circ}$ values. Cy5.5 does have a higher than expected experimental cis-trans energy difference, but thermal reversion is also low, suggesting a higher barrier to ground state photoisomerization. For Cy5, its derivatives, and Cy5.5, the experimental values are closer in magnitude to the DFT energy differences between the cis23 rather than the cis12 isomer, suggesting that cis23 is the photoisomer responsible for the dark state. In Merocyanine 540, however, the cis12, rather than the cis23, appears to be responsible for the photo-induced dark state, based on similarity of calculated isomer energy differences with experimental values.

4.5 Calculated photoisomer excited state energies

Time-dependent DFT excited state calculations further corroborate this interpretation as the calculated cis23 (and cis12 for Merocyanine) vertical transition energies are slightly and appropriately⁵⁰ red-shifted from that of the all-trans isomer absorption. The other isomers exhibit little to no red shift. Because of theoretical limitations of time-dependent

DFT, cyanine transition energies tend to be blue-shifted relative to the experimental values, but can be scaled to appropriate values with a linear correction factor. This has been done previously and the results in this work agree with previous literature values at the B3LYP level of theory.^{51, 121} Experimentally, the trans excitation energy is about 0.1 eV greater than the cis, which best corresponds to the excitation energy differences between the all trans and cis23 isomers. This gives further credence to the notion that the cis23 isomer is responsible for the modulatable dark state, especially when considering the theoretical ground state energy differences match well with the experimental values.

Table 4.2. Ground to excited state transition wavelengths calculated by TDDFT. The functional used was B3LYP, the basis set LanL2DZ, and DMSO solvent using the Gaussian 09 software package.

	Trans (nm)	Cis23 (nm)	Cis12 (nm)	Cis01 (nm)
Cy5	537.51	556.60	542.79	537.01
MHI84	536.20	555.10	541.42	535.83
LO4	537.18	555.38	542.39	539.33
MHI97	539.65	557.86	544.44	541.23
MHI106	536.94	563.55	543.08	536.37
E27	536.12	564.06	548.18	535.63
E63	541.08	565.60	583.31	543.28
E65	540.28	566.54	587.07	542.38
Cy5.5	578.90	596.89	583.19	575.52
Cy7	610.62	640.92	613.47	610.51
Merocyanine 540	491.10	514.15	496.10	495.62

4.6 Theoretical predictions

With the ability to calculate cyanine isomer energies, one has the capability of predicting the energies of different isomers to try to see if any other substituents might give rise to favorable photophysics. Since longer alkyl chain substituents seemed to work well in the compounds tested, theoretical structures with longer alkyl chains or sterically bulkier structures were tested. By using ground state DFT calculations (as described in section

4.4), comparing calculated Cis23-Trans energy differences to the energy differences of the already synthesized molecules allows one to hypothesize which theoretical substituents might result in improved fluorescence enhancement.

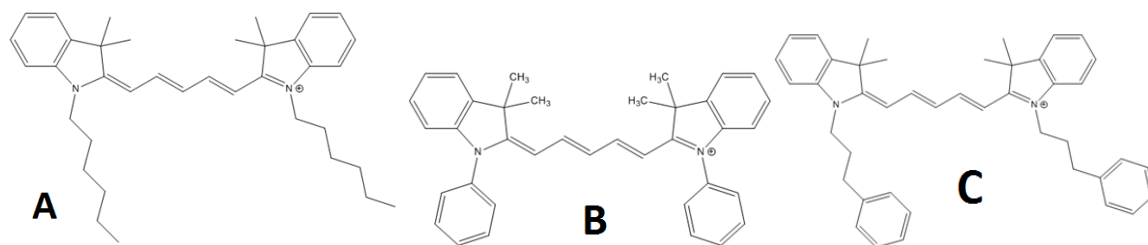


Figure 4.6. Theoretical cyanine structures tested using density functional theory. Structure A has a cis23-Trans energy of 0.137 eV, structure B has a cis23-Trans energy of 0.134 eV, and structure C has a cis23-Trans energy of 1.779 eV.

From these data, it appears that structures A and B have similar cis-trans energy differences to MHI84 and LO4, which exhibited good modulation depth (40-50%). However the energy difference is not as small as in the case of MHI97, suggesting that the Cis23 isomers of these theoretical structures might not show improvements in modulation depth. As the alkyl chains became longer than six carbons, the cis isomers became less stable due to steric hindrance. As shown in structure C, even three carbon chains with phenyl groups at the ends contain too much steric bulk to form a stable cis isomer. The energy difference in that case is greater than an electron volt. Perhaps other substituents to the nitrogen atom on the indole side group could provide more stability to the cis isomer, but in the case of alkyl chains, it appears that butyl chains provide the maximum stability.

Another idea to try was substituents on the indole side chain. In the case of aromatic rings, one electron-donating groups like NH_2 or OH or withdrawing groups such as CF_3 or NO_2 could have an effect on isomerization due to electronic effects, but no effects are seen

in ground state DFT calculations. It appears that bromine or chlorine at the o or m position destabilizes the cis23 isomer.

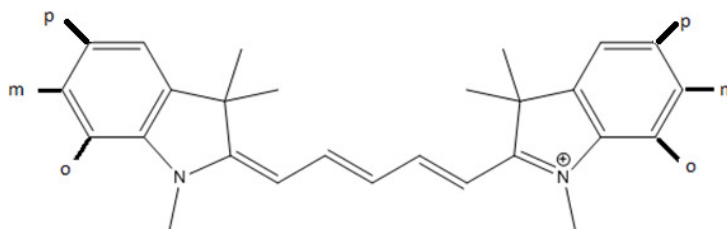


Figure 4.7. Cy5-like structure with substituents labeled at “o,” “m,” and “p” positions.

Table 4.3. Calculated energies comparing cis and all trans ground states for structures with substituents at “o,” “m,” and “p” positions. All data are in eV units.

Dye	Cis23- Trans	Cis12- Trans	Cis01- Trans	Dye	Cis23- Trans	Cis12- Trans	Cis01- Trans
oBr	0.319	0.319	0.058	oNO ₂	0.141	0.325	0.045
mBr	0.311	0.311	0.062	mNO ₂	0.140	0.312	0.060
pBr	0.137	0.310	0.062	pNO ₂	0.141	0.319	0.067
oCl	0.318	0.318	0.064	oNH ₂	0.135	0.307	0.055
mCl	0.311	0.311	0.063	mNH ₂	0.136	0.310	0.064
pCl	0.136	0.309	0.058	pNH ₂	0.131	0.298	0.059
oOH	0.135	0.308	0.072	oCF ₃	0.139	0.327	0.062
mOH	0.149	0.312	0.075	mCF ₃	0.139	0.312	0.061
pOH	0.130	0.304	0.056	pCF ₃	0.141	0.316	0.066

4.7 Testing properties of new cyanine variants

With the earlier analysis of the effects of structural modifications on cyanines, showing how different substituents can tailor photophysical properties for improved

fluorescence modulation, new cyanines were designed by the Henary lab with different substituents in order to tailor the photophysical properties. Fluorescence enhancement, photophysical on and off times, and DFT calculations were performed to characterize these new compounds. Modifications were made to the polymethine bridge and the indole side groups, as well as altogether different side groups. Because photoisomerization is so important to cyanine fluorescence modulation, substituents in the middle of the polymethine bridge are likely to impact modulation parameters. This was seen previously with halogen substitution in the middle of the polymethine bridge. In the new compounds a phenyl substitution was added that may stabilize or destabilize the photoisomer state. Additionally, substituents on the indole side group modify photophysical characteristics. Electron-donating and electron-withdrawing groups could affect the electronic properties of the polymethine bridge chromophore. Lastly, it is interesting to consider a side group other than indole. One common group is benzothiazole, in which a sulfur molecule replaces the dimethyl group on the indole ring. These new compounds were tested for modulation depth, photophysical on and off times, and DFT Cis23-Trans energy differences.

but has less overall enhancement. TRC-84 is water-soluble, unlike most of the other synthesized cyanines, has fairly high enhancement, and seems to have a very long-lived dark state. Computational efforts were originally inconclusive, suggesting that the red-shifted cis23 dark state is lower in energy than the all trans state. But after realizing that the molecule would be de-protonated in water, hydrogens on the carboxylic group were removed and the molecule was assigned a charge of -1 for the calculation, providing a more sensible answer. SP-2-28 is very similar to the previously mentioned MHI84 dye, but has benzothiazolium side groups with sulfur. This causes the ground state to be red-shifted and the cis-photoisomer to be blue-shifted so that they nearly overlap.⁵⁴ Because there is no red-shifted dark state absorption, no fluorescence enhancement is seen upon dual-excitation, but a fair amount of fluorescence is seen with secondary only excitation. ZK-311 also has benzothiazolium side groups, but it has a ring in the center of the polymethine bridge, preventing isomerization around the cis23 bond. As a consequence, there is no fluorescence enhancement or secondary only fluorescence seen.

4.8 Solution additives for manipulation of photophysics

As cyanine dyes have been utilized as fluorophores for biological imaging, certain schemes have been employed to tailor the photophysics in a way that is favorable to the application. For example, a thiol such as beta-mercaptoethanol has been used to inhibit blinking and allow for lower wavelength photoswitching. There are different theories on the mechanism, including covalent attachment to the polymethine chain⁷⁴ or a redox photochemical process.⁷¹ Other additives include triplet quenchers such as Trolox and glutathione, which stabilize fluorescence by inactivating the triplet state, which is

susceptible to blinking and photobleaching.^{65, 70-71, 74, 132-135} On the other hand, it has been shown that adding a triplet enhancer such as ethyl iodide or potassium iodide can increase the yield of both cis and trans triplet states.^{53, 57} Therefore, it is reasonable to assume that the alteration of molecular photophysics could affect the fluorescence modulation observed in cyanine dyes. To look further into this process, different molecules were added to an aqueous Cy5 solution to study how they would affect dark state behavior. Additives were included at high concentrations (~100 mM) to ensure interaction with cyanine molecules in solution.

Table 4.5. Summary of additive effects on Cy5 modulation depth and photophysics. Experiments were conducted in water, Cy5 concentrations were ~1-10 nM while additive concentrations were approximately 100 mM.

Additive	Mod depth	$\tau_{\text{off}}^{\circ}$ (μs)	ϕ_D
None	50 \pm 3%	184 \pm 20	.0014 \pm 2*10 ⁻⁴
Beta-mercaptoethanol	60 \pm 4%	165 \pm 25	.0014 \pm 2*10 ⁻⁴
Beta-mercaptoethylamine	50 \pm 3%	107 \pm 20	.00071 \pm 10 ⁻⁴
L-glutathione, reduced	66 \pm 5%	253 \pm 30	.0016 \pm 2*10 ⁻⁴
Trolox	56 \pm 2%	76 \pm 15	.00092 \pm 10 ⁻⁴
Potassium Iodide	43 \pm 3%	230 \pm 30	.0010 \pm 3*10 ⁻⁴

Modulation frequency scan experiments with a constant primary and modulated secondary laser were performed to determine modulation depth and on and off times. With this information, one could potentially gain insight into molecular photophysics as affected by solution additives. As mentioned, beta-mercaptoethanol is known to affect single molecule photophysics and could potentially impact photoisomer or triplet states. It turns out that modulation depth clearly increases, but there is no discernible effect on the modulation time scale. Perhaps some other effect such as a triplet state could give rise to the increased modulation depth. With beta-mercaptoethylamine, another thiol, the

modulation depth is unchanged compared to Cy5 alone. Glutathione, another thiol and well-known antioxidant in biological systems, increases enhancement the largest amount of any solution additive (50 to 66%). In this case it appears that the dark state lifetime and dark state quantum yield both increase, which could cause increased dark state population recovered by the secondary laser, improving modulation depth. Trolox, another known triplet quencher and antioxidant but not a thiol, increases fluorescence enhancement despite appearing to decrease dark state lifetime and quantum yield. Lastly, potassium iodide is known to increase triplet yield due to a heavy atom effect which increases the intersystem crossing rate. Adding potassium iodide to Cy5 in solution decreases fluorescence enhancement relative to Cy5 while seeming to lengthen the dark state lifetime. Overall, it appears that adding a triplet state quenching molecule to solution increases enhancement, while adding a triplet enhancing molecule decreases enhancement. This may be due to increased population in either the cis or trans triplet state, so experiments exploring the faster timescale dark states may be revealing.

Further experiments were performed using FCS to see if diffusion, triplet, and photoisomer timescales could be resolved and if conclusions could be drawn. A fast time resolution (100 ns) setup with two APD detectors was used to observe any sub-microsecond triplet timescales. However, the results were inconclusive. With three timescales close together in time, it was not possible to resolve using FCS. Increasing primary and secondary laser intensity decreased the triplet timescale in the FCS fit while increasing diffusion time, similar to standard Cy5 FCS experiments. Future experiments could be conducted in which diffusion and photoisomer timescales are better separated

from the triplet, such as immobilization, and then the photoisomer studied by itself, perhaps by quenching the triplet state.

4.9 Conclusions

By looking into cyanine electronic structure, one can develop simple models for energy levels based on the particle in a box or Hückel MO models, allowing one to approximate wave functions and energy levels. Previous research has determined isomerization barrier heights and energy levels by experimental and theoretical techniques. We have built on these results by comparing our modulation data and extracted photophysical times, which agree with previous research and our theoretical framework. Based on our experimental and theoretical data, it appears that the central bond in the pentamethine chain (called cis23 in this work) is most likely the modulatable dark state, as it is a metastable state that is slightly higher in energy than the all trans ground state, and its absorption to a higher electronic level is red-shifted relative to the all trans excitation wavelength. The cis12 state could play a smaller role, though it is higher in energy and has a less red-shifted absorption. In the molecules with higher modulation depths the cis12 could be more involved in the fluorescence recovery. Although modulation depth improvements were seen with longer alkyl chains, increasing chain length or adding bulkier substitutions did not alter the cis-trans energy difference. Perhaps there could be other ways to stabilize the cis23 isomer to further improve modulation depth.

New cyanines and solution additives were also explored. So far newer synthetic cyanine variants have not shown greater modulation depth than Cy5 or MHI97, but other technical improvements are possible, such as longer or shorter modulation timescales and

triplet dark states. It has been observed that solution additives such as triplet quencher or enhancers can affect modulation depth, with triplet quenchers such as beta-mercaptoethanol and l-glutathione increasing modulation depth while enhancing the triplet state with potassium iodide decreasing fluorescence enhancement. At this moment it is unclear why this occurs because there was not a clear trend in the modulation or FCS timescales. Further experiments which isolate the variables (triplet, photoisomer, diffusion) better may elucidate this effect.

CHAPTER 5

OPTICALLY ACTIVATED DELAYED FLUORESCENCE

5.1 Introduction

Fluorescence modulation techniques advance fluorescence imaging by controlling molecular photophysics. Whether through stochastic or deterministic control of dark state residence, transitions to nonfluorescent “dark” states can diminish net fluorescence, but can be optically reversed either thermally, or by co-illumination at a different wavelength that specifically excites the dark state. Such fluorescence modulation offers greater imaging depth and sensitivity by rejecting (non-modulatable) obscuring background emission.^{20, 36, 56, 96-97, 136} Because fluorescence enhancement and modulation result from optically induced rates into and out of photoaccessible dark states, molecular structure and chromophore environment can alter modulation depth and timescales.^{34, 98}

Different dark states appear to offer different mechanisms of modulation, particularly in the cases photoisomer and triplet states. Merocyanine 540 has both photoisomer and triplet dark states that absorb red-shifted relative to the excited state, allowing one to probe the differences between these states. It turns out that upon secondary co-illumination the photoisomer dark state returns to the all trans ground state, while the triplet recovers the singlet excited state, allowing for an optically activated delayed fluorescence effect. The characterization of this state is consistent with a triplet state, and by decreasing the oxygen concentration in the sample environment by purging with nitrogen gas one can lengthen the triplet state ~25-fold. These structural modifications,

solution/environment additives, and different dark states all allow the potential for improved fluorescence modulation.

To further investigate the mechanism of secondary modulation, one can consider whether the secondary laser returns dark state molecules to the ground or excited state of the fluorescence manifold. This has fluorescence imaging implications; it is potentially useful to be able to recover fluorescence with only the secondary laser after primary excitation and turn off. To test this, one can do experiments to “pump” the dark state population and then see the effects when only the secondary laser illuminates the sample. The main experiment performed was pulsed primary excitation with constant (not modulated) secondary excitation. In this scheme one is able to quickly build up the dark state population while looking for any potential secondary effects.

The work in chapter 4 of this thesis, both experimental and theoretical, supports a low-lying photoisomer state, approximately 0.1 eV above the all trans ground state. Conversely, triplet states are known to be much higher in energy (>1 eV), close to the excited singlet state. In fact, much research effort has been devoted to thermally activated delayed fluorescence and triplet harvesting,¹³⁷⁻¹³⁹ effects that couple the triplet and singlet excited states. This allows $S_1 \leftrightarrow T_1$ transitions, causing delayed fluorescence when a molecule undergoes intersystem crossing, reverse intersystem crossing, and eventual fluorescence. This also has been used to increase the efficiency of organic LEDs. Therefore, one could presume that these different dark states could allow for different types of modulation. Based on experiments performed in this work, it appears that upon secondary laser illumination a photoisomer dark state will photoisomerize to the all trans isomer ground state, available for subsequent excitation, while a triplet dark state will

reverse intersystem cross back to the singlet excited state and fluoresce on a delayed timescale.

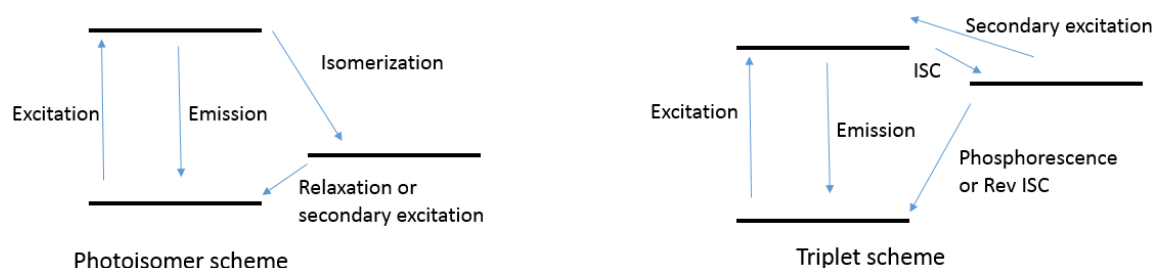


Figure 5.1. Jablonski diagrams illustrating fluorescence recovery pathways via dark state recovery. In the case of a photoisomer, both thermal relaxation and secondary excitation return the dark state to the fluorescent ground state, but in the case of a triplet dark state the excited fluorescence state is recovered, allowing for subsequent fluorescence.

The two molecules studied and compared for triplet vs photoisomer behavior were Cy5 and Merocyanine 540, both of which were studied in chapters 3 and 4. Cy5 and Merocyanine 540 both exhibit fluorescence modulation (40-50%) due to a photoisomer dark state but have different triplet absorptions. Cy5 is known to have a blue-shifted triplet absorption at 625 nm (relative to the ~645 nm singlet absorption) with a 35 μ s lifetime.⁵³ Merocyanine 540, on the other hand, has a red-shifted triplet absorption (~600-650 nm) relative to the singlet absorption (560 nm), with a ~1 μ s lifetime.^{50, 84, 140-141} From this information, one can reason that the triplet absorption in Merocyanine 540 should be susceptible to secondary laser co-illumination, at the same secondary wavelength as used for the photoisomer dark state.

5.2 Cy5 experimental results

In chapter 4, section 4.3 (illustrated in Figure 4.4), primary and secondary modulated cw experiments are used to characterize the energetics photoisomer dark states. The proof of a thermal population helps characterize the cis photoisomer as slightly higher in energy than the all trans ground state. It is also useful to know how the recovery path from the dark state to the fluorescent state, particularly if upon secondary illumination the dark state goes to the fluorescent ground or excited state. If the excited state is recovered, subsequent fluorescence would be expected, whereas in the ground state fluorescence enhancement would be seen upon primary illumination only.

To investigate this, it is useful to excite with a pulsed primary laser and constant secondary laser. With this setup, the primary laser pulse populates the dark state then is shut off, allowing only secondary effects on the populated dark state to be observed. These results can be used to determine the fluorescence recovery pathway from the dark state.

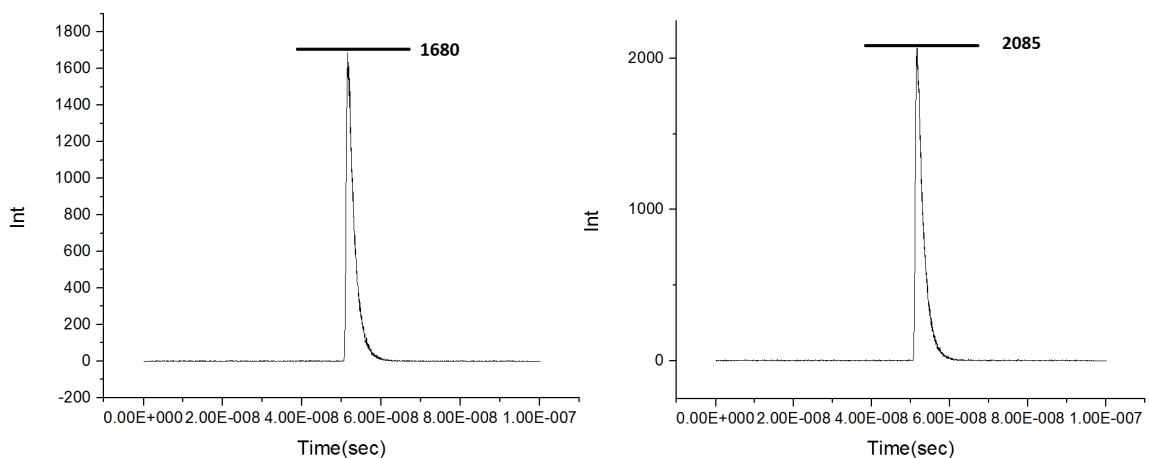


Figure 5.2. Cy5 fluorescence with pulsed primary (647 nm) excitation with and without constant secondary (710 nm) excitation. Left: Pulsed primary with no secondary laser. The peak height is 1680 counts, and the decay is 1 ns. Right: Pulsed primary excitation with constant secondary excitation. In this case the peak height is 2085 counts and the decay is also 1 ns.

From the figure above, one can see that by turning on the secondary laser there is no change in the fluorescence decay, which matches the 1 ns typical Cy5 lifetime, but the primary laser peak height increases by ~24%. This is the same amount of fluorescence enhancement seen with the bulk signal, that is the increase of fluorescence intensity on a CCD or APD detector when the secondary is turned on. From this behavior it appears that the secondary laser will increase the intensity of primary laser fluorescence, but not cause any additional fluorescence upconversion effects. In terms of photophysical mechanism, the secondary laser causes the dark state to recover the fluorescent ground state, not the fluorescent excited state.

5.3 Merocyanine 540 experimental results

Upon primary excitation an exponential fluorescence decay is observed, but this decay disappears with secondary co-illumination due to depopulation of the dark state. However, when the secondary is turned on only in between the primary laser pulses, the primary induced fluorescence decay becomes steeper as a result of a greater initial dark state population. These properties are characteristic of the relatively low energy difference between different isomers. When the energy difference is small enough, the dark state is non-negligibly populated at room temperature.

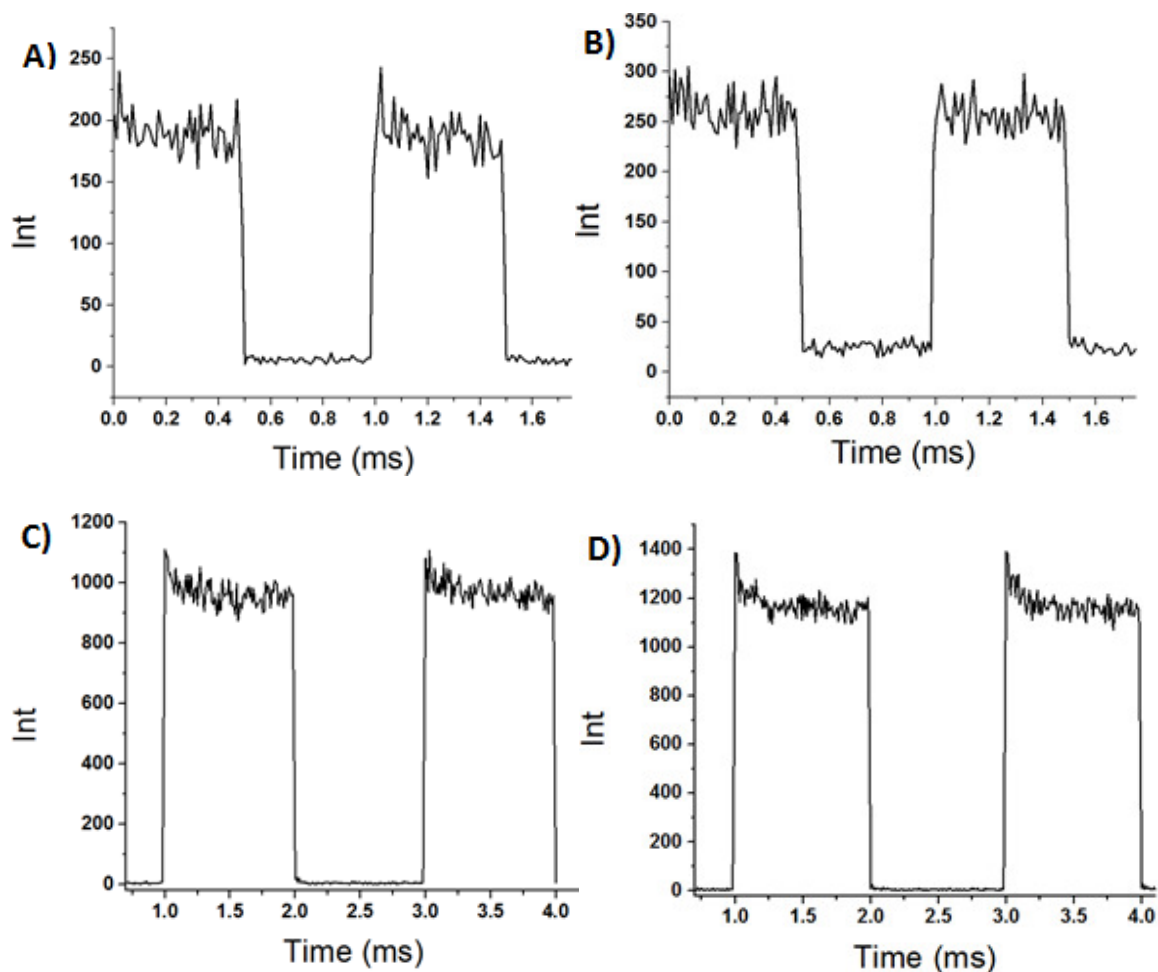


Figure 5.3. Fluorescence of Merocyanine 540 in water. A) modulated primary excitation (543 nm, 600 W/cm²), B) modulated primary plus constant secondary co-illumination (637 nm, 10 kW/cm²), showing elimination of fluorescence decay due to lack of dark state build up. C) modulated primary excitation (5 kW/cm²), D) Alternating modulated primary and secondary (14 kW/cm²) excitation, causing greater fluorescence decay due to photoisomer depopulation to the ground state.

Next, Merocyanine 540 was studied with the pulsed-CW setup. With 1 μ s time resolution, a small shoulder is observed, hinting at fluorescence upconversion due to triplet effects. Faster time resolution reveals a sub-microsecond time scale consistent with triplet state data from the literature, and a dependence on secondary power. By integrating the primary and secondary fluorescence, one finds that the secondary fluorescence to primary fluorescence is .005, or .5%. Since this is much lower than the 40-50% bulk fluorescence

enhancement, one can reason that most of the enhancement observed comes from the photoisomer dark state rather than the triplet dark state.

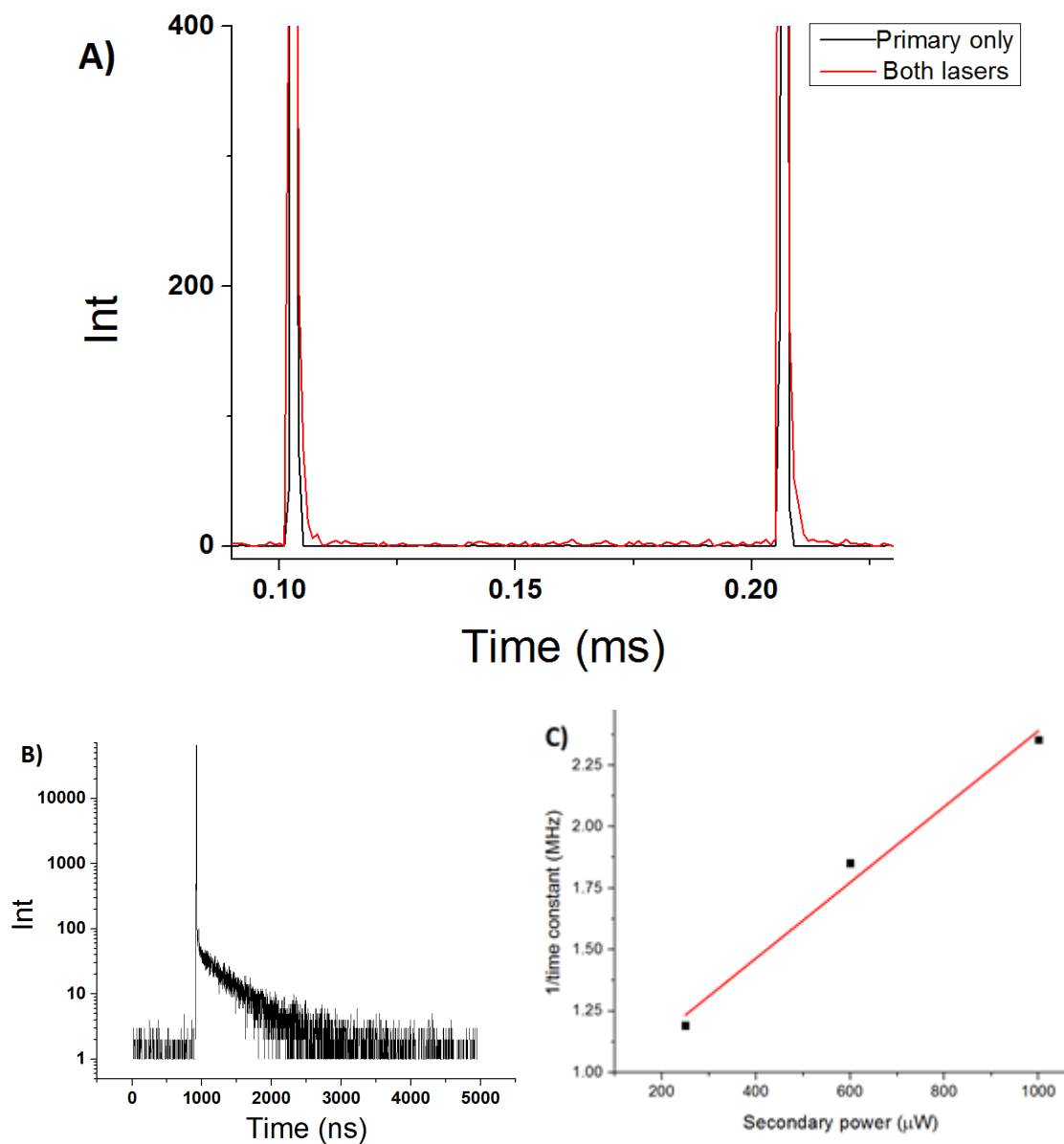


Figure 5.4. Merocyanine 540 fluorescence in aqueous solution using 532 nm pulsed excitation (rep rate 10 kHz) with and without secondary (637 nm) co-illumination. Optically activated delayed fluorescence is observed when the secondary laser is present, presumably due to a repumping of the excited bright state. A) Pulsed primary with and without secondary illumination. With the addition of the secondary laser a slight upconversion tail is observed at the end of the pulse. B) Pulsed primary plus secondary with ~ 1 ns time resolution, showing OADF more clearly. C) Secondary power dependence

of fluorescence decay. Higher power (or intensity due to constant spot size) shortens the observed timescale due to faster depletion of dark state.

The figure above illustrates the ~100 ns timescale fluorescence upconversion observed with Merocyanine 540 which is not observed with Cy5. There is a clear power dependence, with higher power shortening the dark state lifetime. This can be attributed to a power dependence on rate, so that $k_{off} = k_{off}^o + \frac{\sigma_{biso} I_{sec}}{h\nu}$ where k_{off}^o represents the natural dark state decay without secondary while the latter term characterizes the secondary intensity dependence (σ_{biso} is the action cross section for reverse intersystem crossing back to the singlet manifold²²). By plotting the decay rate at different secondary powers (or intensities as the area is constant), one can obtain the y-intercept which is the natural off rate. The timescale obtained matches the ~1 μ s triplet timescale from the literature.⁵⁰

5.4 Triplet state lifetime modifications

Triplet states are readily quenched by molecular oxygen, hastening their nonradiative decay,⁵⁹⁻⁶⁰ and as a consequence are environment dependent. By purging solutions with N₂ gas, one can decrease O₂ content of the sample, extending triplet lifetime. Another way to decrease O₂ content is by introducing an enzymatic oxygen scavenging system consisting of glucose, glucose oxidase, and catalase.⁷⁰⁻⁷¹ Glucose oxidase and catalase enzymes catalyze the reaction of glucose and oxygen to gluconic acid and water, thus decreasing molecular oxygen concentration. Lastly, immobilizing in polyvinyl alcohol (PVA) films significantly extends the secondary laser-excited emission (triplet) lifetime. PVA likely extends the triplet lifetime through rigidification, inhibition of collisional quenching, and low oxygen content/mobility. These environmental effects are illustrated

in Figure 5.5, showing a clear extension of the secondary fluorescence upconversion timescale when compared to merocyanine in water (Figure 5.4). N₂ gas purging and the oxygen scavenging system increase the timescale ~15-fold, while PVA immobilization most dramatically extends repumped fluorescence lifetime, up to ~45 μ s. These data are summarized in Table 5.1.

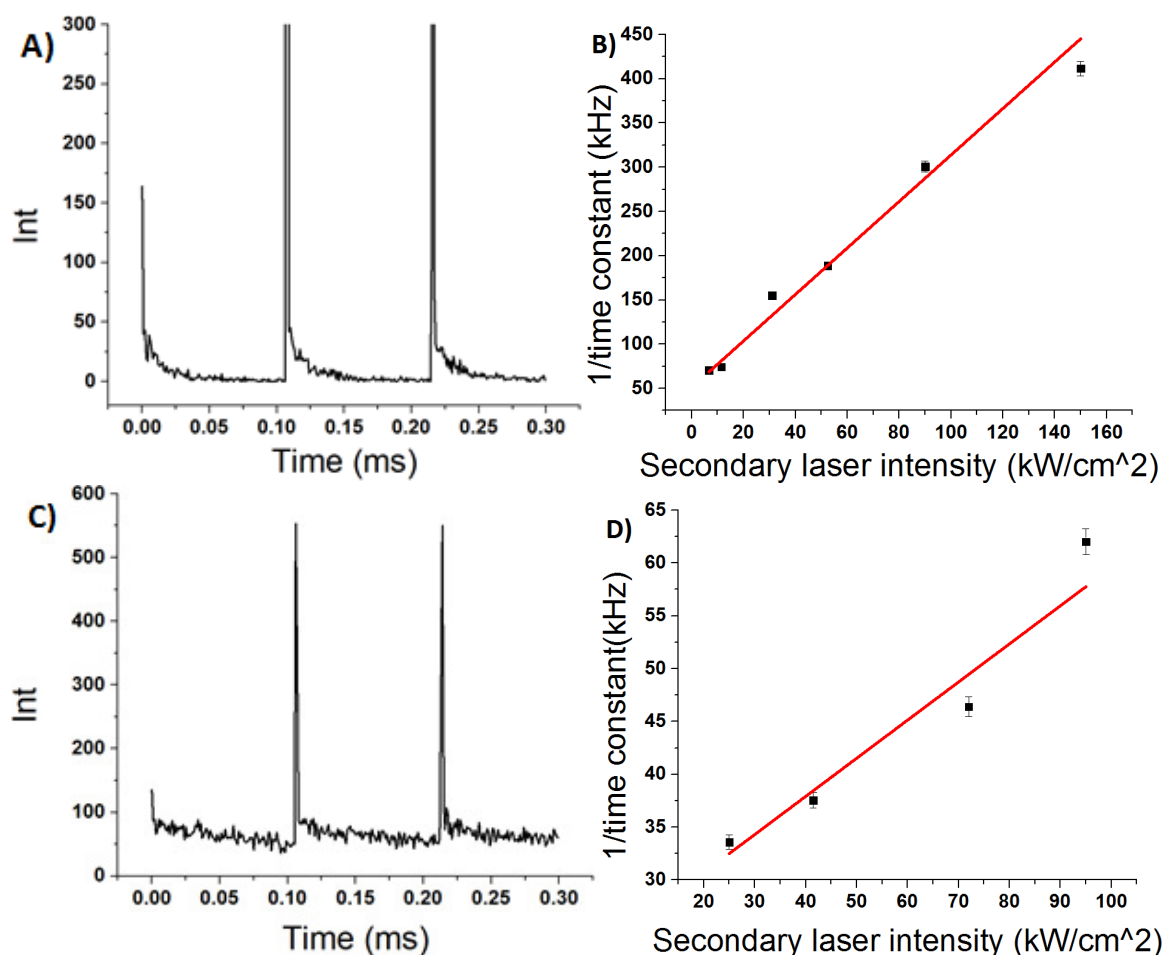


Figure 5.5. A) Pulsed-CW data for Merocyanine 540 in water after nitrogen purging. The secondary fluorescence is much longer lived. B) Secondary power dependence with N₂ gas. The dark state lifetime is 16.1 μ s. C) Pulsed-CW data for Merocyanine 540 in PVA. D) Secondary power dependence in PVA. The dark state lifetime is 45.5 μ s.

Table 5.1. Photophysical OADF properties of Merocyanine 540.

Fluorescence lifetime	775±25 ps
Triplet lifetime in water	1.18±0.175 μ s
Triplet lifetime in water, N ₂ purging	16.1±0.49 μ s
Triplet lifetime in oxygen scavenging system	14.5±2.5 μ s
Triplet lifetime in PVA	45.5±7.3 μ s

In previous work utilizing fluorescence modulation in cyanines, with CW primary and secondary lasers, a photoisomer dark state was responsible, but triplet dark states can work as well, as seen in xanthene dyes.⁹⁶ By performing experiments to distinguish between photoisomer and triplet behavior, one can understand the properties of these dark states. Photoisomer dark states are close in energy to the ground state, on the order of .1 eV, which allows for a small amount of thermal population at room temperature. By pre-illuminating with a secondary laser to deplete this thermal population, a greater fluorescence decay can be seen upon primary laser excitation. This effect has been observed in both Cy5 and Merocyanine 540, confirming the presence of photoisomer dark states. However, no fluorescence is observed by shining a secondary laser without a primary laser, suggesting that photoisomer dark state molecules simply return to the emissive manifold bright state, ready for subsequent fluorescence excitation. This hypothesis is confirmed by the pulsed-CW experiments with Cy5 (Figure 5.2). By distinguishing between primary and secondary effects (the primary laser is on briefly while the secondary is always on) it turns out that the secondary laser increases primary fluorescence intensity without causing any other fluorescence. Ultimately this strongly

suggests that photoisomer dark state, upon secondary laser excitation, returns to the ground state as opposed to the excited state.

Alternatively, a triplet dark state offers different properties than the photoisomer. Because it is higher in energy (>1 eV) it couples to the excited state in the emissive manifold, and experimentally results in optically activated delayed fluorescence, as seen in the pulsed-CW experiments (Figures 5.4 & 5.5). In terms of applicability, this is advantageous because it allows for an upconversion process in which dark state molecules can be repumped as subsequent fluorescence. The red-shifted nature of this secondary excitation allows for detection of fluorescence signal over very little background. The timescales for this process are dependent on the sample environment, primarily O_2 concentration, ranging from very short in aqueous solution in normal air (~ 1 μs), to longer in a nitrogen environment (~ 16 μs) or oxygen scavenging system (~ 15 μs), and even longer in PVA (~ 45 μs). The ability to control triplet lifetime as well as the longer wavelength fluorescence upconversion properties of the modulation of a triplet state promise much use in applications.

The only dark state capable of fluorescence modulation in Cy5 is the *cis* photoisomer. The triplet state in Cy5 absorbs slightly blue-shifted relative to the singlet ground state. There is also a *cis* photoisomer triplet state with a red-shifted absorption,⁵³ but no fluorescence was observed with the pulsed-CW experiment, meaning that there is likely a non-radiative relaxation pathway. In the case of Merocyanine 540, both the photoisomer and triplet state have red-shifted absorptions relative to the ground state absorption so the secondary laser can activate both dark states, as seen in the CW modulation experiments compared to the pulsed-CW results. Therefore, Merocyanine

offers the unique property of having two possible dark states with distinct fluorescence modulation properties.

5.5 Conclusions

Photoisomer and triplet dark states in fluorescent molecules offer different modulation properties due to their bright state recovery pathways. This has been studied in Cy5 and Merocyanine 540 by different fluorescence modulation techniques. In the modulation scheme where a primary laser induces fluorescence and a red-shifted secondary laser excites a dark state, it has been shown that the photoisomer dark state molecules return to the emissive manifold ground state while the triplet dark state molecules return to the excited state. This means that after secondary illumination, fluorescence is observed in triplet dark state molecules, but not in photoisomer dark state molecules. Cy5 only has a photoisomer dark state capable of modulation, but Merocyanine 540 has both photoisomer and triplet dark states, making it capable of both ground and excited state recovery. Furthermore, in Merocyanine 540 the dark states can be controlled by sample environment; eliminating oxygen or immobilizing in PVA increases the triplet dark state lifetime. With this insight, other fluorescent molecules with similar photophysical properties can be tested in a similar protocol, and the fluorescence upconversion observed could be useful in imaging studies to offer background free fluorescence with greater signal sensitivity.

CHAPTER 6

PROTEIN-CHROMOPHORE BINDING MODULATION

6.1 Introduction

Fluorescent proteins are particularly useful due to their biological applications. They can be expressed in cells, and the ability to be modulated allows for acquisition of data with greater signal to background ratio. Photoswitching behavior in FPs was discovered about twenty years ago, when green fluorescent protein (GFP) mutants were studied in single molecule environments. It turned out that upon continuous irradiation with 488 nm excitation, these particular GFP mutants would transition to a nonfluorescent state, from which fluorescence could be recovered by a 405 nm secondary illumination.³⁵ More recently, different types of fluorescent proteins exhibit modulated fluorescence, spanning the visible spectrum from blue to green, cyan, yellow, and red. Both long wavelength fluorescence recovery (SAFIRE) as well as shorter wavelength secondary laser photoswitching mechanisms have been applied to improve fluorescence imaging over biological background.^{34, 36, 136} The protein and chromophore structural dependence of modulation and environmental factors were tested to determine the effects on fluorescence wavelength, modulation depth and characteristic frequencies.

By themselves, FP chromophores (and their structural variants) do not fluoresce brightly in solution when unbound. The fluorescence increases greatly when bound by a protein or aptamer, primarily due to inhibition of the torsional motion of the chromophore.^{33, 90-91, 142-145} As detailed in section 1.5, fluorescent protein chromophore photophysics has been studied by time-resolved spectroscopy, and two processes that are

likely involved in fluorescence modulation are photoisomerization and intramolecular proton transfer.^{37-38, 89} Of particular interest to this research are the human serum albumin (HSA) binding compounds, which have shown to be capable of fluorescence modulation. This process is shown schematically in the figure below, in which a non-emissive chromophore becomes fluorescent upon binding to HSA.

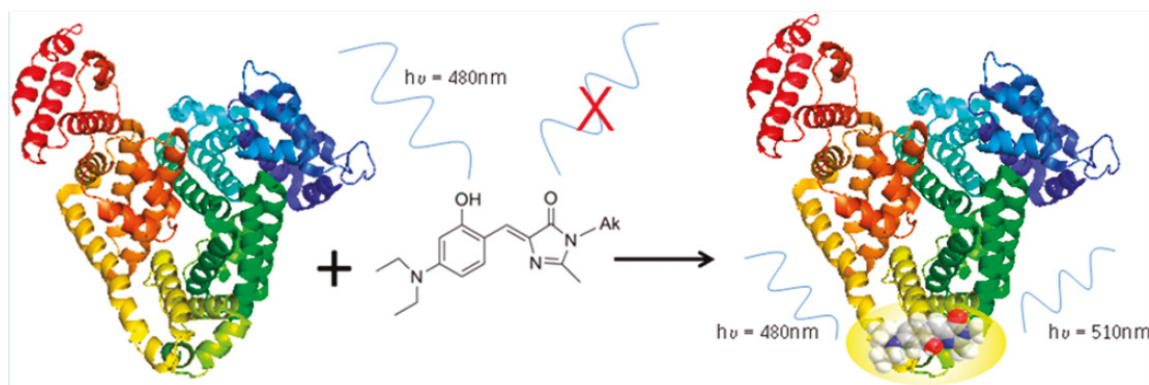
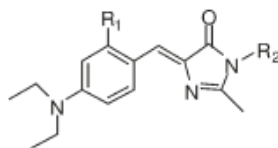


Figure 6.1. Fluorescence activation by binding to HSA.³³ The protein-binding molecule is by itself weakly fluorescent, but becomes much brighter upon encapsulation by the binding pocket of the protein.

This fluorescence “turn-on” effect depends on the molecular structure of the chromophore. As depicted in Figure 6.2, the chromophore has a diethyl amine group at the para position of the aryl ring, and a hydrogen or hydroxy group at the ortho position (R_1), as well as an R_2 substituent--an alkyl chain or butyrate. The optimal substituents turn out to be hydroxy at R_1 and heptyl at R_2 , which, upon binding, increases the fluorescence about seventy times the unbound value. Fluorescence titration of the chromophore with increasing HSA concentration follows a two-site binding model (binding to Sudlow’s sites I and II) with dissociation constants of 240 and 450 nM.³³



	R ₁	R ₂	F/F ₀ ^a		R ₁	R ₂	F/F ₀ ^a
1	H	Me	3	8	OH	pentyl	36
2	H	<i>n</i> -Pr	11	9	OH	hexyl	67
3	H	pentyl	24	10	OH	heptyl	72
4	H	hexyl	20	11	OH	octyl	52
5	H	C ₃ H ₆ CO ₂ H	6	12	OH	undecyl	7
6	OH	Me	30	13	OH	C ₃ H ₆ CO ₂ H	28
7	OH	<i>n</i> -Pr	48				

^a Intensity(bound)/Intensity(unbound) at λ_{em} for 7.5 μ M (0.5 mg/mL) HSA solutions.

Figure 6.2. Different GFP chromophore derivatives and their fluorescence increase upon binding to HSA.³³

GFP chromophore variants that bind to RNA aptamers with a similar fluorescence “turn-on” effect have been analyzed for binding and photoconversion kinetics.¹⁴² Unlike GFP, the RNA aptamer “Spinach” did not exhibit photobleaching but exhibited a recoverable fluorescence decay when primary excitation was turned on and off using square wave modulation. The fluorescence decay was intensity and concentration dependent, and binding kinetics were measured to be $k_{bind} = (6.2 \pm 0.1) * 10^4 \text{ M}^{-1} \text{ s}^{-1}$ and $k_{unbind} = (2.4 \pm 0.1) * 10^{-2} \text{ s}^{-1}$ with $K_D = 390 \text{ nM}$. Most likely, there are concurrent binding and photoconversion effects and it could be that bound chromophores photoconvert to a dark state prior to unbinding.

Different molecules are capable of binding and fluorescing with different properties. The HSA-binding chromophore can also bind to β -lactoglobulin, Bovine Serum

Albumin (BSA), and Rat Serum Albumin (RSA), although the fluorescence is weaker than with HSA. Additionally, different chromophores can bind to cholate aggregates, RNA, or can be used as pH sensors.^{33, 90-91, 142, 145} The RNA aptamer binding chromophores were expressed in *E. coli* and modulated based on the binding/unbinding kinetics to recover signal over background. Thus, the fluorescence “turn on” effect has been shown to have several real world applications, particularly in sensing and fluorescence imaging.

One other fluorescence modulation application for the HSA-binding chromophore is phase advance. Phase advance modulation is based on dark state decay behavior. In the case of modulated sinusoidal excitation, A phase lag can exist due to transitions out of and back into the fluorescent state,¹⁴⁶⁻¹⁴⁷ but a more unexpected phase advance was first discovered in molecules with a triplet dark state,¹⁴⁸⁻¹⁴⁹ and later applied to photoswitchable fluorescent proteins.¹⁵⁰⁻¹⁵¹ The main concept is that over the course of fluorescence emission, intensity is initially high but then decays as molecules transition into the dark state. In the case of sine wave modulation this appears as a pseudo-phase advance in which sine wave fluorescence appears phase advanced relative to an instrument response function or fluorescence from a fluorophore without a dark state. In addition to single and dual laser modulation schemes, phase advance modulation offers another application in which one could discriminate signal from background.

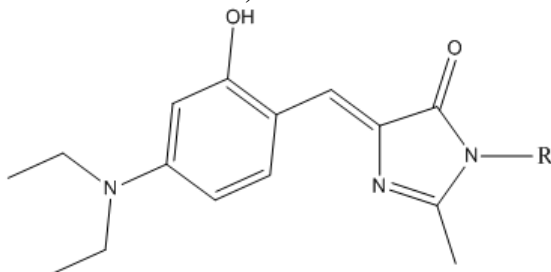
6.2 Fluorescence modulation of protein-binding chromophores

Because different fluorescent proteins have shown long wavelength secondary laser modulation capability, it is reasonable to believe that these photophysics also apply to the structurally similar protein-binding chromophores. Photoisomerization along the middle of

the chromophore is likely to allow the protein binding chromophore to work similar to modulatable fluorescent proteins. Additionally the binding-unbinding processes affect fluorescence intensity and modulation. Compound 10 (described in Figure 6.2) when bound to HSA absorbs around 475 nm and emits around 510 nm. For fluorescence modulation, an experimental setup similar to green fluorescent protein mutant AcGFP³⁶ with a 476 nm primary laser (Argon Ion, Coherent Innova 90) and 561 nm (Sapphire, Coherent) secondary laser works well. After primary illumination, secondary modulation at 561 nm yields fluorescence recovery up to 40%. This result and the corresponding photophysical effects have been studied by experimental methods to elucidate the photophysical mechanism and determine which effects are due to photoswitching compared to binding.

First, the HSA-binding chromophore fluorescence modulation was studied by dual laser (476/561 nm) modulation. Chromophores can be studied on their own in DMSO, though the fluorescence and modulation are minimal (~70-fold less fluorescence and ~4% fluorescence enhancement with >5 kHz modulation frequency). When the chromophores bind to proteins, torsional motions are inhibited and consequently fluorescence brightness and modulation depth increase greatly, while modulation frequency decreases. For this experiment, samples were prepared by combining chromophores and HSA in PBS (pH 7.4). Modulation depth and frequency scans were recorded for various chromophores bound and unbound to HSA, these data are summarized in the table below.

Table 6.1 Summary of HSA binding compounds fluorescence modulation. Modulation depth generally increases while characteristic frequency decreases upon binding. k_{dark} was obtained by fitting to the frequency domain lifetime equation and extrapolating to zero primary intensity (explained in section 3.3).



Name	R	Mod depth (unbound)	Mod depth (bound)	k_{dark} (Hz)
AB113	Heptyl	6%	37%	140
AB120	Octyl	4%	17%	200
AB116	Hexyl	4%	12%	100
AB114	Propyl	4%	10%	375
AB178	Phenyl	3%	4%	n/a
AB177	3-pentyl	5%	0%	n/a

As mentioned, modulation depth increases and characteristic frequency decreases upon binding. Based on the data in table 6.1, it appears that a heptyl R group is optimal for binding and enhancement. Octyl and hexyl, which both differ from heptyl by one carbon atom, have slightly less enhancement while other substituents did not fare as well.

Because modulation timescales observed appear to be fairly slow (>1 ms), it is desirable to eliminate diffusion in and out of the focal volume to ensure molecules don't diffuse before photoconversion between bright and dark states can occur. To achieve this, samples were prepared by adding the protein-binding small molecule to HSA in a PBS solution and combining in a 1% w/v agarose solution to heat and gel. The agarose gel significantly slows diffusion processes.

To analyze modulation timescales, dual laser modulation was first applied using a secondary laser frequency scan as well as a time trace analysis. It appears the modulation

timescales are very slow compared to cyanines, with characteristic frequencies in the 10-100 Hz range. The data for two laser modulation is shown in the figure below.

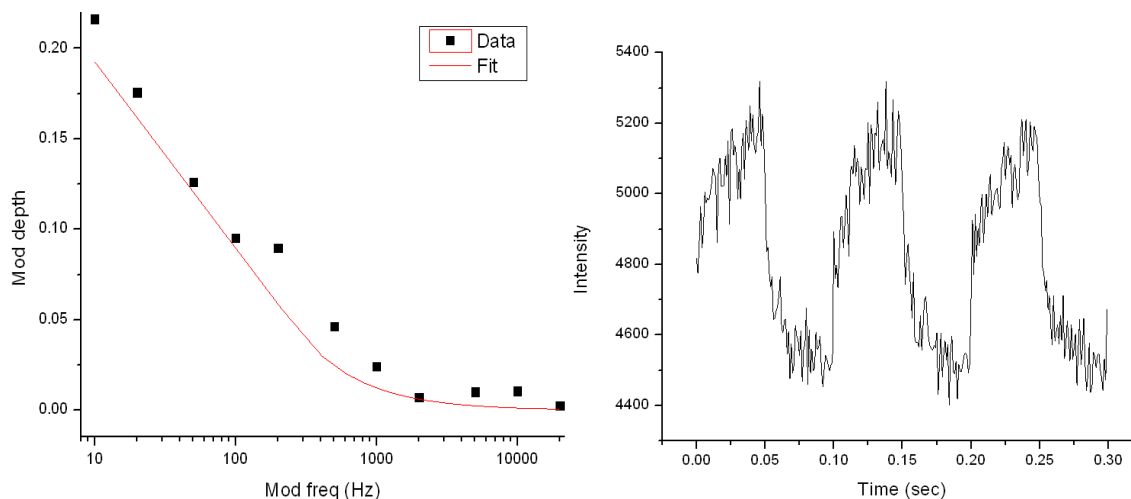


Figure 6.3. Two laser data for the HSA-chromophore complex in which the primary laser is constant and secondary laser is modulated. In the image on the left the modulation depth is recorded over many modulation frequencies while in the image on the right a fluorescence intensity time trace is take over the modulation cycle.

The frequency dependence appears to be less clear than in the case of cyanines, likely due to multiple timescales being involved (potentially photoisomerization, binding, photobleaching), so obtaining clear timescales and a power dependence was very difficult. To complement this approach, a time trace average was taken in which 10 Hz modulation cycles were recorded and fitted with exponential functions. The modulation frequency scan data suggests a timescale in the region of ~20 ms, but the power dependence trend isn't definitive. Analysis of the microtime data shows a clearer trend, with timescales also around 10-20 ms. Higher protein concentration may increase k_{off} frequencies (shorten off times).

Interestingly, and unlike other modulatable fluorophores such as cyanines, the HSA-chromophore complex modulation depth depends on HSA concentration, suggesting

that protein-chromophore binding effects play a role the fluorescence modulation observed. These data are summarized in the table below.

Table 6.2. Concentration dependence of HSA on fluorescence modulation. HSA concentration varies while chromophore concentration stays constant at approximately 5 μM . Laser intensities were approximately 1.4 kW/cm^2 and 5 kW/cm^2 for 476 nm primary and 561 nm secondary excitation, respectively.

HSA concentration	Mod depth
500 nM	13%
750 nM	15%
1 μM	17%
5 μM	27%

For a non-binding fluorophore, fluorescence modulation is concentration-independent because the modulation and DC components are proportional to molecular concentration. However, in the case of binding molecules where only the bound complex is capable of modulation, having a greater number of bound complexes will lead to greater fluorescence recovery and modulation. Therefore, when concentration is within a few orders of magnitude of the binding constant, by increasing the relative protein (or chromophore) concentration modulation depth will increase.

6.3 Time trace analysis of HSA-complex photophysics

One laser experiments in which the sample was illuminated by square wave excitation pulses were also analyzed for fluorescence decay, and the data fit best to a bi-exponential fit, suggesting a fast and slow timescale. The fast timescale is in the range of 10-50 ms, while the slower timescale is around 150-250 ms. It is likely that one timescale applies to a photophysical dark state, and another to chromophore-protein binding. Since the observed modulation timescales for the HSA-complex are in the millisecond range, one

can record the fluorescence time trace and watch the modulation effects in real time by turning the primary and secondary lasers on and off. When the primary laser (476 nm) is turned on, there is a sharp initial decay, followed by a slower decay. The count rate will also continue to drop long term, indicating photobleaching. Thus, there are at least three processes occurring simultaneously: dark state photoconversion, binding/unbinding, and photobleaching. Upon secondary laser (561 nm) illumination some 476 nm-excited fluorescence is recovered, which allows for modulation. Interestingly, the fluorescence recovered by the secondary laser appears to remain relatively constant independent of primary power and as a result the relative fluorescence enhancement decreases with increasing primary intensity. This is an unusual phenomenon; when primary intensity increases, the dark state population typically increases due to a decreased “on time” (the time fluorophores spends in the bright state before transitioning to dark). It is possible that the dark state absorbs the primary laser wavelength, shortening the “off time,” but in that case the fluorescence decay would be less pronounced (less steep), which is not what is seen here. It appears that the binding qualities of the protein-chromophore complex cause a less straightforward path than just bright state \rightarrow dark state \rightarrow bright state, with binding and unbinding states playing a role.

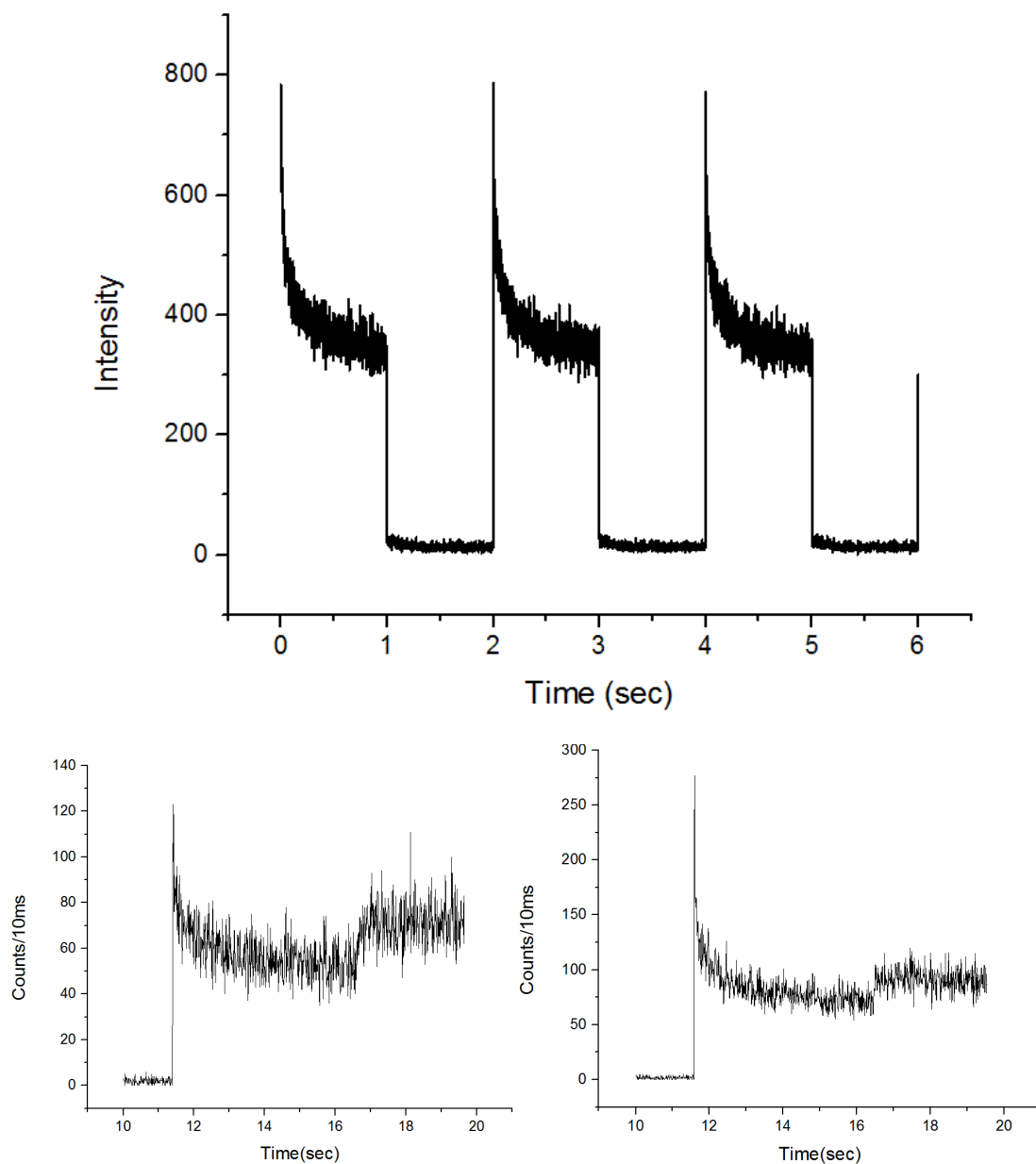


Figure 6.4. Top: Fluorescence time trace of HSA-chromophore complex with only primary illumination modulated at 0.5 Hz showing bi-exponential decay behavior (476 nm, ~ 340 W/cm²). Bottom: Time traces of HSA-chromophore complex beginning with primary only excitation and later a constant fluorescence bump due to secondary laser turn on. Bottom left: Lower primary intensity (100 W/cm²), Bottom right: Higher primary intensity (600 W/cm²).

6.4 Fluorescence phase advance

As mentioned in the chapter introduction, an “anomalous phase advance” exists when over the course of fluorescence emission, intensity is initially high but then decays as molecules transition into the dark state. This appears as an exponential decay during square wave modulation but for of sine wave modulation appears as a pseudo-phase advance compared to non-modulatable fluorescence. This allows one to detect fluorescence modulation by using a lock-in amplifier or time trace analysis. A schematic is shown below.

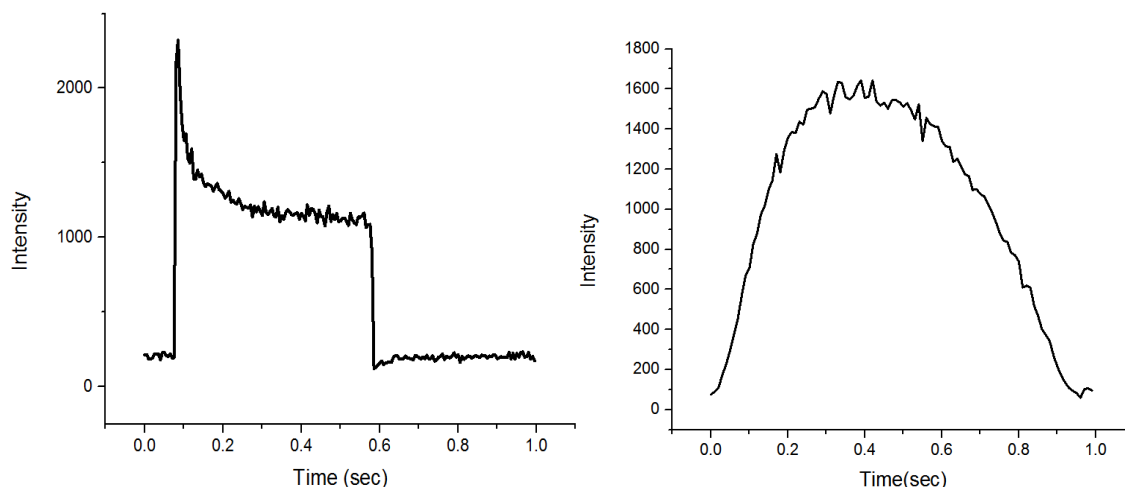


Figure 6.5. HSA-chromophore complex fluorescence with square wave (left) and sinusoidal (right) excitation. With square wave excitation a decay due to dark state behavior is clearly seen, and with sinusoidal excitation a slight phase advance can be observed.

Since this phase advance is due to dark state behavior, the phase advance effect is most pronounced at the conditions for greatest fluorescence decay upon primary excitation, which are low primary intensity and low modulation frequency. The phase advance diminishes or goes away with higher primary power or higher modulation frequency. These characteristics allow for improved signal sensitivity and selectivity if used in fluorescence

imaging, as only fluorophores with the appropriate dark state characteristics will be detected upon demodulation.

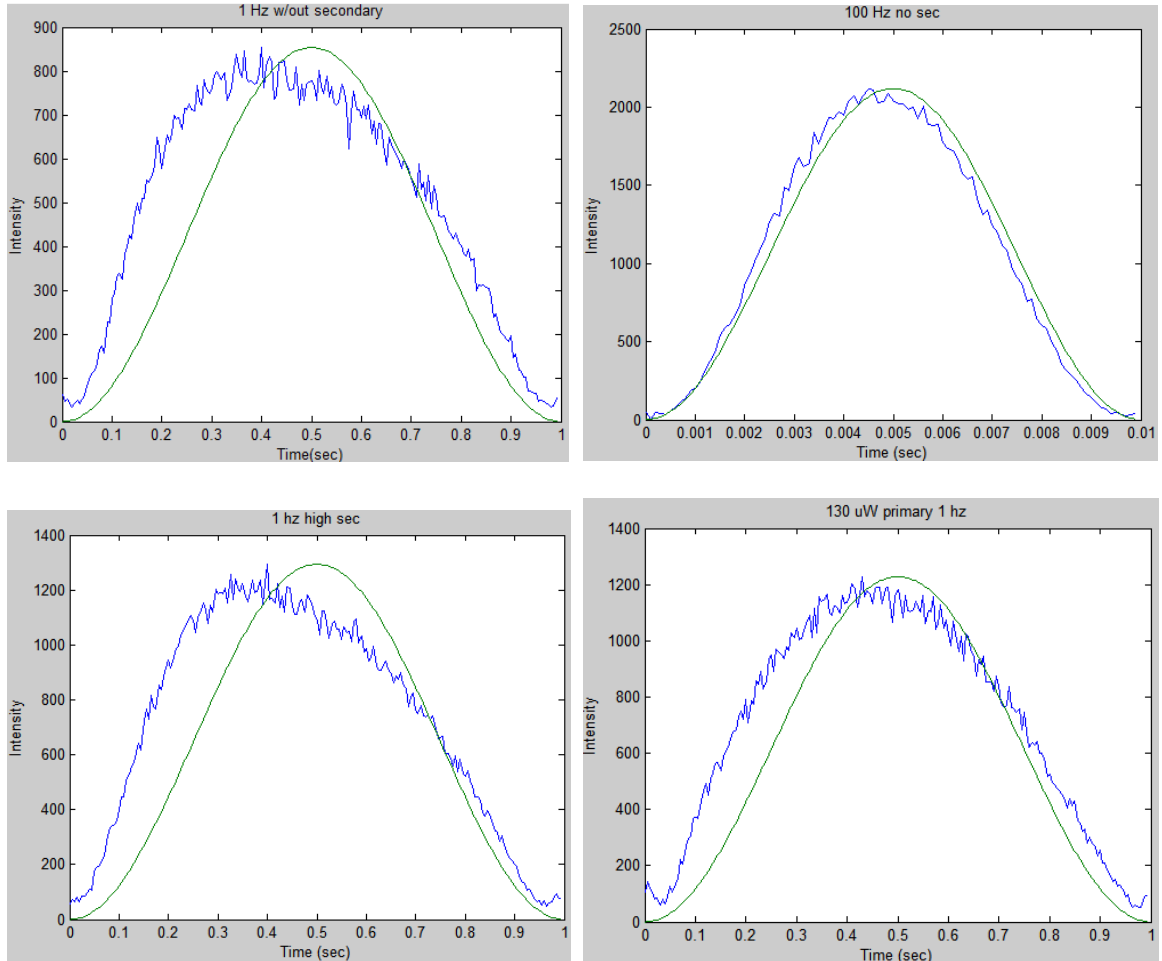


Figure 6.6. Comparison of phase advance with different laser intensity and modulation conditions. A) 1 Hz sine wave modulated primary at 1 kW/cm². B) 100 Hz sine wave modulated primary at 1 kW/cm². C) 1 Hz sine wave modulated primary at 1 kW/cm², plus constant secondary at 100 kW/cm². D) 1 Hz sine wave modulated primary at 13 kW/cm².

Interpreting the figure above, there is a clear phase advance at 1 Hz with low primary, and this phase advance disappears at higher modulation frequency. The addition of a secondary laser or increase of primary laser intensity does not greatly affect the phase advance. This is because all that is needed to observe a phase advance is a primary laser induced

fluorescence decay. The secondary laser does not get rid of this, it only diminishes the decay slightly. Furthermore, increasing the primary laser intensity does not get rid of the phase advance because higher intensity increases the fluorescence decay. Therefore, it appears that the phase advance effect observed in the HSA-chromophore complexes is photophysics dependent, but only modulation frequency affects the degree of phase advance, because at higher modulation frequency the fluorescence is turned on and off faster than the dark state can respond. This could be used in imaging applications: fluorophores with a phase advance could be detected over fluorophores without, and the phase advance can be controlled by laser intensity and modulation frequency.

6.5 Conclusions & Future Work

Protein-binding chromophores, which are known to be susceptible to photoconversion (isomerization, deprotonation, etc.) as well as binding processes, have proven applicability in single and dual laser modulation schemes. In the case of HSA-binding chromophores, GFP structural variants were synthesized and shown to increase fluorescence as well as exhibit modulation. Fluorescence recovery of up to 40% occurs with secondary laser co-illumination, as well as significant dark state decay with square wave primary only illumination. This fluorescence decay property also allows for a pseudo-phase advance, which is dependent on modulation frequency. Analysis of modulation has proven difficult, without a clear intensity or concentration dependence, but seems to yield two timescales, which are presumably due to photoconversion and binding processes, although photobleaching may also play a role.

Moving forward, there may be other ways to isolate and analyze timescales. For example, when studying a RNA aptamer-chromophore binding complex, researchers added low concentrations of chromophore and aptamer and shined a low-intensity lamp on the solution, allowing for the binding to occur slowly so that one could monitor the kinetics.¹⁴² There are also ways to combat photobleaching, such as addition of an oxygen scavenging system. By experimentally isolating single timescales one could be able to tell the different photoconversion processes apart. Also, the addition of dual laser modulation could improve fluorescence imaging applications in which binding and fluorescence turn on are utilized. GFP chromophore structural variants plus binding substrates such as protein binding pockets and RNA aptamers have shown fluorescence turn on and binding activated modulation which could be extended to other molecules and sample environments.

CHAPTER 7

CONCLUSIONS AND OUTLOOK

Various types of fluorescence modulation based on dark state photophysics have been studied in cyanine dyes and protein-binding molecules. Single and dual laser modulation were applied to determine fluorescence enhancement and photophysical on and off times. In Cy5 derivatives it has been shown that dyes with longer alkyl chains on the side groups have higher modulation depth, while dyes with halogens on the polymethine bridge have lower modulation depth. Experimentally high modulation depth is associated with longer modulation timescales and low modulation depth is associated with shorter timescales. Additionally, modulation experiments as well as density functional theory was applied to calculate energetic differences between cyanine isomers. It has been shown experimentally and theoretically that a lower energy dark state photoisomer is associated with higher modulation depth, and a higher energy dark state is associated with lower modulation depth. Furthermore, new cyanine modulation applications have been explored including new dyes, and also certain solution additives can affect modulation depth. More importantly, with a triplet dark state, fluorescence upconversion has been observed in which a red-shifted secondary laser can generate optically activated delayed fluorescence by exciting the triplet state back to the singlet excited state. Lastly, protein-binding fluorophores have been studied and also show fluorescence modulation. Unlike cyanines this modulation depth is concentration dependent (on the protein), and seems to have two timescales associated with it, presumable due to photoisomerization and binding.

Moving forward, these new cyanine modulation and protein-binding modulation applications continue to be studied. New cyanines have been and continue to be synthesized with different properties, and perhaps new cyanines with greater fluorescence enhancement, tunable modulation frequencies, and triplet state fluorescence upconversion will be discovered. On the other hand, different types of binding fluorophores such as RNA aptamer binding GFP derivatives and DNA binding cyanines offer fluorescence turn on effects and new ways to study binding and unbinding effects in concert with fluorescence modulation. The ability to discern between different dark states, their properties and timescales would be useful for future fluorophore design and application.

APPENDIX A

EXTRA MODULATION DATA

SAFIRE modulation depths for other cyanine compounds

Like Cy5.5, its derivatives did not exhibit much modulation depth, and at these low levels of enhancement it was not possible to extract on and off times. But based on this data it appears that compounds with short alkyl chains and no halogen or chlorine on the polymethine bridge result in the highest fluorescence enhancement. Cy5-like compounds with trimethyl amine groups were synthesized in order make the compounds water soluble, but this diminished modulation depth.

Table A1. SAFIRE fluorescence enhancement data for other cyanine derivatives.

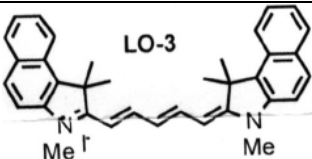
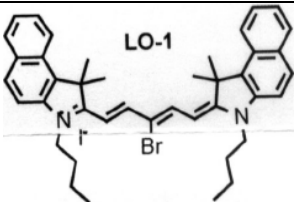
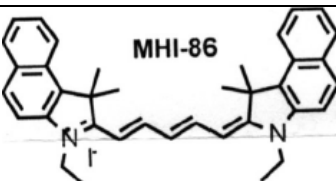
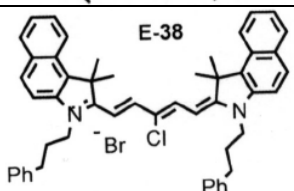
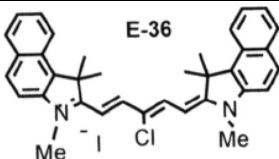
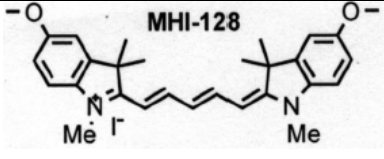
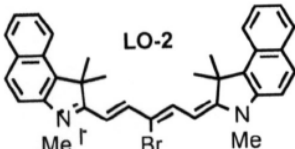
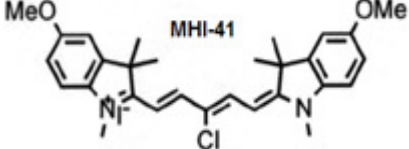
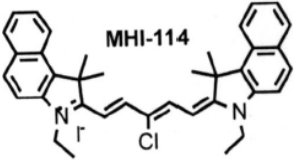
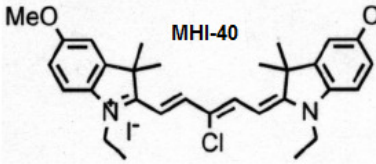
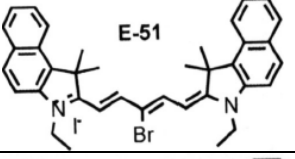
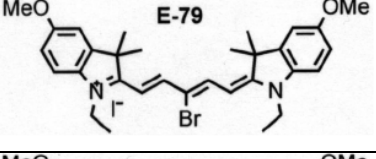
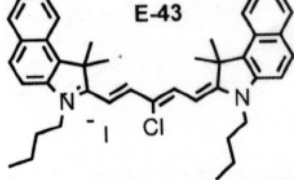
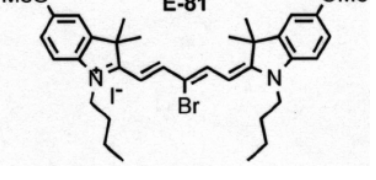
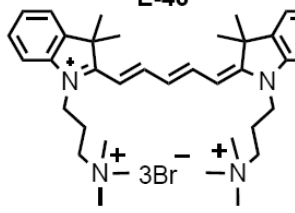
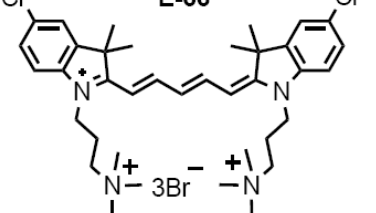
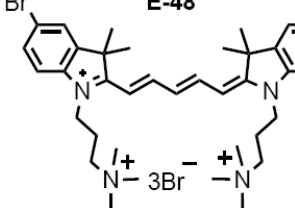
Molecule	Mod depth	Molecule	Mod depth
 <p>LO-3</p>	9.1%	 <p>LO-1</p>	4.3%
 <p>MHI-86</p>	7.3%	 <p>E-38</p>	2.9%
 <p>E-36</p>	7.4%	 <p>MHI-128</p>	9.4%
 <p>LO-2</p>	5.8%	 <p>MHI-41</p>	10.5%

Table A1 (continued).

 <p>MHI-114</p>	4.5%	 <p>MHI-40</p>	8.5%
 <p>E-51</p>	1.9%	 <p>E-79</p>	3.5%
 <p>E-43</p>	6.1%	 <p>E-81</p>	5.3%
 <p>E-46</p>	20%	 <p>E-66</p>	14%
 <p>E-48</p>	18%		

APPENDIX B

SECONDARY INDUCED FLUORESCENCE

Another interesting observation during these experiments has been secondary induced (red-shifted excitation) fluorescence in cyanine dyes. Sometimes when running experiments in our lab we noticed fluorescence detected at approximately 660 nm when exciting at 710 nm. This effect seems to occur despite using the appropriate dichroic filters to eliminate radiation bleed through from the excitation source and only allow emission wavelength radiation to pass, confirming that it is indeed fluorescence emitted from lower energy excitation. One possible explanation for this strange effect that seems to violate energy conservation is that there is a non-negligible thermal population of the cis-photoisomer dark state. The compounds with greater modulation depth and greater thermal dark state population appear to have stronger fluorescence from red-shifted excitation.

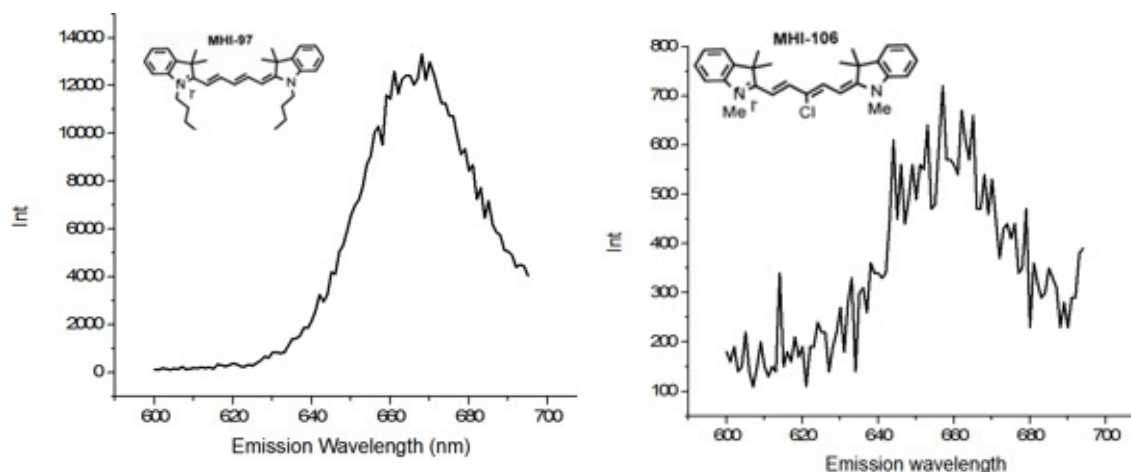


Figure B1. Comparison of secondary fluorescence between MHI-97 (left) and MHI-106 (right). With excitation laser intensity and concentration held constant, MHI-97 has much greater secondary fluorescence.

The difference in energy between 660 and 710 nm light is about .1 eV, close to the experimental and theoretical trans-cis energy differences, perhaps making up the energy deficit. Additionally, vibrational levels have energy spacings of this magnitude. These states could play a role if a higher energy vibrational states of the lowest electronic state are thermally populated. There are also other possibilities, including charge separation states¹⁵² and solvent effects.¹²

To investigate this further, we conducted experiments with pulsed primary and secondary lasers. Fluorescence decays with a 1 ns lifetime characteristic of Cy5 were observed upon both primary and secondary illumination, though the primary-induced fluorescence was much more intense. Upon co-illumination with both lasers, the primary peak increases commensurate to the bulk fluorescence signal while the secondary-only fluorescence is unaffected. This effect is summarized in the figure below.

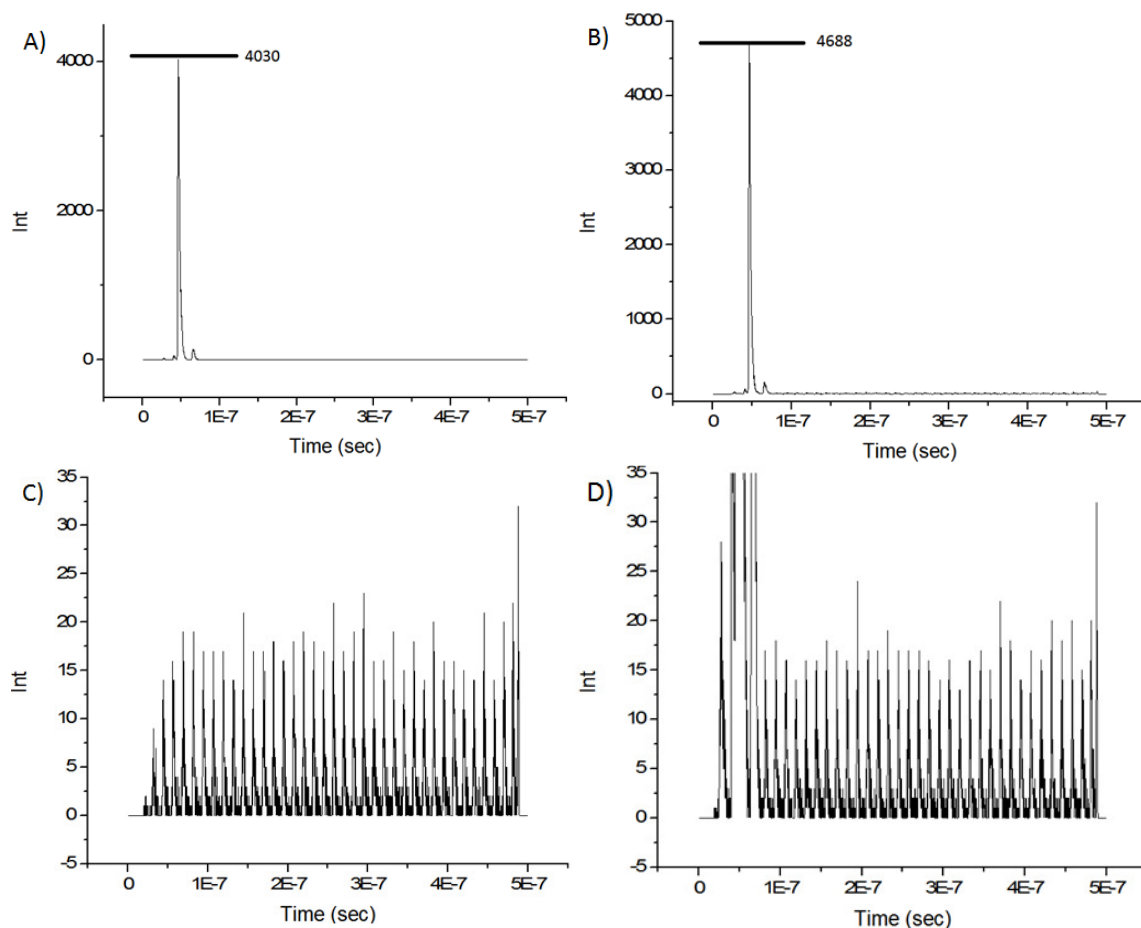


Figure B2. A) Cy5 fluorescence decay with pulsed primary excitation. B) Fluorescence decay with pulsed primary and secondary excitation. C) Fluorescence decay peaks with secondary only excitation. D) Concurrent primary and secondary excitation, zoomed into secondary fluorescence peaks. Upon dual excitation the primary fluorescence peak increases by ~15%, the same as the bulk fluorescence enhancement, while the secondary fluorescence peaks are unchanged.

Thus it appears that a small amount of fluorescence is emitted upon red-shifted excitation with the same fluorescent lifetime as the primary fluorescence, but it appears that this mechanism is independent of fluorescence modulation involving cis-trans photoisomerization. To investigate the possibility of dark state photoisomer thermal population, dye ZK-311 (see section 5.2) with a ring in the middle of the polymethine chain (preventing the possibility of isomerization about the 2-3 bond) was tested for secondary

fluorescence, and fluorescence was observed at 710 nm excitation. This confirms that the secondary fluorescence observed is not due to thermal population of the cis23 isomer. The cis12 isomer is higher in energy so less populated according to the Boltzmann distribution, while the cis01 isomer, according to TD-DFT, does not have a longer wavelength excitation. Because of the lack of dark state modulatability, it appears that this fluorescence from a red-shifted excitation has the same characteristics as standard primary laser induced fluorescence.

Now one has to consider why higher modulation depth molecules exhibit stronger secondary fluorescence. To look beyond isomer thermal population effects, UV-vis spectra were obtained to look for differences in absorption among different cyanines.

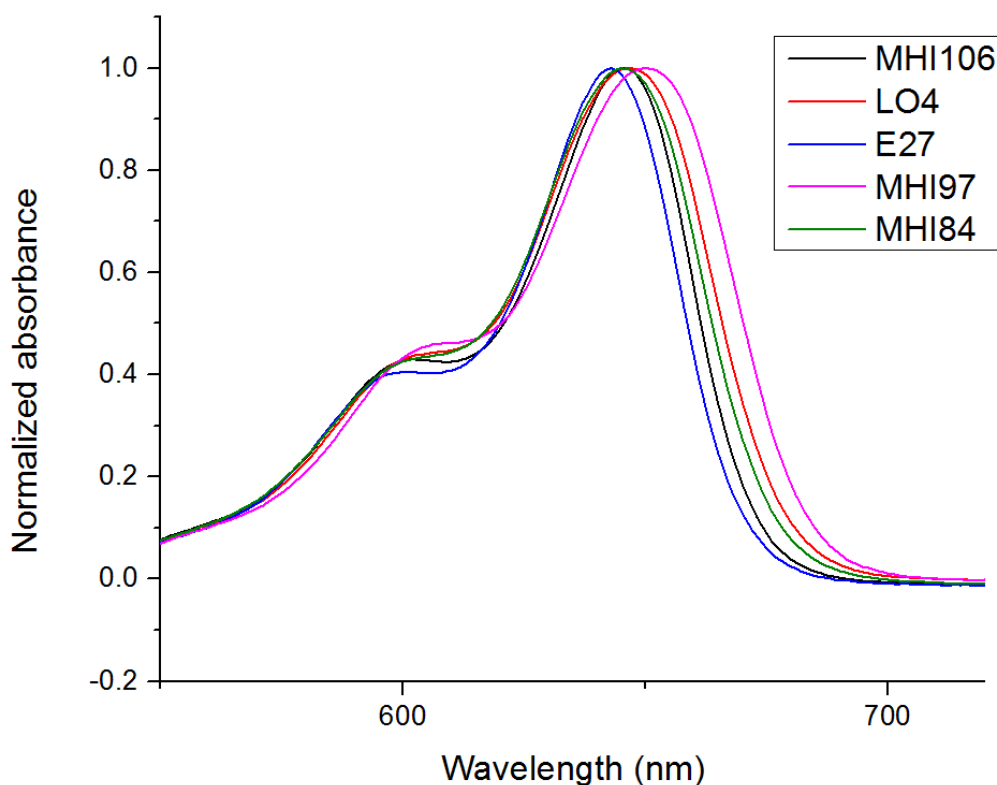


Figure B3. UV-vis absorption spectrum in visible-NIR region. There is a red-shift in the fluorescence from E27 to MHI97, from low to high modulation depth compounds.

There appears to be a clear trend, with lower modulation depth compounds having a blue-shifted absorption maxima compared to higher modulation depth compounds. Therefore it appears that greater secondary fluorescence could simply be due to increased absorbance in the >700 nm region. Perhaps a thermally populated higher level vibrational state accounts for the 0.1 eV energy difference between excitation and emission light, as an “Anti-Stokes” fluorescence effect. A solvent dependence effect was also observed, with solvent refractive index increasing secondary fluorescence.

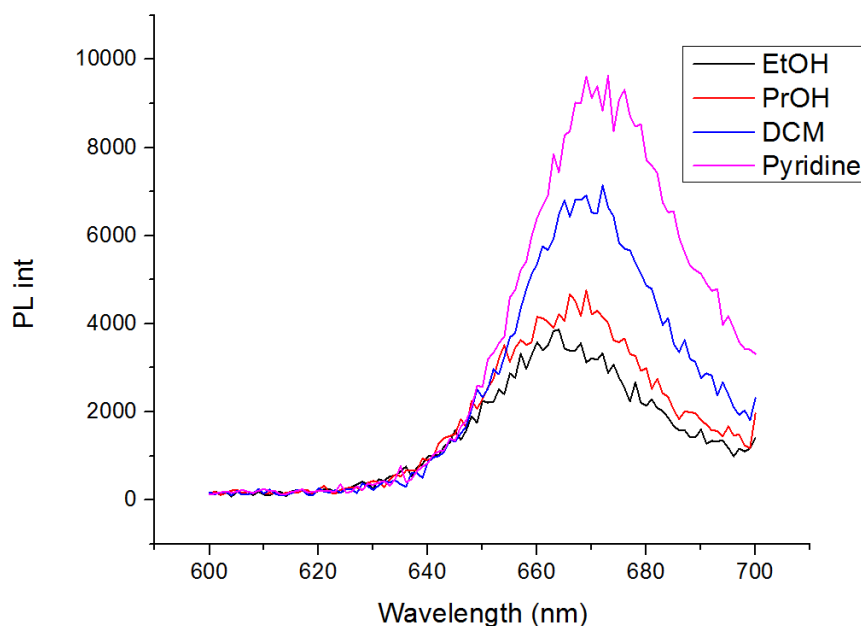


Figure B4. MHI-97 secondary fluorescence (670 nm emission and 710 nm excitation) with varying solvent refractive index, from ethanol (1.36), to propanol (1.39), dichloromethane (1.44), and pyridine (1.51). Increasing refractive index correlates with increasing secondary fluorescence.

If there is greater fluorescence with higher refractive index, this could be due to greater absorption in the >700 nm range. When UV-vis spectra of MHI-97 in different solvents are taken, this does seem to be the case.

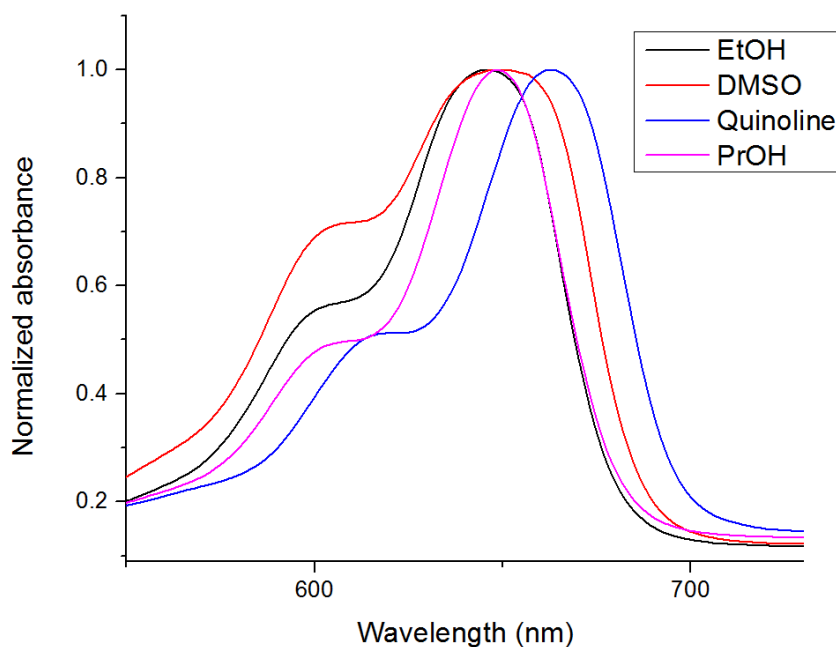


Figure B5. UV-vis absorption of MHI-97 with varying solvent. With increasing refractive index: ethanol (1.36), propanol (1.39), DMSO (1.48), and quinoline (1.63) the maximum absorption appears to shift to higher wavelength.

Curiously, the absorption beyond 700 nm is negligible for most molecules in different solvents, despite the fluorescence detected when excited at that wavelength. However in an excitation scan from 690 – 800 nm where emission is held constant at 665 nm, fluorescence intensity corresponding to the emission scan is observed.

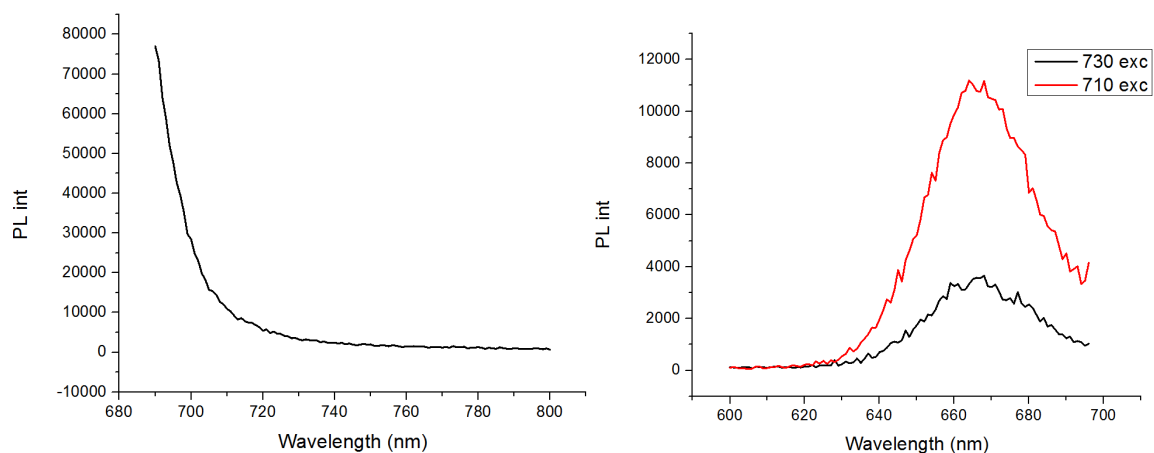


Figure B6. Left: MHI-97 Fluorescence excitation scan from 690-800 nm with emission held constant at 665 nm. Right: Fluorescence emission from 600-700 nm with 710 and 730 nm excitation, the maxima of which correspond to the excitation scan value observed on the left.

There appears to be some degree of fluorescence excitation at wavelengths greater than 700 nm, despite minimal absorbance observed in the UV-vis spectrum. To look into this further, a higher concentration cyanine sample was used to increase 710 nm absorption and compare to 590 nm absorption, the same as the primary laser used in experiments. Then fluorescence emission spectra were compared to see if the absorption and emission data add up.

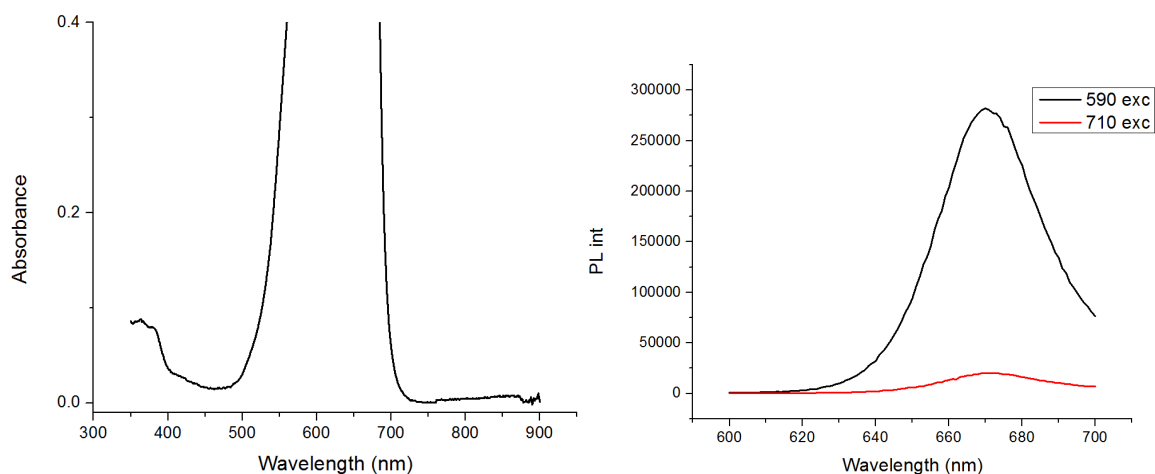


Figure B7. Left: UV-vis absorption of MHI-97 at high concentration ($\sim 100 \mu\text{M}$). Zoomed in, one can observe that the absorbance at 710 nm is 0.02, while the absorbance at 590 nm is 1.04. Right: The fluorescence emission of the same sample at 590 and 710 nm excitation.

At higher concentration, the absorbance at 710 nm is roughly 2% of the absorbance at 590 nm while the ratio of integrated fluorescence from 600-700 nm of 710 to 590 nm is approximately 7%. Although there is a slight discrepancy, one can reason that the fluorescence observed is likely due to anti-Stokes fluorescence,¹⁵³ possibly from a higher vibrational state. Thermal population from a photoisomer state is less likely, and the secondary fluorescence observed behaves similar to primary fluorescence.

In summary, pentamethine cyanine variants that typically absorb at ~ 640 nm and emit fluorescence at ~ 665 nm also exhibit red-shifted (secondary) fluorescence at >700 nm excitation. Initially, it was observed that higher modulation depth compounds had greater secondary fluorescence, and that this could be due to greater dark state thermal population. When studied using our modulation and time-resolved techniques, we determined that this fluorescence has the same characteristic lifetime (1 ns) as typical cyanine fluorescence, and

does not appear to be capable of any form of modulation. To eliminate the dark state thermal population origin hypothesis, the presence of red-shifted fluorescence with molecule ZK-311, with its ring-locked structure, rules out the possibility of cis isomerization about the middle bond where modulation is most likely to occur. After UV-vis analysis, it seems that the higher modulation depth compounds have a red-shifted absorption maximum which could lead to an increased absorption in the >700 nm region. Although the UV-vis absorption in the >700 nm range is almost negligible, corresponding excitation fluorescence is seen in the excitation scan when emission is collected at 665 nm and excitation occurs beyond 700 nm.

APPENDIX C

ADDITIONAL DENSITY FUNCTIONAL THEORY CALCULATIONS

In addition to the Cis23 and Cis12 isomer calculations, computations were performed on the Cis01 isomers and the results are presented in Table S1. The results indicate that (except for E63 and E65) there is a comparatively small energy difference between the Cis01 and all trans ground states when judged against the energy differences of the other photoisomers. In the cases of E63 and E65 the energy differences were comparatively large, perhaps due to steric effects of the bulky side groups. There is also little variation in energy differences among the different dyes, as compared to the other cis photoisomers.

Table C1. Energy differences between the Cis01 isomer and all trans ground states.

Molecule	Cis01-Trans (eV)
MHI84	0.06222
LO4	0.08009
MHI97	0.07670
MHI106	0.06518
E27	0.06695
E63	0.4418
E65	0.4346

Additional computations were run on the Cis01, Cis34, Cis45, Cis56, Cis67, and Cis78 isomers for the commercial dyes, which were asymmetric. For the most part, the asymmetric dye calculations did not differ greatly from the symmetric dyes, except for the Cy5.5 Cis34 and the Cy7 Cis56, which had the same energies as the all trans ground states.

Table C2. Energy differences for asymmetric molecules.

	Cis01- Trans (eV)	Cis34- Trans (eV)	Cis45- Trans (eV)	Cis56- Trans (eV)	Cis67- Trans (eV)	Cis78- Trans (eV)
Cy5	0.09895	0.1345	0.3182	0.08836	N/A	N/A
Cy5.5	0.05018	0	0.3091	0.07516	N/A	N/A
Cy7	0.1463	N/A	N/A	0	0.7242	0.08190
Merocyanine 540	0.2327	0.3242	N/A	N/A	N/A	N/A

APPENDIX D

DENSITY FUNCTIONAL THEORY CALCULATION INPUT

To use Gaussian for electronic structure theory calculations, one needs a great amount of CPU power, beyond what a standard desktop computer can supply. The way this was achieved in this research was by utilizing the Partnership for an Advanced Computing Environment (PACE) at Georgia Tech, which provides a high performance computing infrastructure. In order to perform an electronic structure calculation, one must first input the atomic coordinates of the molecule, along with the molecular charge and multiplicity, and the processors and memory required for the job. An easy way to obtain the molecular coordinates is to draw the desired molecule using a program such as Avogadro, then export the coordinates to a “.com” file which can be ready by Gaussian. From there, one needs to write a PBS (Portable batch system) script to submit the job. Below is the PBS script used to execute jobs to be submitted for calculation by the program Gaussian in this work. For reference, line 3 contains the job name, line 5 requests the nodes and processors per node, line 7 the memory, line 9 the time to complete job, line 11 the cluster name. Additionally, line 17 can be used to email when the job is complete and line 33 contains the file with the atomic coordinates and job specifications.

```
1 #!/bin/bash
2
3 #PBS -N MHI84pNO2cis23exc
4
5 #PBS -l nodes=2:ppn=1
6
7 #PBS -l pmem=2000mb
8
9 #PBS -l walltime=50:00:00
10
```

```
11 #PBS -q force-6
12
13 #-----
14
15 #PBS -j oe
16
17 #PBS -M dmahoney3@gatech.edu
18
19 #PBS -m ae
20
21 #-----
22
23 module purge
24 module load gaussian/G09A02
25
26 export GAUSS_SCRDIR=~/.scratch/$(echo $PBS_JOBID | cut -d. -f1);
27 mkdir $GAUSS_SCRDIR
28
29 #PBS -V
30
31 cd $PBS_O_WORKDIR
32
33 g09 MHI84pNO2cis23exc.com
34
35 rm -rf $GAUSS_SCRDIR
```

APPENDIX E

NUMERICAL SIMULATION OF PHOTOPHYSICS

As explained at the end of the first chapter, the kinetics of three state systems cannot be solved analytically, only numerically, so numerical computer simulations are helpful to see how population dynamics change over time with laser modulation. To model this system, the following parameters are used based on Cy5 photophysics (this simulation written in Mathematica):

```

h = 6.626 * 10-34; (* Planck constant in J s *)
c = 299792458; (*speed of light in m/s*)
λpri = 633 * 10-9; (*pri λ in meters*)
λsec = 710 * 10-9; (*sec λ in meters*)
σ = 4.3 * 10-16; (*absorption cross section in cm-2*)
σbiso = .13 * 10-16; (*reverse photoisomerization cross section*)
T = 1 / (2 * 1000); (*inverse half modulation frequency, Hz*)
ipri = 500 (**Sin[2*Pi*t*T-1] *); (* pri intensity in W/cm2 *)
isec = 1000; (* sec intensity in W/cm2 *)

kpri =  $\frac{\sigma * i_{pri}}{h * c / \lambda_{pri}}$ ;
ksec =  $\frac{\sigma_{biso} * i_{sec}}{h * c / \lambda_{sec}}$ ; (*laser used to deplete dark state*)
krelax = 1 * 109; (* inverse Cy5 lifetime in Hz *)
kISO = 25 * 106; (*photoisomerization rate, Hz*)
kIC = 3.97 * 109; (*internal conversion rate, Hz*)
kTrelax =  $\frac{1}{150 * 10^{-6}}$ ; (*thermal relaxation from photoisomer to S0*)

rateboth =  $\begin{pmatrix} -k_{pri} & k_{relax} + k_{IC} & k_{sec} + k_{Trelax} \\ k_{pri} & -(k_{relax} + k_{IC} + k_{ISO}) & 0 \\ 0 & k_{ISO} & -(k_{sec} + k_{Trelax}) \end{pmatrix}$ ;

rateprobe =  $\begin{pmatrix} -(k_{pri}) & k_{relax} + k_{IC} & k_{Trelax} \\ k_{pri} & -(k_{relax} + k_{IC} + k_{ISO}) & 0 \\ 0 & k_{ISO} & -(k_{Trelax}) \end{pmatrix}$ ; (*pri only*)

init =  $\begin{pmatrix} 1 \\ 0 \\ 0 \end{pmatrix}$ ;

```

```

graphp1 = Plot[MatrixExp[rateprobe*t].init, {t, 0, T}, PlotRange -> Full];
probe1 = MatrixExp[rateprobe*T].init;

graphb2 = Plot[MatrixExp[rateboth*(t-T)].probe1, {t, T, 2 T}, PlotRange -> Full];
both2 = MatrixExp[rateboth*T].probe1;

graphp2 = Plot[MatrixExp[rateprobe*(t-2 T)].both2, {t, 2 T, 3 T}, PlotRange -> Full];
probe2 = MatrixExp[rateprobe*(T)].both2;

graphb3 = Plot[MatrixExp[rateboth*(t-3 T)].probe2, {t, (3 T), (4 T)}, PlotRange -> Full];
both3 = (MatrixExp[rateboth*(T)]).probe2;

graphp3 = Plot[MatrixExp[rateprobe*(t-4 T)].both3, {t, (4 T), (5 T)}, PlotRange -> Full];
probe3 = (MatrixExp[rateprobe*(T)]).both3;

graphb4 = Plot[MatrixExp[rateboth*(t-5 T)].probe3, {t, (5 T), (6 T)}, PlotRange -> Full];
both4 = (MatrixExp[rateboth*(T)]).probe3;

graphp4 = Plot[MatrixExp[rateprobe*(t-6 T)].both4, {t, (6 T), (7 T)}, PlotRange -> Full];
probe4 = (MatrixExp[rateprobe*(T)]).both4;

graphb5 = Plot[MatrixExp[rateboth*(t-7 T)].probe4, {t, (7 T), (8 T)}, PlotRange -> Full];
both5 = (MatrixExp[rateboth*(T)]).probe4;

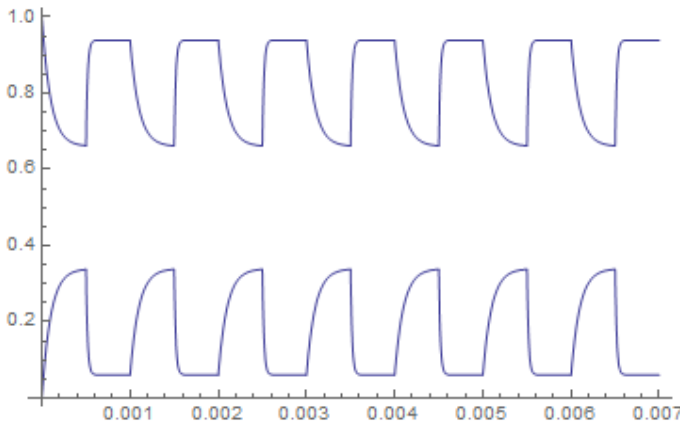
graphp5 = Plot[MatrixExp[rateprobe*(t-8 T)].both5, {t, (8 T), (9 T)}, PlotRange -> Full];
probe5 = (MatrixExp[rateprobe*(T)]).both5;

graphb6 = Plot[MatrixExp[rateboth*(t-9 T)].probe5, {t, (9 T), (10 T)}, PlotRange -> Full];
both6 = (MatrixExp[rateboth*(T)]).probe5;

graphp6 = Plot[MatrixExp[rateprobe*(t-10 T)].both6, {t, (10 T), (11 T)}, PlotRange -> Full];
probe6 = (MatrixExp[rateprobe*(T)]).both6;

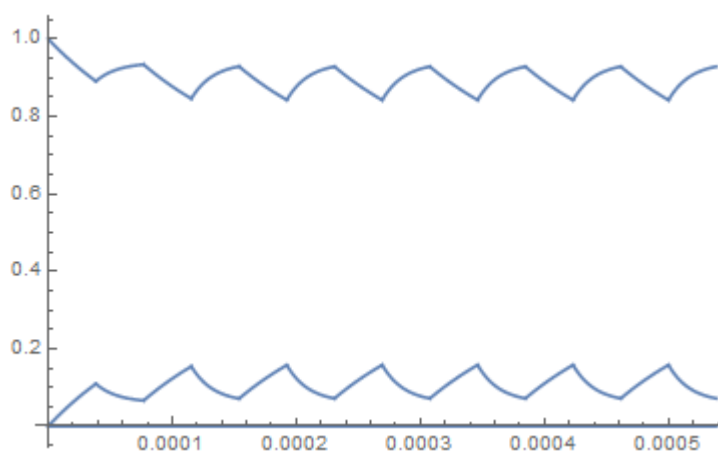
Show[graphp1, graphb2, graphp2, graphb3, graphp3, graphb4, graphp4, graphb5, graphp5,
graphb6, graphp6, graphb7, graphp7, graphb8, PlotRange -> {{0, 14 T}, {0, 1}}]

```



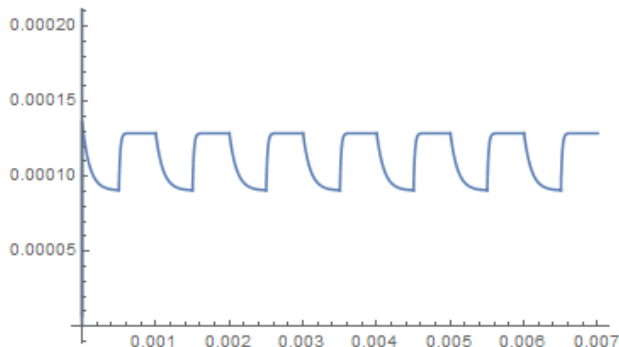
In the output graph the top line refers to the ground state population while the bottom line refers to the dark state population. The graph shows modulation at 1 kHz, which allows for

significant dark state buildup since the decay of the ground state (or increase of dark state) begins to flatten out, signaling steady state kinetics, before the next secondary laser pulse. At higher modulation depths this isn't the case since the dark state hasn't become fully populated before the next modulation cycle when the secondary turns on and depletes the dark state. At 13 kHz modulation frequency the modulation depth has greatly diminished as shown in the figure below.

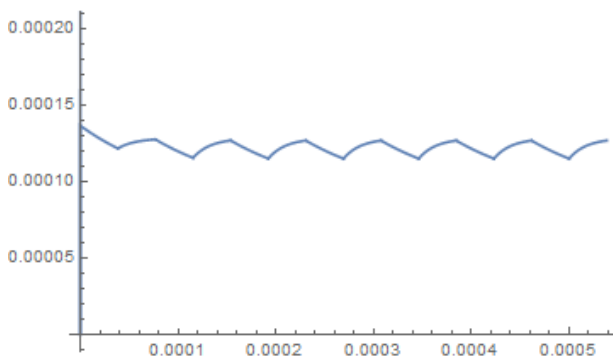


The plots above only show the populations for the ground state and the dark state. It is also possible to observe the fluorescence directly by monitoring the excited state population. To do this, simply zoom in on the y-axis. The excited state (S_1) population is very small because it is so short lived (nanosecond) compared to the ground and dark state.

```
Show[graphp1, graphb2, graphp2, graphb3, graphp3, graphb4, graphp4, graphb5, graphp5,
graphb6, graphp6, graphb7, graphp7, graphb8, PlotRange -> {{0, 14 T}, {0, .0002}}]
```



```
Show[graphp1, graphb2, graphp2, graphb3, graphp3, graphb4, graphp4, graphb5, graphp5,
graphb6, graphp6, graphb7, graphp7, graphb8, PlotRange -> {{0, 14 T}, {0, .0002}}]
```



The figure on the top corresponds to 1 kHz modulation while the figure on the bottom corresponds to 13 kHz. The modulation depth drops significantly from 1 kHz to 13 kHz. The fluorescence waveform looks similar to the ground state population dynamics, albeit a much smaller population, and is opposite from the dark state population dynamics.

Another simpler way to model the photophysics of this type of system is by designating only two states instead of three: on and off instead of S_0 , S_1 and T_1 . In this system “on” represents S_0 and S_1 (the fluorescent manifold) while “off” represents T_1 or the dark state. The on time is effectively the time spent in the bright state before transitioning to the dark state ($k_{exc} * \phi_D$ or the excitation rate times the dark state quantum yield), while the off time is just the dark state lifetime. This model of kinetics has been

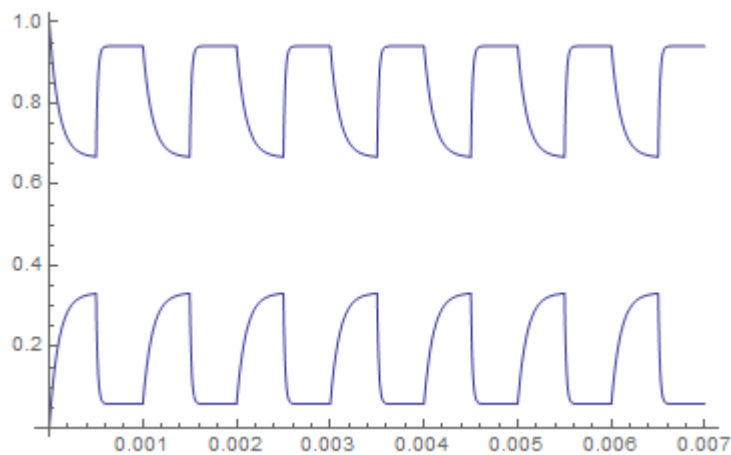
used in single molecule studies,¹⁵⁴ but can be easily applied to bulk samples. The input for this simulation is shown below:

```

h = 6.626 * 10-34;
c = 299792458;
λsec = 710 * 10-9;
kon = (300 * 10-6)-1;
koff = (150 * 10-6)-1;
T = 1 / (2 * 1000);
koffsec = koff +  $\frac{.13 * 10^{-16} * 1000}{h * c / \lambda_{sec}}$ ;
rateprobe =  $\begin{pmatrix} -kon & koff \\ kon & -koff \end{pmatrix}$ ; (*rate for primary only*)
rateboth =  $\begin{pmatrix} -kon & koffsec \\ kon & -koffsec \end{pmatrix}$ ;
init =  $\begin{pmatrix} 1 \\ 0 \end{pmatrix}$ ;

```

While leads to an output similar to that above for 1 kHz modulation.



APPENDIX F

COPYRIGHT PERMISSIONS



Title: Fluorescence microscopy
Author: Jeff W Lichtman and José-Angel Conchello

Logged in as:
Daniel Mahoney

[LOGOUT](#)

Publication: Nature Methods
Publisher: Nature Publishing Group
Date: Dec 1, 2005

Copyright © 2005, Rights Managed by Nature Publishing Group

Order Completed

Thank you for your order.

This Agreement between Daniel P Mahoney ("You") and Nature Publishing Group ("Nature Publishing Group") consists of your license details and the terms and conditions provided by Nature Publishing Group and Copyright Clearance Center.

Your confirmation email will contain your order number for future reference.

[Get the printable license.](#)

License Number	3973720847786
License date	Oct 21, 2016
Licensed Content Publisher	Nature Publishing Group
Licensed Content Publication	Nature Methods
Licensed Content Title	Fluorescence microscopy
Licensed Content Author	Jeff W Lichtman and José-Angel Conchello
Licensed Content Date	Dec 1, 2005
Type of Use	reuse in a dissertation / thesis
Requestor type	academic/educational
Format	print and electronic
Portion	figures/tables/illustrations
Number of figures/tables /illustrations	2
High-res required	no
Figures	Figures 1a&b, 3a
Author of this NPG article	no
Your reference number	
Title of your thesis / dissertation	OPTICAL MODULATION OF FLUOROPHORES BASED ON DARK STATE PHOTOPHYSICS
Expected completion date	May 2017
Estimated size (number of pages)	160
Requestor Location	Daniel P Mahoney 901 Atlantic Drive NW ATLANTA, GA 30332 United States Attn: Daniel P Mahoney
Billing Type	Invoice

Billing address Daniel P Mahoney
901 Atlantic Drive NW

ATLANTA, GA 30332
United States
Attn: Daniel P Mahoney

Total 0.00 USD

ORDER MORE

CLOSE WINDOW

Copyright © 2016 [Copyright Clearance Center, Inc.](#) All Rights Reserved. [Privacy statement](#). [Terms and Conditions](#).
Comments? We would like to hear from you. E-mail us at customercare@copyright.com



Title: NIR fluorescent small molecules for intraoperative imaging
Author: Eric A. Owens, Stephanie Lee, JungMun Choi, Maged Henary, Hak Soo Choi
Publication: Wiley Interdisciplinary Reviews - Nanomedicine and Nanobiotechnology
Publisher: John Wiley and Sons
Date: Jan 30, 2015
© 2015 Wiley Periodicals, Inc.

Logged in as:
Daniel Mahoney

LOGOUT

Order Completed

Thank you for your order.

This Agreement between Daniel P Mahoney ("You") and John Wiley and Sons ("John Wiley and Sons") consists of your license details and the terms and conditions provided by John Wiley and Sons and Copyright Clearance Center.

Your confirmation email will contain your order number for future reference.

[Get the printable license.](#)

License Number	3973721376452
License date	Oct 21, 2016
Licensed Content Publisher	John Wiley and Sons
Licensed Content Publication	Wiley Interdisciplinary Reviews - Nanomedicine and Nanobiotechnology
Licensed Content Title	NIR fluorescent small molecules for intraoperative imaging
Licensed Content Author	Eric A. Owens, Stephanie Lee, JungMun Choi, Maged Henary, Hak Soo Choi
Licensed Content Date	Jan 30, 2015
Licensed Content Pages	11
Type of use	Dissertation/Thesis
Requestor type	University/Academic
Format	Print and electronic
Portion	Figure/table
Number of figures/tables	1
Original Wiley figure/table number(s)	Figure 2
Will you be translating?	No
Title of your thesis / dissertation	OPTICAL MODULATION OF FLUOROPHORES BASED ON DARK STATE PHOTOPHYSICS
Expected completion date	May 2017
Expected size (number of pages)	160
Requestor Location	Daniel P Mahoney 901 Atlantic Drive NW

	ATLANTA, GA 30332 United States Attn: Daniel P Mahoney
Publisher Tax ID	EU826007151
Billing Type	Invoice
Billing address	Daniel P Mahoney 901 Atlantic Drive NW
	ATLANTA, GA 30332 United States Attn: Daniel P Mahoney
Total	0.00 USD



Title: Conformationally Locked Chromophores as Models of Excited-State Proton Transfer in Fluorescent Proteins

Author: Mikhail S. Baranov, Konstantin A. Lukyanov, Alexandra O. Borissova, et al

Publication: Journal of the American Chemical Society

Publisher: American Chemical Society

Date: Apr 1, 2012

Logged in as:

Daniel Mahoney

LOGOUT

Copyright © 2012, American Chemical Society

PERMISSION/LICENSE IS GRANTED FOR YOUR ORDER AT NO CHARGE

This type of permission/license, instead of the standard Terms & Conditions, is sent to you because no fee is being charged for your order. Please note the following:

- Permission is granted for your request in both print and electronic formats, and translations.
- If figures and/or tables were requested, they may be adapted or used in part.
- Please print this page for your records and send a copy of it to your publisher/graduate school.
- Appropriate credit for the requested material should be given as follows: "Reprinted (adapted) with permission from (COMPLETE REFERENCE CITATION). Copyright (YEAR) American Chemical Society." Insert appropriate information in place of the capitalized words.
- One-time permission is granted only for the use specified in your request. No additional uses are granted (such as derivative works or other editions). For any other uses, please submit a new request.

If credit is given to another source for the material you requested, permission must be obtained from that source.



Title: Comprehensive Studies on an Overall Proton Transfer Cycle of the ortho-Green Fluorescent Protein Chromophore

Author: Cheng-Chih Hsieh, Pi-Tai Chou, Chun-Wei Shih, et al

Publication: Journal of the American Chemical Society

Publisher: American Chemical Society

Date: Mar 1, 2011

Copyright © 2011, American Chemical Society

Logged in as:

Daniel Mahoney

[LOGOUT](#)

PERMISSION/LICENSE IS GRANTED FOR YOUR ORDER AT NO CHARGE

This type of permission/license, instead of the standard Terms & Conditions, is sent to you because no fee is being charged for your order. Please note the following:

- Permission is granted for your request in both print and electronic formats, and translations.
- If figures and/or tables were requested, they may be adapted or used in part.
- Please print this page for your records and send a copy of it to your publisher/graduate school.
- Appropriate credit for the requested material should be given as follows: "Reprinted (adapted) with permission from (COMPLETE REFERENCE CITATION). Copyright (YEAR) American Chemical Society." Insert appropriate information in place of the capitalized words.
- One-time permission is granted only for the use specified in your request. No additional uses are granted (such as derivative works or other editions). For any other uses, please submit a new request.

If credit is given to another source for the material you requested, permission must be obtained from that source.

ACS Publications
Most Trusted. Most Cited. Most Read.**Title:**Monitoring Kinetics of Highly
Environment Sensitive States of
Fluorescent Molecules by
Modulated Excitation and
Time-Averaged Fluorescence
Intensity Recording**Author:**Tor Sandén, Gustav Persson,
Per Thyberg, et al**Publication:** Analytical Chemistry**Publisher:** American Chemical Society**Date:** May 1, 2007

Copyright © 2007, American Chemical Society

Logged in as:

Daniel Mahoney

[LOGOUT](#)**PERMISSION/LICENSE IS GRANTED FOR YOUR ORDER AT NO CHARGE**

This type of permission/license, instead of the standard Terms & Conditions, is sent to you because no fee is being charged for your order. Please note the following:

- Permission is granted for your request in both print and electronic formats, and translations.
- If figures and/or tables were requested, they may be adapted or used in part.
- Please print this page for your records and send a copy of it to your publisher/graduate school.
- Appropriate credit for the requested material should be given as follows: "Reprinted (adapted) with permission from (COMPLETE REFERENCE CITATION). Copyright (YEAR) American Chemical Society." Insert appropriate information in place of the capitalized words.
- One-time permission is granted only for the use specified in your request. No additional uses are granted (such as derivative works or other editions). For any other uses, please submit a new request.

If credit is given to another source for the material you requested, permission must be obtained from that source.

CAMBRIDGE
JOURNALS

Title: Cyanine dyes in biophysical research: the photophysics of polymethine fluorescent dyes in biomolecular environments
Author: Marcia Levitus, Suman Ranjit
Publication: Quarterly Reviews of Biophysics
Publisher: Cambridge University Press
Date: Nov 26, 2010

Copyright © 2010, Cambridge University Press

Logged in as:
Daniel Mahoney
Account #:
3001073336

LOGOUT

Order Completed

Thank you for your order.

This Agreement between Daniel P Mahoney ("You") and Cambridge University Press ("Cambridge University Press") consists of your order details and the terms and conditions provided by Cambridge University Press and Copyright Clearance Center.

License number	Reference confirmation email for license number
License date	Oct 21, 2016
Licensed Content Publisher	Cambridge University Press
Licensed Content Publication	Quarterly Reviews of Biophysics
Licensed Content Title	Cyanine dyes in biophysical research: the photophysics of polymethine fluorescent dyes in biomolecular environments
Licensed Content Author	Marcia Levitus, Suman Ranjit
Licensed Content Date	Nov 26, 2010
Licensed Content Volume	44
Licensed Content Issue	1
Start page	123
End page	151
Type of Use	Dissertation/Thesis
Requestor type	Not-for-profit
Portion	Full article
Order reference number	
Territory for reuse	World
Title of your thesis / dissertation	OPTICAL MODULATION OF FLUOROPHORES BASED ON DARK STATE PHOTOPHYSICS
Expected completion date	May 2017
Estimated size(pages)	160
Requestor Location	Daniel P Mahoney 901 Atlantic Drive NW

	ATLANTA, GA 30332 United States Attn: Daniel P Mahoney
Publisher Tax ID	GB823847609
Billing Type	Invoice
Billing address	Daniel P Mahoney 901 Atlantic Drive NW ATLANTA, GA 30332 United States Attn: Daniel P Mahoney
Total	0.00 USD

REFERENCES

1. Tsien, R. Y., Imaging's Future. *Nature Reviews Molecular Cell Biology* **2003**, 5 (9), SS16-SS21.
2. Weissleder, R., A Clearer Vision For In Vivo Imaging. *Nat. Biotechnol.* **2001**, 19 (4), 316-7.
3. Abramowitz M, D. M. Introduction to Microscopy. (accessed June 2).
4. Weissleder, R., Scaling down imaging: molecular mapping of cancer in mice. *Nat. Rev. Cancer* **2002**, 2 (1), 11-18.
5. Sciences, T. R. S. A. o., Scientific Background on the Nobel Prize in Chemistry 2014. Royal Swedish Academy of Sciences: 2014.
6. Raylman, R. R.; Majewski, S.; Lemieux, S. K.; Velan, S. S.; Kross, B.; Popov, V.; Smith, M. F.; Weisenberger, A. G.; Zorn, C.; Marano, G. D., Simultaneous MRI and PET imaging of a rat brain. *Physics in medicine and biology* **2006**, 51 (24), 6371.
7. Feldchtein, F. I.; Gelikonov, G.; Gelikonov, V.; Iksanov, R.; Kuranov, R.; Sergeev, A. M.; Gladkova, N.; Ourutina, M.; Warren, J.; Reitze, D., In vivo OCT imaging of hard and soft tissue of the oral cavity. *Optics express* **1998**, 3 (6), 239-250.
8. Flegler, S. L.; Heckman, J. W.; Klomparens, K. L., *Scanning and transmission electron microscopy: an introduction*. WH Freeman New York:: 1993.
9. Onishi, H.; Iwasawa, Y., STM-imaging of formate intermediates adsorbed on a TiO₂ (110) surface. *Chemical physics letters* **1994**, 226 (1-2), 111-114.
10. Zou, Q.; Leang, K. K.; Sadoun, E.; Reed, M. J.; Devasia, S., Control issues in high-speed AFM for biological applications: Collagen imaging example. *Asian Journal of Control* **2004**, 6 (2), 164-178.
11. Lichtman, J. W.; Conchello, J.-A., Fluorescence microscopy. *Nat Meth* **2005**, 2 (12), 910-919.
12. Lakowicz, J. R., *Principles of Fluorescence Spectroscopy*. Springer US: 2006.

13. Escobedo, J. O.; Rusin, O.; Lim, S.; Strongin, R. M., NIR dyes for bioimaging applications. *Curr. Opin. Chem. Biol.* **2010**, *14* (1), 64-70.
14. Fan, C.; Hsiang, J.-C.; Dickson, R. M., Optical Modulation and Selective Recovery of Cy5 Fluorescence. *ChemPhysChem* **2012**, *13* (4), 1023-1029.
15. Huang, B.; Bates, M.; Zhuang, X., Super-Resolution Fluorescence Microscopy. *Annual Review of Biochemistry* **2009**, *78* (1), 993-1016.
16. Huang, B.; Wang, W.; Bates, M.; Zhuang, X., Three-Dimensional Super-Resolution Imaging By Stochastic Optical Reconstruction Microscopy. *Science* **2008**, *319* (5864), 810-813.
17. Shroff, H.; Galbraith, C. G.; Galbraith, J. A.; Betzig, E., Live-cell photoactivated localization microscopy of nanoscale adhesion dynamics. *Nat Meth* **2008**, *5* (5), 417-423.
18. Biteen, J. S.; Thompson, M. A.; Tselentis, N. K.; Bowman, G. R.; Shapiro, L.; Moerner, W. E., Super-resolution imaging in live *Caulobacter crescentus* cells using photoswitchable EYFP. *Nat Meth* **2008**, *5* (11), 947-949.
19. Egner, A.; Hell, S. W., Fluorescence microscopy with super-resolved optical sections. *Trends in Cell Biology* **2005**, *15* (4), 207-215.
20. Hsiang, J.-C.; Jablonski, A. E.; Dickson, R. M., Optically Modulated Fluorescence Bioimaging: Visualizing Obscured Fluorophores in High Background. *Acc. Chem. Res.* **2014**, *47* (5), 1545-1554.
21. Zheng, J.; Nicovich, P. R.; Dickson, R. M., Highly Fluorescent Noble-Metal Quantum Dots. *Annual Review of Physical Chemistry* **2007**, *58* (1), 409-431.
22. Petty, J. T.; Fan, C.; Story, S. P.; Sengupta, B.; Sartin, M.; Hsiang, J.-C.; Perry, J. W.; Dickson, R. M., Optically Enhanced, Near-IR, Silver Cluster Emission Altered by Single Base Changes in the DNA Template. *J. Phys. Chem. B* **2011**, *115* (24), 7996-8003.
23. Peyser, L. A.; Vinson, A. E.; Bartko, A. P.; Dickson, R. M., Photoactivated Fluorescence from Individual Silver Nanoclusters. *Science* **2001**, *291* (5501), 103-106.
24. Petty, J. T.; Story, S. P.; Hsiang, J.-C.; Dickson, R. M., DNA-Templated Molecular Silver Fluorophores. *The Journal of Physical Chemistry Letters* **2013**, *4* (7), 1148-1155.
25. Choi, S.; Dickson, R. M.; Yu, J., Developing luminescent silver nanodots for biological applications. *Chemical Society Reviews* **2012**, *41* (5), 1867-1891.

26. Patel, S. A.; Richards, C. I.; Hsiang, J.-C.; Dickson, R. M., Water-Soluble Ag Nanoclusters Exhibit Strong Two-Photon-Induced Fluorescence. *Journal of the American Chemical Society* **2008**, *130* (35), 11602-11603.
27. Lim, Y. T.; Kim, S.; Nakayama, A.; Stott, N. E.; Bawendi, M. G.; Frangioni, J. V., Selection of quantum dot wavelengths for biomedical assays and imaging. *Molecular Imaging* **2003**, *2* (1), 50-64.
28. Resch-Genger, U.; Grabolle, M.; Cavaliere-Jaricot, S.; Nitschke, R.; Nann, T., Quantum dots versus organic dyes as fluorescent labels. *Nat Meth* **2008**, *5* (9), 763-775.
29. Pansare, V. J.; Hejazi, S.; Faenza, W. J.; Prud'homme, R. K., Review of Long-Wavelength Optical and NIR Imaging Materials: Contrast Agents, Fluorophores, and Multifunctional Nano Carriers. *Chemistry of Materials* **2012**, *24* (5), 812-827.
30. Zimmer, M., Green Fluorescent Protein (GFP): Applications, Structure, and Related Photophysical Behavior. *Chem Rev* **2002**, *102* (3), 759-781.
31. Tsien, R. Y., THE GREEN FLUORESCENT PROTEIN. *Annual Review of Biochemistry* **1998**, *67* (1), 509-544.
32. Chudakov, D. M.; Matz, M. V.; Lukyanov, S.; Lukyanov, K. A., Fluorescent Proteins and Their Applications in Imaging Living Cells and Tissues. *Physiological Reviews* **2010**, *90* (3), 1103-1163.
33. Baldridge, A.; Feng, S.; Chang, Y.-T.; Tolbert, L. M., Recapture of GFP Chromophore Fluorescence in a Protein Host. *ACS Combinatorial Science* **2011**, *13* (3), 214-217.
34. Jablonski, A. E.; Vegh, R. B.; Hsiang, J.-C.; Bommarius, B.; Chen, Y.-C.; Solntsev, K. M.; Bommarius, A. S.; Tolbert, L. M.; Dickson, R. M., Optically Modulatable Blue Fluorescent Proteins. *J. Am. Chem. Soc.* **2013**, *135* (44), 16410-16417.
35. Dickson, R. M.; Cubitt, A. B.; Tsien, R. Y.; Moerner, W. E., On/off blinking and switching behaviour of single molecules of green fluorescent protein. *Nature* **1997**, *388* (6640), 355-358.
36. Jablonski, A. E.; Hsiang, J.-C.; Bagchi, P.; Hull, N.; Richards, C. I.; Fahrni, C. J.; Dickson, R. M., Signal Discrimination Between Fluorescent Proteins in Live Cells by Long-Wavelength Optical Modulation. *The Journal of Physical Chemistry Letters* **2012**, *3* (23), 3585-3591.

37. Chen, K.-Y.; Cheng, Y.-M.; Lai, C.-H.; Hsu, C.-C.; Ho, M.-L.; Lee, G.-H.; Chou, P.-T., Ortho Green Fluorescence Protein Synthetic Chromophore; Excited-State Intramolecular Proton Transfer via a Seven-Membered-Ring Hydrogen-Bonding System. *Journal of the American Chemical Society* **2007**, *129* (15), 4534-4535.
38. Hsieh, C.-C.; Chou, P.-T.; Shih, C.-W.; Chuang, W.-T.; Chung, M.-W.; Lee, J.; Joo, T., Comprehensive Studies on an Overall Proton Transfer Cycle of the ortho-Green Fluorescent Protein Chromophore. *Journal of the American Chemical Society* **2011**, *133* (9), 2932-2943.
39. Shimomura, O.; Johnson, F. H.; Saiga, Y., Extraction, Purification and Properties of Aequorin, a Bioluminescent Protein from the Luminous Hydromedusan, Aequorea. *Journal of Cellular and Comparative Physiology* **1962**, *59* (3), 223-239.
40. van Thor, J. J., Photoreactions and dynamics of the green fluorescent protein. *Chemical Society Reviews* **2009**, *38* (10), 2935-2950.
41. Zhang, J.; Campbell, R. E.; Ting, A. Y.; Tsien, R. Y., Creating new fluorescent probes for cell biology. *Nat Rev Mol Cell Biol* **2002**, *3* (12), 906-918.
42. Shaner, N. C.; Campbell, R. E.; Steinbach, P. A.; Giepmans, B. N. G.; Palmer, A. E.; Tsien, R. Y., Improved monomeric red, orange and yellow fluorescent proteins derived from *Discosoma* sp. red fluorescent protein. *Nat Biotech* **2004**, *22* (12), 1567-1572.
43. Weissleder, R.; Tung, C.-H.; Mahmood, U.; Bogdanov, A., In Vivo Imaging Of Tumors With Protease-Activated Near-Infrared Fluorescent Probes. *Nat. Biotechnol.* **1999**, *17* (4), 375-378.
44. Frangioni, J. V., In Vivo Near-Infrared Fluorescence Imaging. *Curr. Opin. Chem. Biol.* **2003**, *7* (5), 626-634.
45. Luo, S.; Zhang, E.; Su, Y.; Cheng, T.; Shi, C., A review of NIR dyes in cancer targeting and imaging. *Biomaterials* **2011**, *32* (29), 7127-7138.
46. Henary, M.; Pannu, V.; Owens, E. A.; Aneja, R., Near infrared active heptacyanine dyes with unique cancer-imaging and cytotoxic properties. *Bioorganic & Medicinal Chemistry Letters* **2012**, *22* (2), 1242-1246.
47. Owens, E. A.; Lee, S.; Choi, J.; Henary, M.; Choi, H. S., NIR fluorescent small molecules for intraoperative imaging. *Wiley Interdisciplinary Reviews: Nanomedicine and Nanobiotechnology* **2015**, *7* (6), 828-838.

48. Levitus, M.; Ranjit, S., Cyanine dyes in biophysical research: the photophysics of polymethine fluorescent dyes in biomolecular environments. *Q. Rev. Biophys.* **2011**, *44* (1), 123-51.
49. NHS Esters for Near-Infrared Fluorescence Labeling Reagents.
http://www.licor.com/bio/products/reagents/nhs_esters/nhs_esters.jsp (accessed April 1, 2012).
50. Alarcon, E.; Aspee, A.; Gonzalez-Bejar, M.; Edwards, A. M.; Lissi, E.; Scaiano, J. C., Photobehavior of merocyanine 540 bound to human serum albumin. *Photochem. Photobiol. Sci.* **2010**, *9* (6), 861-869.
51. Bamgbelu, A.; Wang, J.; Leszczynski, J., TDDFT Study of the Optical Properties of Cy5 and Its Derivatives. *J. Phys. Chem. A* **2010**, *114* (10), 3551-3555.
52. Baraldi, I.; Carnevali, A.; Caselli, M.; Momicchioli, F.; Ponterini, G.; Berthier, G., Theoretical and photophysical study of photoisomerism of cyanine dyes: bisphenylaminopentamethine cyanine (BPPC). *J. Mol. Struct.: THEOCHEM* **1995**, *330* (1-3), 403-410.
53. Huang, Z.; Ji, D.; Wang, S.; Xia, A.; Koberling, F.; Patting, M.; Erdmann, R., Spectral Identification of Specific Photophysics of Cy5 by Means of Ensemble and Single Molecule Measurements. *J. Phys. Chem. A* **2006**, *110* (1), 45-50.
54. Meyer, Y. H.; Pittman, M.; Plaza, P., Transient absorption of symmetrical carbocyanines. *Journal of Photochemistry and Photobiology A: Chemistry* **1998**, *114* (1), 1-21.
55. Momicchioli, F.; Baraldi, I.; Berthier, G., Theoretical study of trans-cis photoisomerism in polymethine cyanines. *Chem. Phys.* **1988**, *123* (1), 103-112.
56. Sarkar, S.; Fan, C.; Hsiang, J.-C.; Dickson, R. M., Modulated Fluorophore Signal Recovery Buried within Tissue Mimicking Phantoms. *J. Phys. Chem. A* **2013**, *117* (39), 9501-9509.
57. Widengren, J.; Schwille, P., Characterization of Photoinduced Isomerization and Back-Isomerization of the Cyanine Dye Cy5 by Fluorescence Correlation Spectroscopy. *J. Phys. Chem. A* **2000**, *104* (27), 6416-6428.
58. Dolmans, D. E. J. G. J.; Fukumura, D.; Jain, R. K., Photodynamic therapy for cancer. *Nat Rev Cancer* **2003**, *3* (5), 380-387.

59. Imlay, J. A., Pathways of Oxidative Damage. *Annual Review of Microbiology* **2003**, *57* (1), 395-418.
60. Macdonald, I. J.; Dougherty, T. J., Basic principles of photodynamic therapy. *Journal of Porphyrins and Phthalocyanines* **2001**, *5* (2), 105-129.
61. Umezawa, K.; Citterio, D.; Suzuki, K., Water-soluble NIR Fluorescent Probes Based on Squaraine and Their Application for Protein Labeling. *Analytical Sciences* **2008**, *24* (2), 213-217.
62. Umezawa, K.; Nakamura, Y.; Makino, H.; Citterio, D.; Suzuki, K., Bright, Color-Tunable Fluorescent Dyes in the Visible–Near-Infrared Region. *J. Am. Chem. Soc.* **2008**, *130* (5), 1550-1551.
63. Mishra, A.; Behera, R. K.; Behera, P. K.; Mishra, B. K.; Behera, G. B., Cyanines during the 1990s: A Review. *Chemical Reviews* **2000**, *100* (6), 1973-2012.
64. Fernandez-Suarez, M.; Ting, A. Y., Fluorescent probes for super-resolution imaging in living cells. *Nat Rev Mol Cell Biol* **2008**, *9* (12), 929-943.
65. Heilemann, M.; Margeat, E.; Kasper, R.; Sauer, M.; Tinnefeld, P., Carbocyanine Dyes As Efficient Reversible Single-Molecule Optical Switch. *J. Am. Chem. Soc.* **2005**, *127* (11), 3801-3806.
66. Lukomska, J.; Gryczynski, I.; Malicka, J.; Makowiec, S.; Lakowicz, J. R.; Gryczynski, Z., Two-photon induced fluorescence of Cy5-DNA in buffer solution and on silver island films. *Biochemical and Biophysical Research Communications* **2005**, *328* (1), 78-84.
67. Marder, S. R.; Gorman, C. B.; Meyers, F.; Perry, J. W.; Bourhill, G.; Brédas, J.-L.; Pierce, B. M., A Unified Description of Linear and Nonlinear Polarization in Organic Polymethine Dyes. *Science* **1994**, *265* (5172), 632-635.
68. Hu, H.; Ensley, T. R.; Reichert, M.; Ferdinandus, M. R.; Peceli, D.; Przhonska, O. V.; Marder, S. R.; Jen, A. K. Y.; Hales, J. M.; Perry, J. W.; Hagan, D. J.; Van Stryland, E. W. In *Optimization of the electronic third-order nonlinearity of cyanine-like molecules for all optical switching*, 2014; pp 898303-898303-6.
69. Nguyen, Q. T.; Olson, E. S.; Aguilera, T. A.; Jiang, T.; Scadeng, M.; Ellies, L. G.; Tsien, R. Y., Surgery with molecular fluorescence imaging using activatable cell-penetrating peptides decreases residual cancer and improves survival. *Proceedings of the National Academy of Sciences* **2010**.

70. Rasnik, I.; McKinney, S. A.; Ha, T., Nonblinking and long-lasting single-molecule fluorescence imaging. *Nat Meth* **2006**, 3 (11), 891-893.
71. van de Linde, S.; Loschberger, A.; Klein, T.; Heidebreder, M.; Wolter, S.; Heilemann, M.; Sauer, M., Direct stochastic optical reconstruction microscopy with standard fluorescent probes. *Nat. Protocols* **2011**, 6 (7), 991-1009.
72. Ha, T.; Tinnefeld, P., Photophysics of Fluorescent Probes for Single-Molecule Biophysics and Super-Resolution Imaging. *Annual Review of Physical Chemistry* **2012**, 63 (1), 595-617.
73. Heilemann, M.; van de Linde, S.; Schüttelpelz, M.; Kasper, R.; Seefeldt, B.; Mukherjee, A.; Tinnefeld, P.; Sauer, M., Subdiffraction-Resolution Fluorescence Imaging with Conventional Fluorescent Probes. *Angewandte Chemie International Edition* **2008**, 47 (33), 6172-6176.
74. Dempsey, G. T.; Bates, M.; Kowtoniuk, W. E.; Liu, D. R.; Tsien, R. Y.; Zhuang, X., Photoswitching Mechanism of Cyanine Dyes. *Journal of the American Chemical Society* **2009**, 131 (51), 18192-18193.
75. Huang, Z.; Ji, D.; Xia, A.; Koberling, F.; Patting, M.; Erdmann, R., Direct Observation of Delayed Fluorescence from a Remarkable Back-Isomerization in Cy5. *Journal of the American Chemical Society* **2005**, 127 (22), 8064-8066.
76. Awad, M.; McCarthy, P.; Blanchard, G., Photoisomerization of Cyanines. A comparative study of oxygen-and sulfur-containing species. *The Journal of Physical Chemistry* **1994**, 98 (5), 1454-1458.
77. Chibisov, A. K.; Zakharova, G. V.; Gorner, H., Effects of substituents in the polymethine chain on the photoprocesses in indodicarbocyanine dyes. *J. Chem. Soc., Faraday Trans.* **1996**, 92 (24), 4917-4925.
78. Vogt, G.; Krampert, G.; Niklaus, P.; Nuernberger, P.; Gerber, G., Optimal control of photoisomerization. *Physical review letters* **2005**, 94 (6), 068305.
79. Naqvi, K. R.; Sharma, D.; Hoytink, G., On the long-lived transient absorption observed in nanosecond laser photolysis studies of two polymethine cyanine dyes. *Chemical Physics Letters* **1973**, 22 (2), 226-229.
80. Weigel, A.; Pfaffe, M.; Sajadi, M.; Mahrwald, R.; Improta, R.; Barone, V.; Polli, D.; Cerullo, G.; Ernsting, N. P.; Santoro, F., Barrierless photoisomerisation of the "simplest cyanine": Joining computational and femtosecond optical spectroscopies to trace the full reaction path. *Physical Chemistry Chemical Physics* **2012**, 14 (38), 13350-13364.

81. Su-Fan Wang, T. Z., Yu-Cheng Huang, Shi-Yong Ye, DFT Investigation on the Trans-cis Photoisomerization of Pentamethine Cyanine Dye Model Molecule. *Chinese J. Struct. Chem.* **2011**, 30 (3), 401-411.
82. Improta, R.; Santoro, F., A theoretical study on the factors influencing cyanine photoisomerization: the case of thiacyanine in gas phase and in methanol. *Journal of chemical theory and computation* **2005**, 1 (2), 215-229.
83. Jia, K.; Wan, Y.; Xia, A.; Li, S.; Gong, F.; Yang, G., Characterization of photoinduced isomerization and intersystem crossing of the cyanine dye Cy3. *The Journal of Physical Chemistry A* **2007**, 111 (9), 1593-1597.
84. Widengren, J.; Seidel, C. A., Manipulation and characterization of photo-induced transient states of Merocyanine 540 by fluorescence correlation spectroscopy. *Physical Chemistry Chemical Physics* **2000**, 2 (15), 3435-3441.
85. Mandal, D.; Pal, S. K.; Sukul, D.; Bhattacharyya, K., Photophysical processes of merocyanine 540 in solutions and in organized media. *The Journal of Physical Chemistry A* **1999**, 103 (41), 8156-8159.
86. Hoebeke, M.; Pieite, J.; Van de Vorst, A., Viscosity-dependent isomerization and fluorescence yields of merocyanine 540. *Journal of Photochemistry and Photobiology B: Biology* **1990**, 4 (3), 273-282.
87. Conyard, J.; Kondo, M.; Heisler, I. A.; Jones, G.; Baldrige, A.; Tolbert, L. M.; Solntsev, K. M.; Meech, S. R., Chemically Modulating the Photophysics of the GFP Chromophore. *The Journal of Physical Chemistry B* **2011**, 115 (6), 1571-1577.
88. Hsu, Y.-H.; Chen, Y.-A.; Tseng, H.-W.; Zhang, Z.; Shen, J.-Y.; Chuang, W.-T.; Lin, T.-C.; Lee, C.-S.; Hung, W.-Y.; Hong, B.-C.; Liu, S.-H.; Chou, P.-T., Locked ortho- and para-Core Chromophores of Green Fluorescent Protein; Dramatic Emission Enhancement via Structural Constraint. *Journal of the American Chemical Society* **2014**, 136 (33), 11805-11812.
89. Baranov, M. S.; Lukyanov, K. A.; Borissova, A. O.; Shamir, J.; Kosenkov, D.; Slipchenko, L. V.; Tolbert, L. M.; Yampolsky, I. V.; Solntsev, K. M., Conformationally Locked Chromophores as Models of Excited-State Proton Transfer in Fluorescent Proteins. *Journal of the American Chemical Society* **2012**, 134 (13), 6025-6032.
90. Lee, J.-S.; Baldrige, A.; Feng, S.; SiQiang, Y.; Kim, Y. K.; Tolbert, L. M.; Chang, Y.-T., Fluorescence Response Profiling for Small Molecule Sensors Utilizing the Green Fluorescent Protein Chromophore and Its Derivatives. *ACS Combinatorial Science* **2010**, 13 (1), 32-38.

91. Baldridge, A.; Amador, A.; Tolbert, L. M., Fluorescence Turn On by Cholate Aggregates. *Langmuir* **2011**, 27 (7), 3271-3274.
92. Sandén, T.; Persson, G.; Thyberg, P.; Blom, H.; Widengren, J., Monitoring Kinetics of Highly Environment Sensitive States of Fluorescent Molecules by Modulated Excitation and Time-Averaged Fluorescence Intensity Recording. *Analytical Chemistry* **2007**, 79 (9), 3330-3341.
93. Sandén, T.; Persson, G.; Widengren, J., Transient State Imaging for Microenvironmental Monitoring by Laser Scanning Microscopy. *Analytical Chemistry* **2008**, 80 (24), 9589-9596.
94. Spielmann, T.; Xu, L.; Gad, A. K. B.; Johansson, S.; Widengren, J., Transient state microscopy probes patterns of altered oxygen consumption in cancer cells. *FEBS Journal* **2014**, 281 (5), 1317-1332.
95. Widengren, J., Fluorescence-based transient state monitoring for biomolecular spectroscopy and imaging. *J. R. Soc., Interface* **2010**.
96. Richards, C. I.; Hsiang, J.-C.; Dickson, R. M., Synchronously Amplified Fluorescence Image Recovery (SAFIRE). *J. Phys. Chem. B* **2009**, 114 (1), 660-665.
97. Richards, C. I.; Hsiang, J.-C.; Khalil, A. M.; Hull, N. P.; Dickson, R. M., FRET-Enabled Optical Modulation for High Sensitivity Fluorescence Imaging. *Journal of the American Chemical Society* **2010**, 132 (18), 6318-6323.
98. Mahoney, D. P.; Owens, E. A.; Fan, C.; Hsiang, J.-C.; Henary, M. M.; Dickson, R. M., Tailoring Cyanine Dark States for Improved Optically Modulated Fluorescence Recovery. *The Journal of Physical Chemistry B* **2015**, 119 (13), 4637-4643.
99. Wang, L. V.; Hu, S., Photoacoustic tomography: in vivo imaging from organelles to organs. *Science* **2012**, 335 (6075), 1458-1462.
100. Rosencwaig, A.; Gersho, A., Theory of the photoacoustic effect with solids. *Journal of Applied Physics* **1976**, 47 (1), 64-69.
101. Zhang, H. F.; Maslov, K.; Stoica, G.; Wang, L. V., Functional photoacoustic microscopy for high-resolution and noninvasive in vivo imaging. *Nature biotechnology* **2006**, 24 (7), 848-851.
102. Becker, W., *Advanced time-correlated single photon counting techniques*. Springer Science & Business Media: 2005; Vol. 81.

103. Becker, W.; Bergmann, A.; Hink, M.; König, K.; Benndorf, K.; Biskup, C., Fluorescence lifetime imaging by time-correlated single-photon counting. *Microscopy research and technique* **2004**, *63* (1), 58-66.
104. Birch, D. J.; Imhof, R. E., Time-domain fluorescence spectroscopy using time-correlated single-photon counting. In *Topics in fluorescence spectroscopy*, Springer: 2002; pp 1-95.
105. lab, D. K. Time Correlated Single Photon Counting.
http://smos.sogang.ac.kr/wiki/index.php/Time_Correlated_Single_Photon_Counting (accessed June 28).
106. Haustein, E.; Schwille, P., Single-molecule spectroscopic methods. *Current opinion in structural biology* **2004**, *14* (5), 531-540.
107. Moerner, W.; Fromm, D. P., Methods of single-molecule fluorescence spectroscopy and microscopy. *Review of Scientific Instruments* **2003**, *74* (8), 3597-3619.
108. Krichevsky, O.; Bonnet, G., Fluorescence correlation spectroscopy: the technique and its applications. *Reports on Progress in Physics* **2002**, *65* (2), 251.
109. Haustein, P. S. a. E., *Fluorescence Correlation Spectroscopy: An Introduction to its Concepts and Applications*. Gottingen, Germany.
110. Widengren, J.; Mets, U.; Rigler, R., Fluorescence correlation spectroscopy of triplet states in solution: a theoretical and experimental study. *The Journal of Physical Chemistry* **1995**, *99* (36), 13368-13379.
111. Laurence, T. A.; Ly, S.; Bourguet, F.; Fischer, N. O.; Coleman, M. A., Fluorescence correlation spectroscopy at micromolar concentrations without optical nanoconfinement. *The Journal of Physical Chemistry B* **2014**, *118* (32), 9662-9667.
112. Conoptics Modulation Systems. www.conoptics.com/modulation-systems/ (accessed July 21).
113. Parr, R. G., Density functional theory of atoms and molecules. In *Horizons of Quantum Chemistry*, Springer: 1980; pp 5-15.
114. Kohn, W.; Becke, A. D.; Parr, R. G., Density functional theory of electronic structure. *The Journal of Physical Chemistry* **1996**, *100* (31), 12974-12980.

115. Hohenberg, P.; Kohn, W., Inhomogeneous electron gas. *Physical review* **1964**, *136* (3B), B864.
116. Kohn, W.; Sham, L. J., Self-consistent equations including exchange and correlation effects. *Physical review* **1965**, *140* (4A), A1133.
117. Becke, A. D., A new mixing of Hartree–Fock and local density-functional theories. *The Journal of chemical physics* **1993**, *98* (2), 1372-1377.
118. Hanwell, M. D.; Curtis, D. E.; Lonie, D. C.; Vandermeersch, T.; Zurek, E.; Hutchison, G. R., Avogadro: an advanced semantic chemical editor, visualization, and analysis platform. *Journal of Cheminformatics* **2012**, *4* (1), 1-17.
119. Frisch, M. J.; Trucks, G. W.; Schlegel, H. B.; Scuseria, G. E.; Robb, M. A.; Cheeseman, J. R.; Scalmani, G.; Barone, V.; Mennucci, B.; Petersson, G. A.; Nakatsuji, H.; Caricato, M.; Li, X.; Hratchian, H. P.; Izmaylov, A. F.; Bloino, J.; Zheng, G.; Sonnenberg, J. L.; Hada, M.; Ehara, M.; Toyota, K.; Fukuda, R.; Hasegawa, J.; Ishida, M.; Nakajima, T.; Honda, Y.; Kitao, O.; Nakai, H.; Vreven, T.; Montgomery, J. J. A. *Gaussian 09, revision B.01*, Gaussian, Inc.: Wallingford, CT, 2009.
120. Bertolino, C. A.; Ferrari, A. M.; Barolo, C.; Viscardi, G.; Caputo, G.; Coluccia, S., Solvent effect on indocyanine dyes: A computational approach. *Chem. Phys.* **2006**, *330* (1–2), 52-59.
121. Champagne, B.; Guillaume, M.; Zutterman, F., TDDFT investigation of the optical properties of cyanine dyes. *Chem. Phys. Lett.* **2006**, *425* (1–3), 105-109.
122. Beckford, G.; Owens, E.; Henary, M.; Patonay, G., The solvatochromic effects of side chain substitution on the binding interaction of novel tricarbocyanine dyes with human serum albumin. *Talanta* **2012**, *92*, 45-52.
123. Choi, H. S.; Gibbs, S. L.; Lee, J. H.; Kim, S. H.; Ashitate, Y.; Liu, F.; Hyun, H.; Park, G.; Xie, Y.; Bae, S.; Henary, M.; Frangioni, J. V., Targeted zwitterionic near-infrared fluorophores for improved optical imaging. *Nat Biotech* **2013**, *31* (2), 148-153.
124. Chapman, G.; Henary, M.; Patonay, G., The Effect of Varying Short-Chain Alkyl Substitution on the Molar Absorptivity and Quantum Yield of Cyanine Dyes. *Anal. Chem. Insights* **2011**, *6* (2561-ACI-The-Effect-of-Varying-Short-Chain-Alkyl-Substitution-on-the-Molar-Abso.pdf), 29.
125. Bates, M.; Blosser, T. R.; Zhuang, X., Short-Range Spectroscopic Ruler Based On A Single-Molecule Optical Switch. *Phys. Rev. Lett.* **2005**, *94* (10), 108101.

126. van der Velde, J. H. M.; Ploetz, E.; Hiermaier, M.; Oelerich, J.; de Vries, J. W.; Roelfes, G.; Cordes, T., Mechanism Of Intramolecular Photostabilization In Self-Healing Cyanine Fluorophores. *ChemPhysChem* **2013**, *14* (18), 4084-4093.
127. Bates, M.; Huang, B.; Dempsey, G. T.; Zhuang, X., Multicolor Super-Resolution Imaging With Photo-Switchable Fluorescent Probes. *Science* **2007**, *317* (5845), 1749-1753.
128. Flors, C., Photoswitching Of Monomeric And Dimeric DNA-intercalating Cyanine Dyes For Super-resolution Microscopy Applications. *Photochem. Photobiol. Sci.* **2010**, *9* (5), 643-648.
129. Baker, T. A.; Gellene, G. I., A hybrid ab initio/free electron computational model for conjugated dye molecules: Simple cyanines and oxonols. *J. Comput. Chem.* **2000**, *21* (11), 943-953.
130. Jacquemin, D.; Zhao, Y.; Valero, R.; Adamo, C.; Ciofini, I.; Truhlar, D. G., Verdict: Time-Dependent Density Functional Theory "Not Guilty" of Large Errors for Cyanines. *Journal of Chemical Theory and Computation* **2012**, *8* (4), 1255-1259.
131. Bahnick, D. A., Use of Huckel Molecular Orbital Theory in Interpreting the Visible Spectra of Polymethine Dyes: An Undergraduate Physical Chemistry Experiment. *Journal of Chemical Education* **1994**, *71* (2), 171.
132. Kwok, S. J. J.; Choi, M.; Bhayana, B.; Zhang, X.; Ran, C.; Yun, S.-H., Two-photon excited photoconversion of cyanine-based dyes. *Scientific Reports* **2016**, *6*, 23866.
133. Altman, R. B.; Terry, D. S.; Zhou, Z.; Zheng, Q.; Geggier, P.; Kolster, R. A.; Zhao, Y.; Javitch, J. A.; Warren, J. D.; Blanchard, S. C., Cyanine fluorophore derivatives with enhanced photostability. *Nat Meth* **2012**, *9* (1), 68-71.
134. Zheng, Q.; Jockusch, S.; Zhou, Z.; Altman, R. B.; Warren, J. D.; Turro, N. J.; Blanchard, S. C., On the Mechanisms of Cyanine Fluorophore Photostabilization. *The Journal of Physical Chemistry Letters* **2012**, *3* (16), 2200-2203.
135. van de Linde, S.; Aufmkolk, S.; Franke, C.; Holm, T.; Klein, T.; Löschberger, A.; Proppert, S.; Wolter, S.; Sauer, M., Investigating Cellular Structures at the Nanoscale with Organic Fluorophores. *Chemistry & Biology* **2013**, *20* (1), 8-18.
136. Chen, Y.-C.; Jablonski, A. E.; Issaeva, I.; Bourassa, D.; Hsiang, J.-C.; Fahrni, C. J.; Dickson, R. M., Optically Modulated Photoswitchable Fluorescent Proteins Yield Improved Biological Imaging Sensitivity. *Journal of the American Chemical Society* **2015**, *137* (40), 12764-12767.

137. Zhang, Q.; Li, B.; Huang, S.; Nomura, H.; Tanaka, H.; Adachi, C., Efficient blue organic light-emitting diodes employing thermally activated delayed fluorescence. *Nat Photon* **2014**, *8* (4), 326-332.
138. Zhang, Q.; Li, J.; Shizu, K.; Huang, S.; Hirata, S.; Miyazaki, H.; Adachi, C., Design of Efficient Thermally Activated Delayed Fluorescence Materials for Pure Blue Organic Light Emitting Diodes. *Journal of the American Chemical Society* **2012**, *134* (36), 14706-14709.
139. Dias, F. B.; Bourdakos, K. N.; Jankus, V.; Moss, K. C.; Kamtekar, K. T.; Bhalla, V.; Santos, J.; Bryce, M. R.; Monkman, A. P., Triplet Harvesting with 100% Efficiency by Way of Thermally Activated Delayed Fluorescence in Charge Transfer OLED Emitters. *Advanced Materials* **2013**, *25* (27), 3707-3714.
140. Redmond, R. W.; Kochevar, I. E.; Krieg, M.; Smith, G.; McGimpsey, W. G., Excited State Relaxation in Cyanine Dyes: A Remarkably Efficient Reverse Intersystem Crossing from Upper Triplet Levels. *The Journal of Physical Chemistry A* **1997**, *101* (15), 2773-2777.
141. Aramendia, P. F.; Krieg, M.; Nitsch, C.; Bittersmann, E.; Braslavsky, S. E., THE PHOTOPHYSICS OF MEROCYANINE 540. A COMPARATIVE STUDY IN ETHANOL AND IN LIPOSOMES. *Photochemistry and Photobiology* **1988**, *48* (2), 187-194.
142. Han, K. Y.; Leslie, B. J.; Fei, J.; Zhang, J.; Ha, T., Understanding the Photophysics of the Spinach–DFHBI RNA Aptamer–Fluorogen Complex To Improve Live-Cell RNA Imaging. *Journal of the American Chemical Society* **2013**, *135* (50), 19033-19038.
143. Laptinok, S. P.; Conyard, J.; Page, P. C. B.; Chan, Y.; You, M.; Jaffrey, S. R.; Meech, S. R., Photoacid behaviour in a fluorinated green fluorescent protein chromophore: ultrafast formation of anion and zwitterion states. *Chemical Science* **2016**, *7* (9), 5747-5752.
144. Filonov, G. S.; Moon, J. D.; Svensen, N.; Jaffrey, S. R., Broccoli: Rapid Selection of an RNA Mimic of Green Fluorescent Protein by Fluorescence-Based Selection and Directed Evolution. *Journal of the American Chemical Society* **2014**, *136* (46), 16299-16308.
145. You, M.; Jaffrey, S. R., Structure and mechanism of RNA mimics of green fluorescent protein. *Annual review of biophysics* **2015**, *44*, 187-206.
146. Querard, J.; Markus, T.-Z.; Plamont, M.-A.; Gauron, C.; Wang, P.; Espagne, A.; Volovitch, M.; Vríz, S.; Croquette, V.; Gautier, A.; Le Saux, T.; Jullien, L., Photoswitching Kinetics and Phase-Sensitive Detection Add Discriminative Dimensions for Selective Fluorescence Imaging. *Angewandte Chemie International Edition* **2015**, *54* (9), 2633-2637.

147. Quérard, J.; Le Saux, T.; Gautier, A.; Alcor, D.; Croquette, V.; Lemarchand, A.; Gosse, C.; Jullien, L., Kinetics of Reactive Modules Adds Discriminative Dimensions for Selective Cell Imaging. *ChemPhysChem* **2016**, *17* (10), 1396-1413.
148. Gatzogiannis, E.; Zhu, X.; Kao, Y.-T.; Min, W., Observation of Frequency-Domain Fluorescence Anomalous Phase Advance Due to Dark-State Hysteresis. *J. Phys. Chem. Lett.* **2011**, *2* (5), 461-466.
149. Zhu, X.; Min, W., Frequency-domain phase fluorometry in the presence of dark states: A numerical study. *Chem. Phys. Lett.* **2011**, *516* (1–3), 40-44.
150. Manna, P.; Jimenez, R., Time and Frequency-Domain Measurement of Ground-State Recovery Times in Red Fluorescent Proteins. *The Journal of Physical Chemistry B* **2015**, *119* (15), 4944-4954.
151. Chen, Y.-C.; Dickson, R. M., Improved Fluorescent Protein Contrast and Discrimination by Optically Controlling Dark State Lifetimes. *The Journal of Physical Chemistry Letters* **2017**, *8* (4), 733-736.
152. Lu, D.; Chen, G.; Perry, J. W.; Goddard, W. A., Valence-Bond Charge-Transfer Model for Nonlinear Optical Properties of Charge-Transfer Organic Molecules. *Journal of the American Chemical Society* **1994**, *116* (23), 10679-10685.
153. Przhonska, O.; Slominsky, Y.; Stahl, U.; Daehne, S., Excited-state relaxation processes in polymethine dye molecules in polymeric media. *Journal of Luminescence* **1996**, *69* (2), 105-113.
154. Yip, W.-T.; Hu, D.; Yu, J.; Vanden Bout, D. A.; Barbara, P. F., Classifying the photophysical dynamics of single-and multiple-chromophoric molecules by single molecule spectroscopy. *The Journal of Physical Chemistry A* **1998**, *102* (39), 7564-7575.